DEVELOPMENT OF FLEXIBLE ORGANIC ELECTROCHEMICAL TRANSISTOR BASED ON BIOPOLYMER ELECTROLYTE AND ITS PERFORMANCE OPTIMIZATION

BO SUN

FACULTY OF ENGINEERING UNIVERSITI MALAYA KUALA LUMPUR

DEVELOPMENT OF FLEXIBLE ORGANIC ELECTROCHEMICAL TRANSISTOR BASED ON BIOPOLYMER ELECTROLYTE AND ITS PERFORMANCE OPTIMIZATION

BO SUN

DISSERTATION SUBMITTED IN FULFILMENT OF THE REQUIREMENTS FOR THE DEGREE OF MASTER OF ENGINEERING SCIENCE

FACULTY OF ENGINEERING UNIVERSITI MALAYA KUALA LUMPUR

UNIVERSITI MALAYA ORIGINAL LITERARY WORK DECLARATION

Name of Candidate: BO SUN

Matric No: S2106028/1

Name of Degree: MASTER OF ENGINEERING SCIENCE

Title of Project Paper/Research Report/Dissertation/Thesis ("this Work"):

DEVELOPMENT OF FLEXIBLE ORGANIC ELECTROCHEMICAL TRANSISTOR BASED ON BIOPOLYMER ELECTROLYTE AND ITS PERFORMANCE OPTIMIZATION

Field of Study:

MICROELECTRONICS

I do solemnly and sincerely declare that:

- (1) I am the sole author/writer of this Work;
- (2) This Work is original;
- (3) Any use of any work in which copyright exists was done by way of fair dealing and for permitted purposes and any excerpt or extract from, or reference to or reproduction of any copyright work has been disclosed expressly and sufficiently and the title of the Work and its authorship have been acknowledged in this Work;
- (4) I do not have any actual knowledge nor do I ought reasonably to know that the making of this work constitutes an infringement of any copyright work;
- (5) I hereby assign all and every rights in the copyright to this Work to the Universiti Malaya ("UM"), who henceforth shall be owner of the copyright in this Work and that any reproduction or use in any form or by any means whatsoever is prohibited without the written consent of UM having been first had and obtained;
- (6) I am fully aware that if in the course of making this Work I have infringed any copyright whether intentionally or otherwise, I may be subject to legal action or any other action as may be determined by UM.

Candidate's Signature	Date:	3/3/2025

Subscribed and solemnly declared before,

Witness's Signature Date: 3 Mac 2025

Name:

Designation:

ABSTRACT

Neuromorphic devices are gaining attention for their ability to mimic biological

synapses, with organic electrochemical transistors (OECTs) emerging as promising

candidates due to their high transconductance, low voltage operation, and strong

electrolyte gating. However, conventional OECTs often rely on liquid electrolytes or

synthetic polymers, posing challenges in stability, sustainability, and scalability. In this

study, we develop a biodegradable, flexible OECT using a solid-state chitosan-based

biopolymer electrolyte, a PEDOT:PSS semiconductor channel, and a low-cost screen-

printing process, enabling scalable fabrication. The chitosan electrolyte, reinforced with

salt, enhances ion transport, charge carrier density, and electric double layer (EDL)

formation, improving device performance. Our optimized OECTs achieve an on-state

current of 0.19 ± 0.03 mA at 0.6 V, an on/off ratio of 0.3×10^3 , and a transconductance

of 0.416 ± 0.05 mS, while maintaining mechanical robustness over 300 bending cycles

and thermal stability from 30 to 75 °C. The biodegradable electrolyte offers an

environmentally friendly alternative, reducing electronic waste and enabling sustainable

transient electronics. This study introduces one of the latest solid-state polymer

electrolytes for OECTs, demonstrating how electrolyte engineering can optimize ion

transport and interfacial dynamics. With scalable fabrication, competitive performance,

and eco-friendly design, this work provides a promising approach for bioelectronics,

neuromorphic computing, and AI-driven applications.

Keywords: OECTs, Polymer electrolyte, Flexible, PEDOT:PSS, Biodegradable.

ABSTRAK

Peranti neuromorfik semakin mendapat perhatian kerana keupayaannya meniru sinaps biologi, dengan transistor elektrokimia organik (OECT) muncul sebagai calon yang menjanjikan disebabkan transkonduktans tinggi, operasi voltan rendah, dan pengawalan elektrolit yang kuat. Walau bagaimanapun, OECT konvensional sering bergantung pada elektrolit cecair atau polimer sintetik, yang menimbulkan cabaran dalam kestabilan, kelestarian, dan kebolehkembangan. Dalam kajian ini, kami membangunkan OECT yang boleh biodegradasi dan fleksibel menggunakan elektrolit biopolimer berasaskan kitosan dalam keadaan pepejal, saluran semikonduktor PEDOT:PSS, dan proses cetakan skrin kos rendah, yang membolehkan fabrikasi berskala besar. Elektrolit kitosan, yang diperkuat dengan garam, meningkatkan pengangkutan ion, ketumpatan pembawa cas, dan pembentukan lapisan dua elektrik (EDL), sekali gus memperbaik prestasi peranti. OECT yang dioptimumkan ini mencapai arus keadaan hidup (on-state) sebanyak 0.19 ± 0.03 mA pada 0.6 V, nisbah arus hidup/mati (on/off) sebanyak 0.3×10^3 , dan transkonduktans sebanyak 0.416 ± 0.05 mS, sambil mengekalkan kekukuhan mekanikal melebihi 300 kitaran lenturan serta kestabilan terma dalam lingkungan suhu 30 hingga 75 °C. Elektrolit yang boleh biodegradasi ini menawarkan alternatif mesra alam, mengurangkan sisa elektronik dan membolehkan pembangunan elektronik sementara yang lestari. Kajian memperkenalkan salah satu elektrolit polimer keadaan pepejal terkini untuk OECT, serta membuktikan bagaimana kejuruteraan elektrolit dapat mengoptimumkan pengangkutan ion dan dinamik antara muka. Dengan fabrikasi berskala besar, prestasi kompetitif, dan reka bentuk mesra alam, kajian ini membuka jalan baharu untuk bioelektronik, pengkomputeran neuromorfik, dan aplikasi berasaskan kecerdasan buatan (AI).

Kata kunci: OECTs, Elektrolit Polimer, Fleksibel, PEDOT:PSS, Boleh terurai.

ACKNOWLEDGEMENTS

I express my deepest gratitude to my supervisors, Dr. Sharifah Fatmadiana Wan

Muhamad Hatta, Prof. Norhayati Soin, and Prof. Dr. Mohd Fakhrul Zamani Abdul

Kadir, for their invaluable guidance, encouragement, and mentorship. Dr. Sharifah

Fatmadiana, in particular, has played a crucial role in shaping my research journey and

fostering my growth as a researcher.

A heartfelt thank you to my teammates, Fazliyatul Azwa Binti Md Rezali, Dr.

Maliya, and Dr. Nabila, for their support, skill-sharing, and assistance throughout my

research. Special thanks to Fazliyatul Azwa for her significant contributions to my

writing and presentations.

I am also profoundly thankful for the friendships I've developed here in a foreign

land, which have enriched my life and provided continuous motivation and support.

Most importantly, I owe my sincerest gratitude to my family, whose unwavering

support and love have been my foundation. Their sacrifices have enabled me to

complete my research, and my love for them is everlasting.

This dissertation reflects not only my efforts but the collective support and

encouragement of all mentioned. To everyone who has been a part of this journey, thank

you.

Bo Sun

June 2024

iv

TABLE OF CONTENTS

Abstract	ii
Abstrak	ii
Acknow	ledgementsiv
List of F	iguresix
List of T	Sables xiv
List of S	lymbols and Abbreviationsxv
List of A	Appendicesxx
СНАРТ	TER 1: INTRODUCTION1
1.1	Background of Research
1.2	Problem Statement
1.3	Motivation4
1.4	Aims and Objectives5
1.5	Scope of Work7
1.6	Dissertation Outline
СНАРТ	ER 2: LITERATURE REVIEW10
2.1	Introduction
2.2	Biological Synapse10
2.3	Synaptic Transistors Based on Field-Effect Transistor
2.3	.1 Floating-gate Synaptic Transistor14
2.3	.2 Electrolyte-gate Synaptic Transistors

2.3.3 Ferroelectric-gate Synaptic Transistors
2.4 Synaptic Transistor Based on Organic Electrochemical Transistor20
2.4.1 Working Mechanism and Characterization of OECTs21
2.4.2 Structure of OECTs23
2.4.3 Material of OECTs
2.4.4 Application of OECTs
2.5 Summary
CHAPTER 3: RESEARCH METHODOLOGY
3.1 Introduction
3.2 Flow Chart of Overall Project Methodology
3.3 Experimental Section
3.3.1 Organic Semiconductor Synthesis
3.3.2 Polymer Electrolyte Preparation
3.3.3 Fabrication of OECTs Based on Rigid Si Wafer Substrate
3.3.4 Fabrication of OECTs Based on Flexible PET Substrate
3.3.5 Characterization
3.4 Experimental Design of Electrical Characteristics
3.5 Experimental Design of Mechanical Properties

3.5.1 Mechanical Robustness Testing4
3.5.2 Temperature Testing
3.6 Optimization Solution5
3.6.1 Effect of Structure in OECT5
3.6.2 Effect of Ethylene Glycol (EG) Doping in PEDOT:PSS
3.6.3 Effect of Salt Addition to The Polymer Electrolyte
CHAPTER 4: RESULTS AND DISCUSSIONS5
4.1 Introduction
4.2 Analysis on Performance of Rigid OECTs on Si Wafer5
4.2.1 The Exhibition of Physical Rigid OECTs5
4.2.2 Surface Morphology of Rigid OECTs5
4.2.3 The Electrical Characteristics of Rigid OECTs5
4.2.4 Adjustment of Experimental Conditions
4.3 Analysis on Performance of Flexible OECTs Based on Chitosan Electrolyte
on PET Substrate6.
4.3.1 Dielectric Properties of The Solid-State Chitosan-Based Polymer
Electrolyte6
4.3.2 Investigated Structures of Flexible Chitosan-based OECTs6.
4.3.3 The Electrical Characteristics of Flexible Chitosan-based OECTs 6.

4.3.4 The Mechanical Properties of Flexible Chitosan-based OEC	CTs69
4.3.5 Degradable Characterization	73
4.3.6 Optimization of Flexible Chitosan-based OECTs	74
4.4 Summary	79
CHAPTER 5: CONCLUSION AND FUTURE WORKS	81
References	84
List of Publications and Papers Presented	94
APPENDIX	95

LIST OF FIGURES

Figure 1.1: Diagram of overall works involved in this study
Figure 2.1: (a) Schematic illustration of neurons and synapse in human brain (Chen et al., 2019). (b)Typical artificial synapse based on OECTs
Figure 2.2: Schematic diagram of (a) the configuration of floating-gated transistor, (b) the mechano-plastic MoS ₂ synaptic transistor and (c) trapped/de-trapped of electrons by Au nanoparticles across HfO ₂ tunneling layer (X. Yang et al., 2020)
Figure 2.3: (a) Schematic of the flexible synaptic transistors based on semiconducting CNTs. (b) Image of the paper substrate being bent to accommodate the flexible CNT synaptic transistors (Kim et al., 2017).
Figure 2.4: Schematics of (a) the configuration of electrolyte-gated transistor, (b) casein electrolyte-based electric-double-layer (EDL) synaptic transistors on glass substrates, (c) a three-layer fully connected artificial neural network (ANN) for handwritten Modified National Institute of Standards and Technology (MNIST) recognition
Figure 2.5: (a) Schematic diagrams of ITO synaptic transistor, (b) extracted electrical parameters as a function of bending cycles. (c) Images of biodegradable ITO synaptic transistors (Yu et al., 2018).
Figure 2.6: Schematic diagrams of (a) configuration of ferroelectric-gated transistor and (b) In ₂ O ₃ ferroelectric transistor to mimic the biological synapse, (c) the simulated recognition accuracy as a function of the training epoch for WIL-FST (Ferroelectric transistor with Al ₂ O ₃ layer) (Luo et al., 2023).
Figure 2.7: Schematic diagrams of (a) tunable BT NPs/P(VDF-TrFE) ferroelectric gate dielectric layer-based synaptic transistor and (b) the working mechanism of artificial intrinsic-synaptic tactile sensory organ induced by tactile stimulation (Lee et al., 2020).
Figure 2.8: (a) The relationship between $g_{\rm m}$ and $I_{\rm D}$ as a function of $V_{\rm G}$ in the P-type OECT. (b) The response time required to change the state from 'OFF' to 'ON' (Paterson et al., 2018)
Figure 2.9: The schematic diagrams of (a) EDL formation and (b) electrochemical doping in OECT (Lee et al., 2021)
Figure 2.10: Figure 2.10: The schematic diagrams of (a) top-gated structure, (b) bottom-gated structure, (c) side-gated structure and (d) extended-gated structure (Torricelli et al., 2021).

Figure 2.11: Illustrations of (a) aqueous salt electrolyte, where the first solvation shells of both cations and anions are showed, (b) ionic liquids (ILs) electrolyte, which contain pure cations and anions, (c) polymer electrolytes, where the polyethylene oxide-like polymer chains align with the salt cations and anions, (d) ion gel electrolytes based on an ABA triblock copolymer and IL, (e) polyelectrolytes, where the bottom one is based on the polymerization of anions (polyanion), while the higher one is based on the polymerization of cations (polycation) (Huang et al., 2021)
Figure 2.12: (a) Schematic of an OPV integrated with an OECT, with the associated circuit schematic and a picture of the combined device. (b) Photograph of the self-powered integrated device mounted to the rat heart (Park et al., 2018). (c) Schematic of the ECG monitoring and signals acquired by SSOECT based on p(g1T2-g5T2)29
Figure 2.13: (a) Schematic components in the wearable OECT patch for multiplexed sensing of Al^{3+} and Ca^{2+} ions. (b) Photograph of flexible OECTs attached on different deformable surfaces and I_D response curve of the OECT to saliva under different volumes.
Figure 2.14: Schematics of (a) the transparent stretchable sensor array for temperature measurement on skin, (b) a flexible pressure sensor based on OECTs
Figure 2.15: (a) Schematic of artificial tactile system made up by an artificial afferent nerve and a biological efferent nerve. (b) Photograph of action measurement of cockroach leg
Figure 2.16: Schematics of (a) sound location using a neuro-transistor-based artificial neural network, (b) sound location by the human brain binaural effect
Figure 3.1: Research method for the development and analysis of flexible OECTs 36
Figure 3.2: General overview of the research workflow
Figure 3.3: Illustration of (a) pristine PEDOT:PSS solution, (b) filtered by 0.45 µ m filter and (c) added with different amount of EG
Figure 3.4: General preparation process of biopolymer electrolytes42
Figure 3.5: The overall step-by-step fabrication scheme of the OECT on silicon substrates
Figure 3.6: The procedure in fabricating OECT on flexible PET substrate45
Figure 3.7: Schematic diagrams of OECT design of (a) top-gated (b) bottom-gated (c) side-gated, and (d) channel size, $W\&L = 1.5 \times 0.5$ mm
Figure 3.8: List of electrical characteristics investigated in this study

Figure 3.9: Schematics of (a) bending testing and (b) temperature testing50
Figure 3.10: List of optimization methods for enhancing performance of OECTs 52
Figure 4.1: The photographs of rigid OECTs fabricated using three types polymer electrolytes on Si wafer. (a) Schematic diagram of structure of rigid OECT on Si wafer. Images of OECT based on (b) chitosan, length and width are 0.416 mm and 3.959 mm, (c) methylcellulose, length and width are 0.507 mm and 2.596 mm and (d) fish gelatin, length and width are 0.374 mm and 3.585 mm
Figure 4.2: The photographs of (a) Bruker Dektak XT measuring the thickness and (b) the stylus of Bruker Dektak XT touching surface of Si substrate
Figure 4.3: (a) The photograph of FESEM equipment, FEI QUANTA 450 FEG. (b) FESEM image of solid-state chitosan electrolyte on Si substrate
Figure 4.4: (a) The photograph of SCS parameter analyzer, Keithley 4200A and (b) probes connected with electrodes of rigid OECTs to measure the electrical properties. 57
Figure 4.5: Schematics of rigid OECTs structures and corresponding electrical characteristics. Illustrations of OECT (a) with chitosan-based electrolyte, (b) with methylcellulose-based electrolyte and (c) with fish gelatin-based electrolyte. (d-f) Transfer characteristics corresponding to (a-c). (g-i) Corresponding output curves of the transistors.
Figure 4.6: Photographs of deposition of chitosan-based electrolyte by spin-coating under (a) 3000 rpm for 30 s, (b) under 1000 rpm for 60 s and (c) under 2000 rpm for 60 s
Figure 4.7: Photographs of chitosan-based electrolyte film formation under 1000 rpm for 60 s. (a) Before UV curing. (b) After UV curing. 61
Figure 4.8: Annealing of chitosan-based electrolyte film under different temperature and duration. (a) Below 80 $^{\circ}$ C, less than 15 min. (b) Over 80 $^{\circ}$ C62
Figure 4.9: Design of the chitosan-based polymer electrolyte for the OECTs. (a) Microstructures and chemical structures of chitosan, dextran, and LiClO ₄ . (b) Schematic diagram of the organic polymer electrolyte
Figure 4.10: Flexible OECTs architecture. (a) Schematic illustration of the top-gated OECT. The channel length (L) and width (W) are 500 μ m and 1500 μ m, respectively. Photographs of (b) an array of top-gated OECTs on a flexible substrate while being bent and (c) one top-gated OECT, clearly showing the PEDOT:PSS layer and electrolyte layer. The green arrow indicates the direction of the transport of charge carriers64
Figure 4.11: (a) Schematic illustration of bottom-gated OECTs, top-gated OECTs and side-gated OECTs. The green arrow indicates the direction of the transport of charge

carriers. (b) Top views of OECTs with corresponding structures under digital microscope.
Figure 4.12: (a) Transfer characteristics of top-gated OECTs (red, solid line), bottom-gated OECTs (green, solid line), and side-gated OECTs (orange, solid line) measured at $V_D = -0.6$ V and (b) their associated transconductances. (c) Output curve of top-gated OECTs. The inset arrows refer to the sweep direction. All measurements were performed in a chitosan-based polymer electrolyte with the PEDOT:PSS channel66
Figure 4.13: (a) Double sweeping transfer curves of top-gated OECTs with different scanning rates, showing slight hysteresis. (b) Comparison of normalized on-state current and maximum transconductance for previously reported OECTs and the chitosan-based OECT developed herein. To obtain a fair comparison among the reported works on the topic of OECTs, the peak on-current and maximum transconductance were normalized by the channel dimension (dW/L) .
Figure 4.14: The long-term stability of chitosan-based OECTs. (a) Transfer and (b) the associated transconductance curves of chitosan-based OECTs measured over time 69
Figure 4.15: Device performance of flexible chitosan-based top-gated OECTs at two bending states. (a) Photographic images of the chitosan-based OECTs bended on a 3D printed rigid semicylinder and (b) attached on a flat PCB board. (c) Corresponding transfer and gm characteristics for the flexible chitosan-based OECTs during bending at a bending radius of 40 mm and flat state
Figure 4.16: Device performance of flexible chitosan-based top-gated OECTs at different bending radii. (a) Photographic images of four 3D printed rigid semicylinders with different bending radii ($R = 40, 50, 70, \text{ and } 100 \text{ mm}$). Cycle stabilities of (b) peak I_{on} and (c) g_{m} of flexible devices in terms of bending times at various bending radii ($R = 40, 50, 70, \text{ and } 100 \text{ mm}$).
Figure 4.17: Long-term stability of the (a) peak $I_{\rm on}$ of flexible devices and (b) $g_{\rm m}$ as a function of bending duration at various bending radii (R = 40, 50, 70, and 100 mm). All measurements were performed in the chitosan-based top-gated OECTs72
Figure 4.18: (a) Transfer characteristics and the associated transconductance of chitosan-based top-gated OECTs at different temperatures ranging from 30 to 75 $^{\circ}$ C (b) Corresponding maximum $g_{\rm m}$ value and $V_{\rm Th}$ as a function of the operating temperature.
Figure 4.19: (a) Schematic illustration of the degradation experiment. (b) Degradable behavior of the self-supporting OECTs in watered damp soil in 45 s (humidity: 67%, temperature: 30 ° C)
Figure 4.20: Effect of EG doping on the device performance. (a) Normalized $R_{sq}/R_{sq}(0)$ of the PEDOT: PSS film as a function of EG concentrations. (b) Transfer characteristics

and (c) associated transconductance of chitosan-based OECTs under different EG
concentrations as a function of gate voltage76
Figure 4.21: Effect of different weight percentages of LiClO ₄ on device performance.
FESEM images of LiClO ₄ with weight percentages of (a) 20 wt%, (b) 30 wt%, and (c)
40 wt%. (d) Transfer characteristics and (e) corresponding transconductance of
chitosan-based OECTs with different LiClO ₄ weight percentages as a function of gate
voltage. (f) I_{on} and g_m of the devices with different LiClO ₄ weight percentages78

LIST OF TABLES

Table 2.1: The advantages and drawbacks of diverse synaptic transistors
Table 2.2: Summary of material, synaptic function and application of new OECTs developed in recent years
Table 3.1: Designation of the PEDOT:PSS with different amounts of EG39
Table 3.2: Designation of the electrolytes with different type of polymers42
Table 3.3: Experimental conditions and facilities used for OECTs on Si wafer43
Table 3.4: Experimental conditions and facilities used of flexible OECTs46
Table 3.5: Specification of each facilities applied for OECTs measurement
Table 3.6: Experimental design for mechanical properties of OECTs50
Table 4.1: Average thickness of each layer of three types OECTs56
Table 4.2: Comparison of the electrical performances for recently reported OECTs 68
Table 4.3: Electrical properties of OECTs with different LiClO ₄ weight percentage 79

LIST OF SYMBOLS AND ABBREVIATIONS

For example:

AI : Artificial intelligence

IoT : Internet of things

CMOS : Conventional complementary-metal-oxide-semiconductor

ANNs : Artificial neural networks

OFET : Organic field effect transistor

OECT : Organic electrochemical transistor

EDL : Electric double-layer

 $V_{\rm G}$: Gate voltage

 $I_{\rm D}$: Drain current

G: Transconductance

g_m : Maximum transconductance

 I_{on} : On-state current

 $R_{\rm sq}$: Sheet resistance

L : Channel length

W: Chaneel width

D: Thickness

 $I_{\rm on}/I_{\rm off}$: On-off current ratio

 V_{Th} : Threshold voltage

T : Temperature

SS : Subthreshold swing

CVD : Chemical vapor deposition

EG : Ethylene glycol

FETs : Field-effect transistors

IPSC : Inhibitory postsynaptic current

IPSP : Inhibitory postsynaptic potential

MOSFET : Metal-oxide-semiconductor field-effect transistor

FGTs : Floating gate transistors

TENG : Triboelectric nanogenerator

PPF : Paired-pulse facilitation

PPD : Paired-pulse depression

STP : Short-term plasticity

LTP : Long-term plasticity (LTP)

STDP : Spike-timing-dependent plasticity

EPSC : Post-synaptic current

PPF : Paired pulse facilitation

PPD : Paired pulse depression

EGTs : Electrolyte-gate synaptic transistors

ANN : Artificial neural network

MNIST : Modified national institute of standards and technology

SM : Sensory memory

STM : Short-term memory

LTM : Long-term memory

FEGTs : Ferroelectric-gate synaptic transistors

SA : Slow adaptation

OSC : Organic semiconductor

IL : Ionic liquid

HOMO : Highest occupied molecular orbital

OPVs : Organic photovoltaic cells

ECG : Electrocardiographic

SSOECT : Solid-state OECT

EIS : Electrochemical impedance spectroscopy

FTIR : Fourier transform infrared spectroscopy

SCS : Semiconductor characterization system

FESEM : Emission scanning electron microscopy

SA : Slow adaptation

LOD : Limit of detection

UV : Ultraviolet

S : Source

D : Drain

PET : Poly(ethylene terephthalate)

PS-PEO-PS : Poly(styrene-block-ethylene-oxide-block-styrene)

PVDF-HFP : Poly(vinylidene fluoride-co-hexafluoropropylene)

PVPA-AA : Poly(vinylphosphonic acid-co-acrylic acid)

[EMIM][TFSI] : 1-ethyl-3-methylimidazolium bis(trifluoromethylsulfonyl) imide

[BMIM][PF6] : 1-butyl-3-methylimidazolium hexafluorophosphate

EG : Ethylene glycol

Na⁺ : Sodium

CNT : Carbon nanotube

IGZO : Indium-gallium-zinc oxide

ITO : Indium tin oxide

In₂O₃ : Indium oxide

HZO: $Hf_{0.5}Zr_{0.5}O_2$

PEDOT:PSS : Poly(3,4-ethylenedioxythiophene) polystyrene sulfonate

PPy : Polypyrrole

P3HT : Poly(3-hexylthiophene)

DMSO : Dimethyl sulfoxide

BBL : Poly(benzimid azobenzophenanthroline)

NaCl : Sodium chloride

KCl : Potassium chloride

PBS : Phosphate-buffered saline

DEME⁺ : Diethylmethyl(2-methoxyethyl)ammonium

EMIM⁺ : 1-ethyl-3- methylimidazolium

BMIM⁺ : 1-butyl-3-methylimidazolium

HMIM⁺ : 1-hexyl-3-methylimidazolium

TFSI : Bis(trifluoromethylsulfonyl)imide

FSI : Bis(fluorosulfonyl) imide

DCA : Dicyanamide

BF4 : Tetrafluoroborate

PEO : Poly (ethylene oxide)

PVA : Poly(vinyl alcohol)

PS-PEA-PS : Polystyrene-b-poly(ethyl acrylate)-b-polystyrene

PS-PMMA-PS : Poly(styrene-b-methyl methacrylate-b-styrene)

PVDF : Polyvinylidene fluoride

PSSH : Poly(styrene sulfonic acid)

PSSNa : Poly(styrene sulfonic acid sodium salt)

P(VPA-AA) : Poly[(vinyl phosphonic acid)-co-(acrylic acid)]

Si : Silicon

MC : Methylcellulose

Dex : Dextran

FS : Fish gelatin

CS : Chitosan

NH₄PF₆ : Ammonium Hexafluorophosphate

LiClO₄ : Lithium Perchlorate

Ag : Silver

LIST OF APPENDICES

APPENDIX A	95
APPENDIX B	96
APPENDIX C	97
APPENDIX D	98
APPENDIX E	99
APPENDIX F	100
APPENDIX G	101
APPENDIX H	
APPENDIX I	
APPENDIX J	
APPENDIX K	
APPENDIX L	107
APPENDIX M	108

CHAPTER 1: INTRODUCTION

1.1 Background of Research

With the emergence of artificial intelligence (AI) technology (Nguyen et al., 2022) and development of Internet of Things (IoT), conventional complementary-metal-oxide-semiconductor (CMOS) transistors, based on the von Neumann architecture, face limitations in processing bigger and more data due to their sequential data flow and high power consumption (Backus, 1978; Shim et al., 2019). Brain-inspired synaptic transistors have emerged as a promising alternative, as they can parallelly process information in one single device and exhibit cognitive functionalities (Lee et al., 2020), such as electrolyte-gated transistors, field effect transistors, nanoparticles transistors.

Artificial synaptic transistors, based on organic semiconductor materials, possessed substantial potential for the establishment of flexible devices (H. Wang et al., 2019; Wang et al., 2018). This is largely due to the compatibility of organic semiconductors with large-scale fabrication techniques such as ink-jet printing and coating, which are ideal for solution processing methods. Moreover, organic materials yield several advantages including the facilitation of ionic transport, the ability to modify functional groups, biodegradability, and the capacity to establish anaerobic interfaces with liquid electrolytes. Given these attributes, artificial neural networks (ANNs) utilizing organic synaptic transistors are poised to facilitate the development of flexible neural morphological systems capable of complex signal processing in future applications (Shao et al., 2021). In addition, some organic synaptic electronics can be decomposed in nature without causing pollution (Y. Yang, X. Zhao, C. Zhang, et al., 2020). Moreover, organic synaptic transistors can record action potentials from neurons and bridge the gap between biology and electronics because they are biocompatible.

As the representatives of organic synaptic transistors, organic field effect transistor (OFET) (Cramer et al., 2012) and organic electrochemical transistor (OECT) (Liang et al., 2020) have been investigated and applied for biochemical signal recording and transduction of bio-electrical signals from cells and tissues (Campana et al., 2014) due to their low power consumption and drain contact resistances. Both are designed with the characteristics of ionic conduction. The migration of ions builds an electric double-layer (EDL), which is used to mimic the synaptic functions. However, the ionic-electronic interaction occurs at the single electrolyte-semiconductor contact in OFETs. By contrast, OECTs enable EDL and electrochemical reactions two working processes, the ionic-electronic interaction includes the whole three-dimensional volume of the material channel for ion-permeable semiconductors. This operational mode endows OECTs with stronger EDL with less working voltage.

Therefore, OECTs, operating as electrolyte-gated synaptic transistors, hold the potential to mimic the computational principles of the human brain due to ion-modulation behaviors (Yang et al., 2017), offering advantages in various applications ranging from neuromorphic devices (Van De Burgt et al., 2017) to transducers for biological sensing such as detection of glucose (Rezali et al., 2022), ions, antibody-antigen interaction (Strakosas et al., 2015). Nevertheless, the state of the art OECTs are commonly made of silicon (Si) (Lai et al., 2019) or glass substrates (Kim et al., 2022), suffer from several drawbacks such as stiffness, poor bio-compatibility. In addition, most of the reported OECTs with inorganic materials are not environment-friendly, and even harmful or toxic, which are not biocompatible and cannot be applied to human tissues or skin (Mao et al., 2019). Since the electrolytes in the OECTs may be either liquid or solid-state (Yang et al., 2017), majority of liquid electrolytes are not suitable for large area preparation, compared to liquid electrolyte, solid ion electrolyte offers greater flexibility, reduced leakage, and a superior safety profile, a proper flexible

OECTs based solid electrolyte is highly desired (Lu et al., 2020). For these issues, this study is carried out to develop a flexible organic electrochemical transistor based on the solid-state organic polymer electrolyte to offer an alternative solution for neuromorphic computing against existing products. This dissertation introduces a simple but low-cost fabrication of OECTs by integrating organic semiconductor PEDOT:PSS, organic chitosan-based solid polymer electrolyte with flexible Poly(ethylene terephthalate) (PET) substrate by the simple screen printing and drop casting deposition techniques under low heating temperature ≤ 120 °C.

1.2 Problem Statement

Organic electrochemical transistors (OECTs) have garnered significant attention as promising candidates for next-generation neuromorphic devices (Menon et al., 2023; Pecqueur et al., 2018) and bioelectronics (Braendlein et al., 2017) due to their unique ionic-electronic coupling and high transconductance. However, the reliance on aqueous electrolytes in OECTs introduces substantial challenges, particularly in terms of fluidity, which needs protective layers to prevent channel swelling (Jo et al., 2020). This susceptibility to environmental factors such as humidity, temperature fluctuations, and oxidants compromises the long-term stability of OECTs. Additionally, for wearable electronic applications, such as glucose detection (Rezali et al., 2023) and cardiac signal recording (Park et al., 2018), OECTs must be flexible enough to adhere to biological surfaces. The presence of aqueous electrolytes limits the device's adaptability to curved and uneven surfaces (Tarabella et al., 2020), restricting its potential in flexible electronics. Moreover, ensuring stable operation across a wide range of temperatures, including extreme conditions, remains a crucial challenge. To address these limitations, there is a need for the development of solid-state electrolytes that can provide efficient ionic gating while maintaining mechanical flexibility and environmental stability.

1.3 Motivation

One promising approach to overcoming these limitations is the development of ionic gel-based solid-state electrolytes, composed of polymeric matrices and ionic liquids. These materials exhibit excellent solubility (Lee et al., 2011), mechanical flexibility (Dathbun et al., 2019), and stretchability (Jang et al., 2018), making them well-suited for wearable and flexible devices. Various polymer-ionic liquid combinations have been explored, including poly(styrene-block-ethylene-oxide-block-styrene) PS-PEO-PS (Cho, Lee, Xia, et al., 2008), poly(vinylidene fluoride-co-hexafluoropropylene) PVDF-HFP (Lee et al., 2012), poly(vinylphosphonic acid-co-acrylic acid) PVPA-AA (Yan et al., 2020). liquids 1-ethyl-3-methylimidazolium and ionic such bis(trifluoromethylsulfonyl) imide [EMIM][TFSI] (Cho, Lee, He, et al., 2008) and 1butyl-3-methylimidazolium hexafluorophosphate [BMIM][PF6] (Chae et al., 2016). While these ionic gels demonstrate promising properties, their complex synthesis, highcost copolymers, and potential toxicity of ionic liquids pose significant challenges to their widespread adoption.

To overcome these issues, natural biopolymers such as cellulose (Dai et al., 2018) and dextran (Y. Yang, X. Zhao, C. Zhang, et al., 2020) offer viable alternatives due to their ionic conduction capabilities, low cost, biocompatibility, and biodegradability. These materials have shown promise in reducing environmental impact (Li et al., 2020) and conserving non-renewable resources. However, challenges remain in the synthesis and processing of these biopolymer-based ionic gels. Cellulose-based gels require specific solvents and chemical modifications to enhance ionic conductivity, limiting their applicability in printed electronics (Jo et al., 2020). Dextran, despite its high hydrophilicity (Y. Yang, X. Zhao, S. Wang, et al., 2020) and ion transport efficiency, exhibits high viscosity, complicating the film formation process. While solid-state organic biopolymer electrolytes have been studied for energy applications like

supercapacitors (Aziz et al., 2022), their mechanical robustness and thermal stability in bioelectronics, particularly in OECTs, remain underexplored. Therefore, the development of a new class of solid-state organic polymer electrolytes that are non-volatile, biocompatible, and biodegradable is essential for advancing OECT technology, particularly for applications in wearable and flexible bioelectronics.

1.4 Aims and Objectives

The primary aim of this research is to propose and develop a new organic electrochemical transistor (OECT) that is both biodegradable and flexible. These innovative OECTs will utilize biopolymer electrolyte and organic channel composed of PEDOT:PSS, aligning with the growing need for environmentally friendly and sustainable electronic components. This development is anticipated to provide a meaningful guidance for organic synaptic electronics by introducing a viable alternative to conventional, hard electronic devices, and represents a remarkable advance toward developing natural biopolymers in the fabrication of bio-integrated devices. To achieve the overarching aim, this dissertation is structured around the following detailed sub-objectives:

- 1. To design and fabricate a biopolymer-based organic electrochemical transistors (OECTs) by exploring the various solid-state biopolymer electrolytes and organic semiconductor channels based on screen printing. To optimize OECT key performance metrics including on-state current, on/off current ratio, and transconductance, by tuning parameters such as biopolymer-based electrolyte compositions and salt concentrations as well as transistor configurations.
- 2. To assess the mechanical robustness and environmental stability of the flexible chitosan-based organic electrochemical transistors (OECTs) across different conditions, including bending cycles, long-term bending, and temperature

fluctuations to ensure their reliability for practical applications in bioelectronics and wearable electronics.

Traditional methods, such as photolithography for fabrication of OECTs require specialized equipment like spin coating, thermal evaporation, or chemical vapor deposition (CVD). These complicated techniques not only escalate the overall cost of OECTs but also hinder its potential for widespread adoption and use. Screen-printing method can be considered for OECTs, which making the fabrication process both costeffective and accessible. Progressing further, the electrical characteristics need to be meticulously tested across various configurations, exploring how structural and design changes affect performance. This critical analysis is aimed at revealing the fundamental operational mechanisms of OECTs, essential for enhancing their practical application. An integral part of the endeavor involves experimenting with different polymer electrolytes to boost the electrical performance of OECTs. By varying organic polymer types and adjusting electrolyte salt concentrations, the goal is to pinpoint the optimal mix for superior conductivity and functionality, pushing the boundaries of what these OECTs can achieve. The optimization continues by tweaking the channel material, specifically assessing how different ethylene glycol (EG) doping levels in PEDOT: PSS influence the device's electrical traits. This fine-tuning process not only seeks to improve conductivity but also aims at elevating the overall efficiency of the OECTs. In addition, this study also rigorously evaluates the OECTs for durability, focusing on their mechanical robustness, temperature stability, and resistance to degradation. This is crucial for their application in wearable and implantable technologies, ensuring the devices can endure real-world physical stresses and environmental conditions. Through the successful accomplishment of these objectives, this research aims to contribute significantly to the field of organic synaptic transistors, providing a sustainable, flexible, and efficient alternative to traditional electronic components. This work is expected to

pave the way for the next generation of eco-friendly electronic devices, with broad implications for biomedical engineering, wearable technology, and beyond.

1.5 Scope of Work

The aim of this study is to develop a flexible organic electrochemical transistor using the organic polymer blend materials as a solid-state polymer electrolyte and the PEDOT: PSS as the conducting channel.

The study involves architecture design and corresponding sample fabrication, as well as electrical performance evaluation and optimization. The entire fabrication process must be carried out using low-temperature deposition below 120 °C on a flexible PET substrate by utilizing screen or inkjet printing. To achieve long-term stability and desirable transconductance at a low operating voltage of 1 V, the electrical characteristics involve conducting transfer curve (I_D - V_G) and output curve (I_D - V_D) measurements across different OECT configurations. The configurations of OECTs cover a range of popular architectures from the top-gate, followed by bottom-gate and then to recently advanced side-gate.

Optimal architecture of OECTs are evaluated by integrating with various organic polymer electrolytes, such as the different electrolyte composition and salt concentration, the polymer electrolyte is varied to investigate their impact on the device's electrical properties. This comprehensive analysis enables the identification of the optimal electrolyte for achieving high-performance OECTs in neuromorphic computing. In addition, to further improve performance of OECTs, the conducting channel is optimized. It has been reported that the conductivity of PEDOT: PSS can be improved by addition of the ethylene glycol (EG) (Kim et al., 2011), the concentration of EG doping was investigated.

Considering their prospective use in wearable electronics, this study also thoroughly investigates the mechanical robustness, temperature stability, and biodegradability of chitosan-based organic electrochemical transistors (OECTs). These parameters are critical for ensuring the durability and environmental compatibility of the OECTs under the variable conditions which would encounter in real-world applications. Figure 1.1 shows the overview of the works involved in this study.

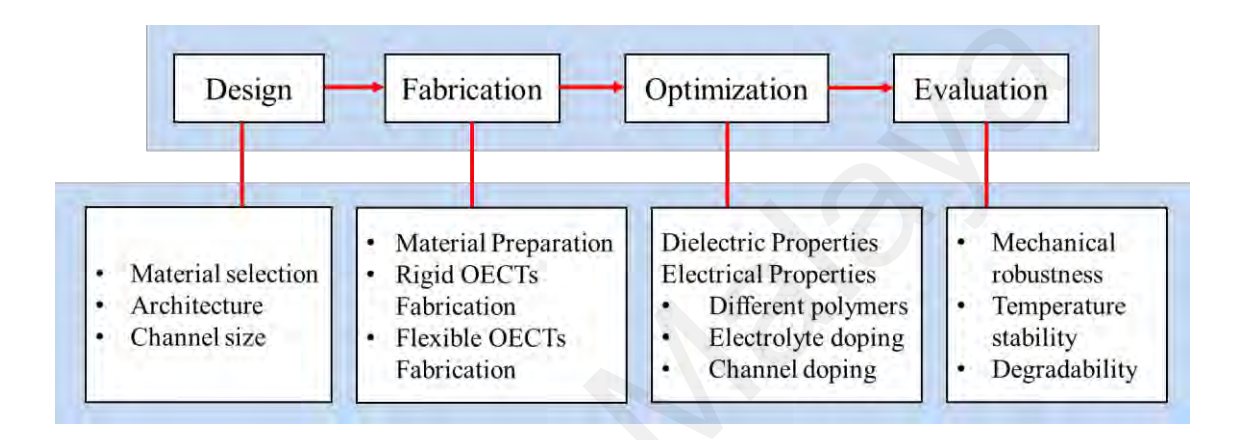


Figure 1.1: Diagram of overall works involved in this study

1.6 Dissertation Outline

This thesis is structured as follows:

Chapter 2 provides a depth literature review on the current research progress in the field of synaptic organic electrochemical transistors. A brief overview of both operation mechanism and synaptic behaviors of organic synaptic transistors are introduced. In addition, this chapter presents on the various material, popular architectures and advanced fabrication techniques specifically for solution-processed electrolyte-gated transistors.

Chapter 3 highlights a comprehensive overview of the experimental design and detailed procedures for fabricating and measuring chitosan-based OECTs based on PEDOT: PSS. The chapter begins with a detailed description of the overall project flow,

which includes a list of potential materials and architecture. It also presents a flowchart of the fabrication process and diagrams illustrating advanced fabrication techniques, as well as the characterization methods implemented in the OECTs. Additionally, this chapter details the methodologies used to measure the dielectric properties of the electrolyte and the electrical characteristics observed in this research. It also describes the mechanical analysis methods employed to achieve optimized performance in solution-processed OECTs.

Chapter 4 presents experimental findings to substantiate the feasibility of proposed flexible OECTs based on the solid-state organic polymer electrolytes. This chapter not only proposes the usage of solution processed, natural biopolymers in the hard OECTs based on silicon substrate, but also utilizes the experimental data of the hard OECTS and proposes the corresponding flexible substrate as well as the development of flexible OECTs. Moreover, this work investigates the electrical characteristics of a flexible OECTs based on solid-state biopolymer electrolyte and reveals the relationship between the OECTs performance characteristics, and the doping of electrolytes and channel. Additionally, this work investigates the mechanical characteristics of the flexible OECTs and biodegradability to imitate operation application a real-word scenario.

Chapter 5 comprises of summary and future work. This chapter concludes and discusses the possible future works for this field of research, and some suggestions are offered.

CHAPTER 2: LITERATURE REVIEW

2.1 Introduction

This chapter describes in detail on the fundamental aspects in artificial synaptic transistors based on OECTs. It starts with an overview of synaptic transistors, detailing the operation mechanisms and behaviors of bio-synapses. The reviews extend to artificial synaptic transistors, present a broader review of variations, specifically organic field-effect transistors (FETs) and organic electrochemical transistors (OECTs), and other technologies, contextualize their developments and applications. In addition, attention is then given to the impact of the electrical-double-layer (EDL) effect on device performance, a critical aspect for understanding the operational efficiency of these transistors. Besides, design strategies in OECT development are presented next, covering working principles, characteristics, architecture, active materials and electrolytes. This provides a comprehensive view of current capabilities and future directions in OECT technology. Furthermore, the reviews take into accounts the integration of OECTs in neuromorphic computing, emphasizing their potential to advance neuromorphic engineering and artificial intelligence systems.

2.2 Biological Synapse

With the increasing maturity of artificial intelligence (AI) and big data, the conventional von Neumann architecture computers suffer from low processing speed and excessive power consumption because of a physical bottleneck that results from the physical separation of memory and computation components (Backus, 1978; Shim et al., 2019) when processing large amounts of data. In contrast, the human brain's highly parallel and fault-tolerant neural network enables it to carry out complicated computations and memories at minimal energy consumption concurrently. Hence, the brain-like electronics are expected to point out a new direction of bioinspired electronics for the next-generation intelligent neurorobotics (Han et al., 2019).

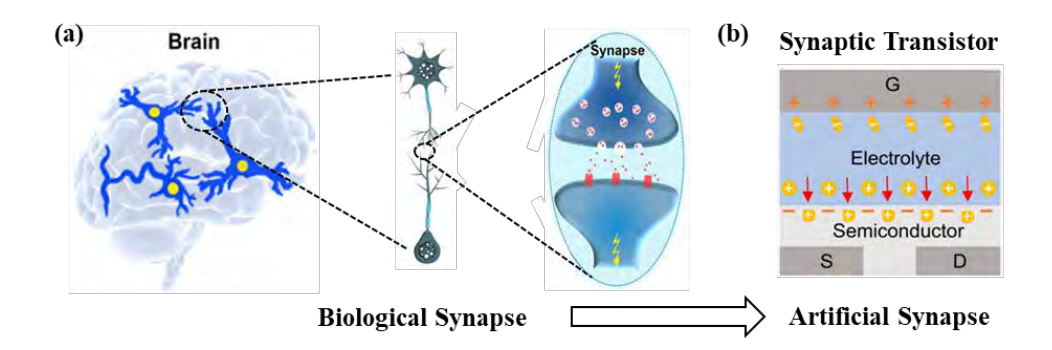


Figure 2.1: (a) Schematic illustration of neurons and synapse in human brain (Chen et al., 2019). (b) Typical artificial synapse based on OECTs

Human brain comprises of more than 10¹¹ neurons transmitted by 10¹⁵ synapses, which regulates motion, thinking, learning, and memory (Drachman, 2005). As fundamental components of the human nervous system, synapses modulate the strength of neuronal connections while concurrently storing and processing information. Figure 2.1 depicts a schematic diagram of a biological synapse, which primarily comprises the presynaptic terminal, the synaptic cleft, and the postsynaptic Neurotransmitters are released into the synaptic cleft in response to a neuronal signal that reaches the presynaptic terminal. Subsequently, some of these neurotransmitters bind to receptors on the postsynaptic terminal. Many of these receptors are coupled with ion channels, which are capable of allowing positively charged ions to pass into or out of the cell (Royer & Paré, 2003), as illustrated in Figure 2.1. Normally, the ion channel at excitatory synapses permits sodium (Na⁺) to enter the cell, producing an excitatory postsynaptic current/potential (EPSC/EPSP) (Takagi, 2000). This increases the possibility that the postsynaptic neuron will generate an action potential. Instead, at inhibitory synapses, an inhibitory postsynaptic current/potential (IPSC/IPSP) is generated, which tends to move the postsynaptic neuron away from the threshold required to generate an action potential. In this manner, when neuronal spikes reach the synapses, the connection between two neurons, also referred to as synaptic weight, is modified through synaptic plasticity (Smith et al., 2000). This adaptability is regarded

as the principal mechanism underlying the learning and memory functions in the brain (Markram et al., 2012).

2.3 Synaptic Transistors Based on Field-Effect Transistor

Since the concept of "neuromorphic electronic systems" was first proposed by Carver Mead in 1990 (Mead, 1990), various synaptic devices based on two-terminal and threeterminal structures have been developed to emulate the information processing functions of the human brain. Initially, two-terminal devices such as memristors (S. Wang et al., 2019) and phase-change memories (Tuma et al., 2016) were extensively explored for applications like image recognition and data classification, primarily due to their low power consumption and simplistic device architectures (Yang et al., 2021). More recently, three-terminal transistors have attracted considerable attention in the field of synaptic devices, overshadowing memristors because of their capabilities in parallel processing and memory functions. Field-effect transistors (FETs), as a typical one of three-terminal transistors, exhibit a structure remarkably similar to biological synapses. In these devices, the gate voltage (V_G) typically serves as the pre-synaptic input terminal, while the source-drain channel current (I_D) acts as the post-synaptic output terminal. The dielectric layer mimics the synaptic cleft and may consist of materials such as ionic electrolytes or ferroelectrics, paralleling the transmission of neurotransmitters from the pre-synapse to the post-synapse through carrier transportation. In recent years, innovative derivatives of FET structures, such as organic electrochemical transistors (OECTs) (Kim et al., 2022) and organic floating gate transistors (Zhang et al., 2017), have been introduced, effectively imitating the behavior of biological synapses. OECTs, for example, transmit signals through the movement of ions into the channel, akin to the mechanism used by the human brain for electrical signal transmission between synapses. Additionally, OECTs demonstrate high capacitance due to the formation of an electric double-layer effect (EDL) in the

electrolyte (Emelyanov et al., 2016), which enables the control voltage and response time (τ) of these transistors comparable to those of biological synapses (Figure 2.1 b). Moreover, given their biocompatibility and flexibility, OECTs have a broader range of applications, including in neural interfaces, brain-like chips, and artificial limbs, and others (Williamson et al., 2015). To better compare each of the new reported synaptic transistors, the devices developed in recent years, as well as their configurations, synaptic functions, and applications, are summarized in Table 2.1.

Table 2.1: The advantages and drawbacks of diverse synaptic transistors

Type	Configuration	Advantages	Drawbacks
FGTs	Floating gate	Non-volatile memory	Complex fabrication
		High density	Large operating voltage
EGTs	Top gate	Low operating voltage Flexible substrates	Electrolyte instability
FEGTs	Top gate	Non-volatile memory	Complex fabrication
		Fast switching	Large operation voltage
OECTs	Top gate Bottom gate	Low energy consumption	Material instability
		Biocompatibility	Longer operating time
		High transconductance	Longer operating time

In 1959, the first successful Metal-Oxide-Semiconductor Field-Effect Transistor (MOSFET) was fabricated by Kahng (Kahng, 1960) at Bell Labs, which is based on semiconductor materials and capable of modulating and amplifying electrical signals. Today, MOSFETs are widely used in both analog and digital circuits. The fundamental operating principle of ordinary FETs is the gate voltage (V_G), which may be used to control the current I_{SD} of the source (S) and drain (D). When the gate voltage is

removed, the carriers that have accumulated in the channel are immediately released (Li et al., 2022), demonstrating the volatile behavior of the FETs.

2.3.1 Floating-gate Synaptic Transistor

Due to the float gate (second gate) between the tunneling and blocking dielectric layers of floating gate transistors (FGTs), the floating-gate layer's conductivity is sufficient to draw in and hold onto the electrical charges. This sandwich structure enables to change the conductance of channel and further endows the FGTs with the ability to mimic artificial synapses. Recently, Wang et al. proposed a mechano-plastic synaptic transistor based on MoS₂, integrated with a triboelectric nanogenerator (TENG) to harness mechanical displacement for synaptic modulation (X. Yang et al., 2020). The semiconductor layers and floating-gate were constituted by monolayer MoS₂ and Au nanoparticles, respectively. Synaptic weights of artificial synapses were further regulated by triboelectric potential change with mechanical displacement, giving rise to synaptic mechano-plasticity (Figure 2.2). Au nanoparticles enhanced the charge trapping and retention, which successfully imitated synaptic behaviors such as the paired-pulse facilitation/depression (PPF/PPF). Nevertheless, it is worth noting that short-term plasticity (STP) and long-term plasticity (LTP) barely concurrently achieved because of the strong charge-retention ability of the floating gate layer on floating-gate synaptic transistor.

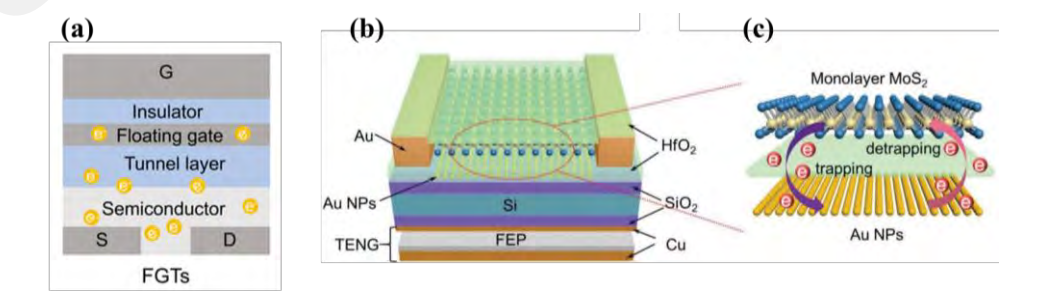


Figure 2.2: Schematic diagram of (a) The configuration of floating-gated transistor, (b) The mechano-plastic MoS₂ synaptic transistor and (c) Trapped/de-trapped of electrons by Au nanoparticles across HfO₂ tunneling layer (X. Yang et al., 2020)

Using an Au layer as a floating gate to regulate the charge storage, Kim et al. (2017) created a flexible synaptic transistor based on highly purified, pre-separated 99% semiconducting carbon nanotube (CNT) with changeable weight update linearity and variation margin (Figure 2.3). The channel conductance of the CNT semiconductor was modulated by charges stored at the Au floating gate, which was adjusted by applying gate voltage pulses, which adjust the weight update linearity and variation margin. The CNT-based transistors' altered channel conductance demonstrated synaptic excitatory and inhibitory properties, which correlate to the IPSC and EPSC processes. The study also incorporated a simplified spike-timing-dependent plasticity (STDP) scheme for simulating pattern recognition tasks. The incorporation of CNT transistors into a neuromorphic system that is flexible and paper-based demonstrated the possibility of future uses in flexible and disposable electronics.

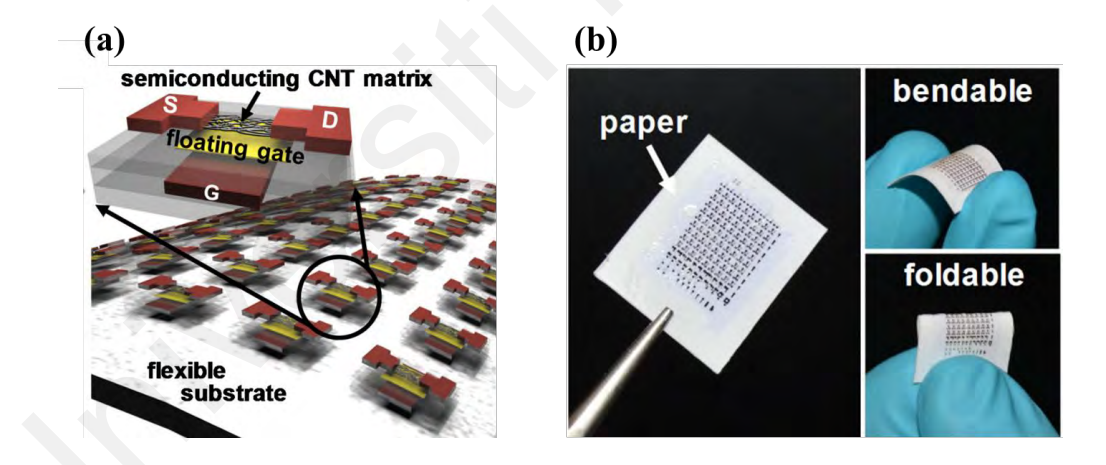


Figure 2.3: (a) Schematic of the flexible synaptic transistors based on semiconducting CNTs. (b) Image of the paper substrate being bent to accommodate the flexible CNT synaptic transistors (Kim et al., 2017)

Compared to conventional FETs, floating-gate transistors can easily capture charges through thermal emission and quantum tunneling, retaining them at the floating-gate layer for an extended period. This leads to changes in threshold voltage and subsequently alters the channel conductance. Hence, floating-gate synaptic transistors exhibit stable performance to simulate crucial synaptic behaviors including excitatory

post-synaptic current (EPSC), paired pulse facilitation (PPF), paired pulse depression (PPD), short-term plasticity (STP), long-term potentiation (LTP), and repeated learning processes.

2.3.2 Electrolyte-gate Synaptic Transistors

Electrolyte-gate synaptic transistors (EGTs) in artificial synapses have been intensively investigated own to low power consumption. EGTs were characterized by the electrolyte, which are ionic conduction and electronic insulation, applying a positive bias to the gate induces cations in electrolyte migrate towards the interface between the semiconductor and electrolyte, thus forming a double electric layer (EDL), this EDL effectively regulates the conductance of the channel. Hence, the synaptic function is implemented in an EDL by controlling carrier transport, as illustrated in Figure 2.4 (a).

Recently, a biocompatible electrolyte-gated synaptic transistors have been fabricated using indium-gallium-zinc oxide (IGZO) as semiconductor channel and a casein as organic electrolyte owing to the advantages of abundant, biodegradable, non-toxic, and capable of low-cost solution processing (Figure 2.4 (b)) (J. Sun et al., 2018). Anions and cations collected at the interfaces between the electrolyte and the channel when the V_G pulse was applied to the gate electrode. Short-term plasticity was attained by modulating the channel conductance and the holes that accumulated within it. Furthermore, the device also exhibited significant synaptic behaviors, including EPSC, PPF, STDP, and reliable potentiation and depression. Moreover, the performance of these synaptic transistors in simulating a three-layer artificial neural network (ANN) for handwritten digit recognition from the MNIST dataset achieved a high recognition rate of 90% as illustrated in Figure 2.4 (c). This indicates that the development of such casein electrolyte based synaptic transistor provides a biocompatible and environmentally friendly option for application in neuromorphic systems.

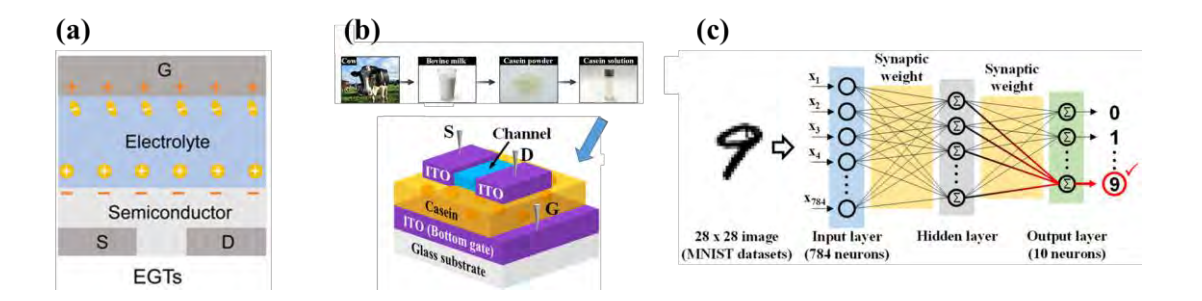


Figure 2.4: Schematics of (a) The configuration of electrolyte-gated transistor, (b) Casein electrolyte-based electric-double-layer (EDL) synaptic transistors on glass substrates, (c) A three-layer fully connected artificial neural network (ANN) for handwritten Modified National Institute of Standards and Technology (MNIST) recognition

Wearable "green" electronics, such as flexible organic transistors, are also a popular trend owing to their great compatibility with wrinkled surface of human skin and friendly to environment. Yu et al. (2018) have fabricated a flexible environmentally friendly synaptic device using solution-processed chitosan-based polysaccharide as the gate dielectric because of their excellent biocompatibility and biodegradability. On a flexible polyethylene terephthalate (PET) substrate, an electrolyte/indium tin oxide (ITO) film was used as an interfacial-modified layer to produce synaptic devices (Figure 2.5 (a)).

The transitions from sensory memory (SM) to short-term memory (STM) and from STM to long-term memory (LTM) were successfully mimicked, showing the device's ability to emulate complex memory behaviors. The electrical parameters of the device also remained quite stable after 500–1000 bending cycles, exhibiting good mechanical reliability (Figure 2.5 b). Furthermore, the synthetic synapses were easily dissolved in deionized (DI) water, suggesting possible uses for green neuromorphic devices.

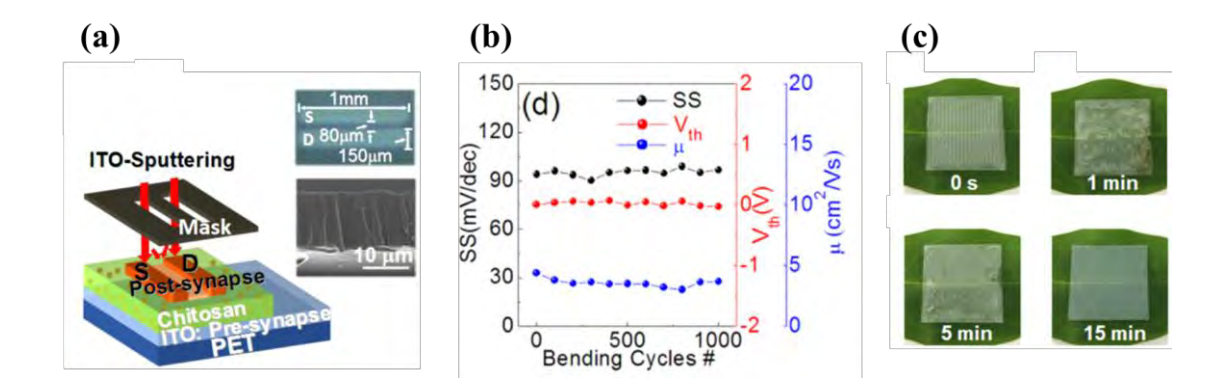


Figure 2.5: (a) Schematic diagrams of ITO synaptic transistor, (b) Extracted electrical parameters as a function of bending cycles. (c) Images of biodegradable ITO synaptic transistors (Yu et al., 2018)

In conclusion, the low-energy-consuming electrolyte-gated synaptic transistors mimic the basic properties of synapses. To enhance device performance, scalability, durability, and electrolyte instability should all be optimized.

2.3.3 Ferroelectric-gate Synaptic Transistors

Meanwhile, the ferroelectric-gate synaptic transistors (FEGTs) also have attracted increasing interest owing to the advantages of non-volatile polarization states, and high-speed operation. When applying voltage spike (V_G) on the gate electrode, the polarization state of the ferroelectric material is controlled subsequently, which further adjusted the channel conductance (Figure 2.6 (a)).

In 2023, Luo. et al. (2023) have illustrated a solution-processed indium oxide (In₂O₃) ferroelectric transistor gated by ferroelectric Hf_{0.5}Zr_{0.5}O₂ (HZO), as shown in Figure 2.6 (b). With a low energy consumption of 490 fJ per spike event, this device demonstrated good durability (>1000 cycles) with a large dynamic range $G_{\text{max}}/G_{\text{min}} = 32.2$, successfully simulating long-term potentiation/depression (LTP/D) up to 101 effective conductance states. Besides, the device achieved predominately high handwritten image recognition accuracy of 96.5% in simulation of artificial neural network (Figure 2.6 (c)).

This work revealed the feasibility of developing low-cost, high-performance, and energy-efficient FEGTs.

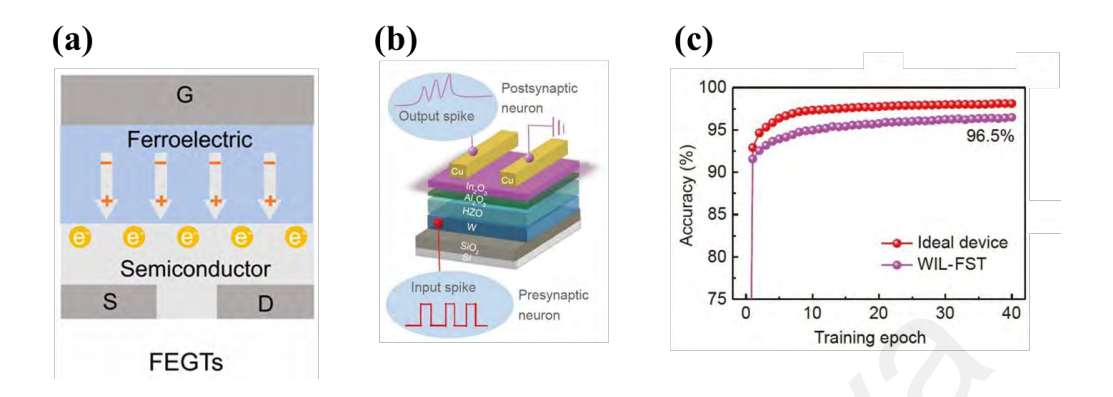
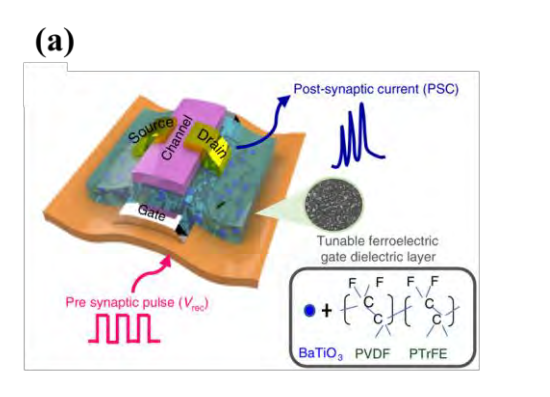


Figure 2.6: Schematic diagrams of (a) Configuration of ferroelectric-gated transistor and (b) In₂O₃ ferroelectric transistor to mimic the biological synapse, (c) The simulated recognition accuracy as a function of the training epoch for WIL-FST (Ferroelectric transistor with Al₂O₃ layer) (Luo et al., 2023)

Y. R. Lee et al. (2020) reported an artificial intrinsic-synaptic tactile sensory organ based on flexible ferroelectric-gate transistors, with the aid of BT NP (20 wt% BaTiO₃)/P(VDF-TrFE) nanocomposite as the organic ferroelectric gate dielectric and pentacene as organic semiconductor layer to imitate the structure and function of the human touch sensory organs (Figure 2.7 (a)). The tunability of synaptic weight and sensory memory functions were achieved by varying the compositions of BT NPs to P (VDF-TrFE). Moreover, a triboelectric-capacitive coupling phenomenon was used by the gadget to function. First, triboelectric charge transfer caused by touch stimulation causes the dipoles in the ferroelectric gate dielectric to align. These modifications then alter the channel conductance of the ferroelectric-gate transistor, which in turn alters the post-synaptic current (PSC). Hence, this process allows the device to mimic various synaptic functions, including slow adaptation (SA), filtering, and sensory memory. In addition, the device's ability to process tactile information in a self-energy transducing manner, combined with its mechanical flexibility, positioned it as a promising candidate for applications in intelligent soft electronic skins, neuro-robotics, and autonomous systems.



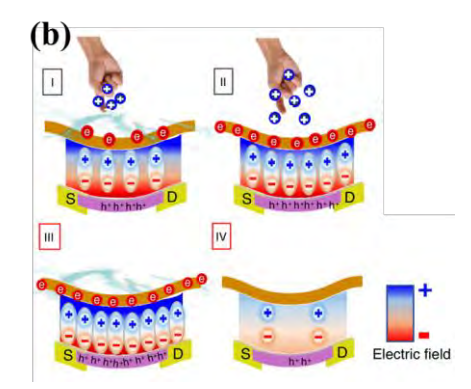


Figure 2.7: Schematic diagrams of (a) Tunable BT NPs/P(VDF-TrFE) ferroelectric gate dielectric layer-based synaptic transistor and (b) The working mechanism of artificial intrinsic-synaptic tactile sensory organ induced by tactile stimulation (Lee et al., 2020)

In the future, it will be necessary to lower the high operating voltage needed to switch the polarization state of ferroelectric materials, despite the fact that ferroelectric synaptic transistors exhibit excellent multidomain polarization for modulating multilevel channel conductance with a large on/off ratio and excellent multidomain structures.

2.4 Synaptic Transistor Based on Organic Electrochemical Transistor

In contrast to the conventional EGTs stated previously, on the basis of the double electron layer, OECTs also have the basic working process of electrochemical reaction. Electrochemical doping results from the electrolyte's ions diffusing into the semiconductor channel at high gate voltages and specific electrolyte concentrations. Similar to the method used by living things to transfer electrical messages across synapses, the ions that penetrate the majority of the channel during electrochemical doping alter the semiconductor's conductivity and channel shape. Hence, the formation of EDL and electrochemical doping endow OECT an efficient ion-to-electron transducer, as indicated in Figure 2.1 (b), which is capable of controlling voltage and response time (τ) of the OECTs comparable to that of the biological synapses. In addition, the simplicity of processing organic conjugated polymers and the ability to

modify their properties through chemical synthesis greatly aid in the development of OECTs. Those advancements allow OECTs to be flexible and biocompatible using low-cost manufacturing (e.g., printing techniques (Berggren et al., 2007)). Thus, numerous studies have demonstrated the possibility of OECTs in broad practical applications, including biological neural interfaces, biological and chemical sensors, biomolecule sensing, barrier tissues sensing, and recently COVID-19 detection.

2.4.1 Working Mechanism and Characterization of OECTs

As a typical organic 3-terminals transistors, OECTs was first developed and reported by Wrighton at el. (1984), where the P-type polymer semiconductor polypyrrole(PPy) was applied as electrolyte, the transistors worked well in the broad PH range (White et al., 1984). The structure of OECTs is comprised of electrodes (gate, source, and drain), electrolyte, and organic semiconductor (OSC), Normally, the current in OSC (I_D) can be affected by applying gate voltage (V_G), which change the carrier concentration between channel and electrolyte. The relation between I_D and V_G can be described by the transfer curve, and the transconductance (g_m) is extracted from the slope of the transfer curve:

$$g_m = \frac{\partial I_D}{\partial V_G}. (2.1)$$

where $g_{\rm m}$ is the most important parameter for characterizing the electrical performance of OECT. The higher $g_{\rm m}$ indicates that OECT has a better ability to amplify the gate signal into $I_{\rm D}$, consequently leading to better performance. The relationship between $I_{\rm D}$, $V_{\rm G}$ and $g_{\rm m}$ are illustrated in Figure 2.8 (a). According to Bernard model (Bernards & Malliaras, 2007), the $g_{\rm m}$ of OECT can be calculated as follows:

$$g_m = \frac{W}{I} \cdot \mu \cdot d \cdot C^* \cdot (V_{th} - V_G). \tag{2.2}$$

where W, and L represent the channel width and length, respectively, μ represents the carrier mobility, d is the channel thickness, C^* is the capacitance per unit volume of electrolyte, V_{Th} and V_{G} are the threshold voltage and the gate voltage, respectively.

Besides g_m , the response time (τ) is deemed as another crucial parameter for OECTs, which describes the time when the current in the device changes from 'OFF' to 'ON' as shown in Figure 2.8 (b). Normally, response time could achieve to microseconds, and under comparable circumstances, it is positively connected with the device's size, meaning that the larger the device, the slower the response. In contrast, it is inversely correlated with g_m . Additionally, according to Bernard's model, the total capacitance of the channel and the electrolyte resistance multiply to determine the τ of OECTs. Consequently, discovering materials with better volume permittivity and ion mobility under the constraint of fixed device size is expected to produce larger g_m and shorter τ , since only μ and C^* are connected to channel and electrolyte materials (Paterson et al., 2018).

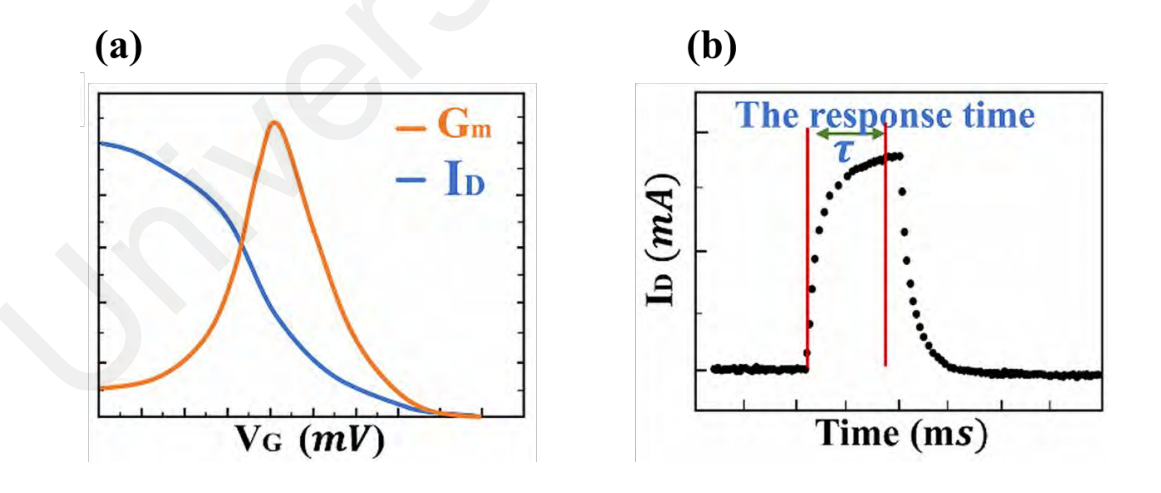


Figure 2.8: (a) The relationship between g_m and I_D as a function of V_G in the P-type OECT. (b) The response time required to change the state from 'OFF' to 'ON' (Paterson et al., 2018)

As aforementioned, the migration of ions in the electrolyte can lead to the EDL formation and electrochemical doping effect, both working mechanisms coupled

efficiently enhance the g_m of OECTs. In the light of the Stern model (Gongadze et al., 2011), the ions from electrolyte will form an EDL at the interfaces between the electrolyte and other materials. The Helmholtz plate is the plate that is right next to the interface. The diffuse layer, which is where the plate is weak on ions further from the interfaces, both Helmholtz and diffuse layers are important components of EDL (Figure 2.9 (a)). Meanwhile, EDL formed at interfaces can be seen as the parallel plate capacitors with high capacitance, which can easily manipulate I_D by inputting a small V_G , greatly saving power consumption (Lee et al., 2021). Under the effect of EDL, ions in electrolyte are easier to penetrate into the channel and react with OSC. When the energy level formed by those ions is lower than the highest occupied molecular orbital (HOMO) in OSC, the electrons can be trapped in the HOMO, which is equivalent to creating a hole and conducting electricity as shown in Figure 2.9 (b).

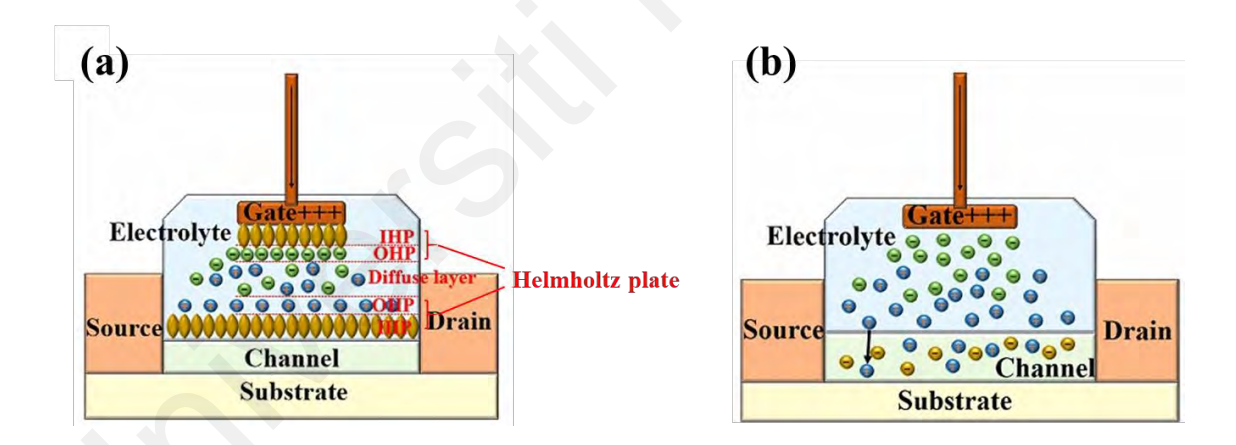


Figure 2.9: The schematic diagrams of (a) EDL formation and (b) electrochemical doping in OECT (Lee et al., 2021)

2.4.2 Structure of OECTs

According to the position of electrodes, OECT can be constructed via four different architectures as shown in Figure 2.10: Top-gate bottom-contact, bottom-gate top-contact, side-gate and extended-gate.

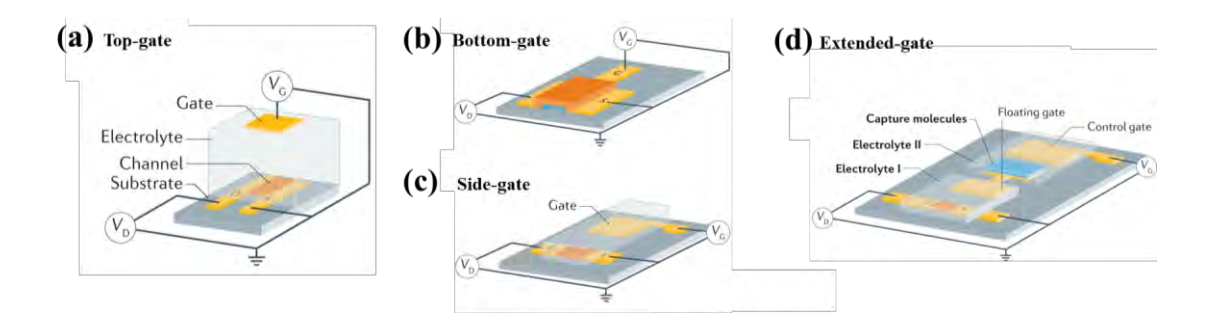


Figure 2.10: Figure 2.10: The schematic diagrams of (a) Top-gated structure, (b) Bottom-gated structure, (c) Side-gated structure and (d) Extended-gated structure (Torricelli et al., 2021)

The top-gate bottom-contact geometry is the most prevalent configuration in OECTs, where the gate electrode is positioned directly above the electrolyte. In this structure, the electrolyte, which can be a biological fluid, allows for the direct probing of chemical, biological, or ionic properties, making it predominantly utilized in electrophysiology studies. In contrast, the less common bottom-gate top-contact geometry features a solid electrolyte that insulates the gate electrode from the semiconductor channel. This configuration is especially useful for physiological recordings in which neural signals are recorded by placing a biocompatible semiconductor channel—like PEDOT:PSS directly in contact with human tissue (Cea et al., 2020). Another distinctive structure is the side-gated geometry, where the gate is located in the same plane as the semiconductor channel. In this design, the side gate functions as a global gate, biasing several nearby semiconductor channels simultaneously, which is typically employed in neuromorphic applications (Koutsouras et al., 2019). The fourth architecture is the floating-gate design, characterized by two separate electrolyte Sections (I and II) connected via a gold electrode with two pads, termed the floating gate. In this design, the control gate and the semiconductor channel are both capacitively connected to the floating gate via the electrolytes, a configuration commonly employed in biological or chemical sensing applications (White et al., 2018).

2.4.3 Material of OECTs

As introduced in Section 2.4.1, it indicates that the properties and functions of OECTs are closely correlated to material applied. So far, the electrode materials of OECTs mainly focus on Pt, Ag and Au. For further innovation on materials, the electrolyte materials and channel materials of OECTs are expected as a new breakthrough.

Channel: With the fast development of wearable electronics and biosensors, OSC materials have attracted more interest in the channel applied for OECTs. The conductive polymers are the most common channel materials, of which the commonly used for OECTs is p-type OSC, include poly(3,4-ethylenedioxythiophene) polystyrene sulfonate (PEDOT:PSS), polypyrrole(PPy), and Poly(3-hexylthiophene) (P3HT). Among these, PEDOT:PSS is particularly popular due to its high electrical conductivity, chemical stability, and insolubility in water. However, PEDOT:PSS has drawbacks, like the presence of PSS makes the device prone to reacting with environmental water, leading to corrosion, and the intrinsic low conductivity because of the ambiguous phase segregation. Several studies have addressed this issue by incorporating cross-linking agents or additives, for instance, doping with secondary solvents of ethylene glycol (EG) (Kim et al., 2011), dimethyl sulfoxide (DMSO) (Nagata et al., 2015), and glycerol (Palumbiny et al., 2014) et al. Compared to the P-type channel materials, there are very few studies on OECTs based on N-type materials at present due to the low charge carrier mobilities and instability. (H. Sun et al., 2018) depicted poly(benzimid azobenzophenanthroline) (BBL) as an n-type conjugated polymer for OECTs, the device exhibited a high amplification but very slow switching speed with respect to ptype materials. In future, the design of n-type materials for OECTs should concentrate on the enhancement of ion movement in the film that providing high electronic mobility. Table 2.1 compiles major OSC materials used in channel of OECTs in recent years.

Electrolyte: Electrolyte is another crucial factor for realization of the high performance OECTs, ionic conductors but electrical insulators make up electrolyte. Electrolyte materials for OECTs can be liquids, gels, or solids, in contrast to standard gate dielectrics for FETs, which are solids like silicon dioxide. Based on the compositions and physical states, electrolytes for OECTs can be generally classified into five different types (Figure 2.11): aqueous salt electrolytes, ionic liquid (IL) electrolytes, polymer electrolytes, ion gel electrolytes and polyelectrolytes.

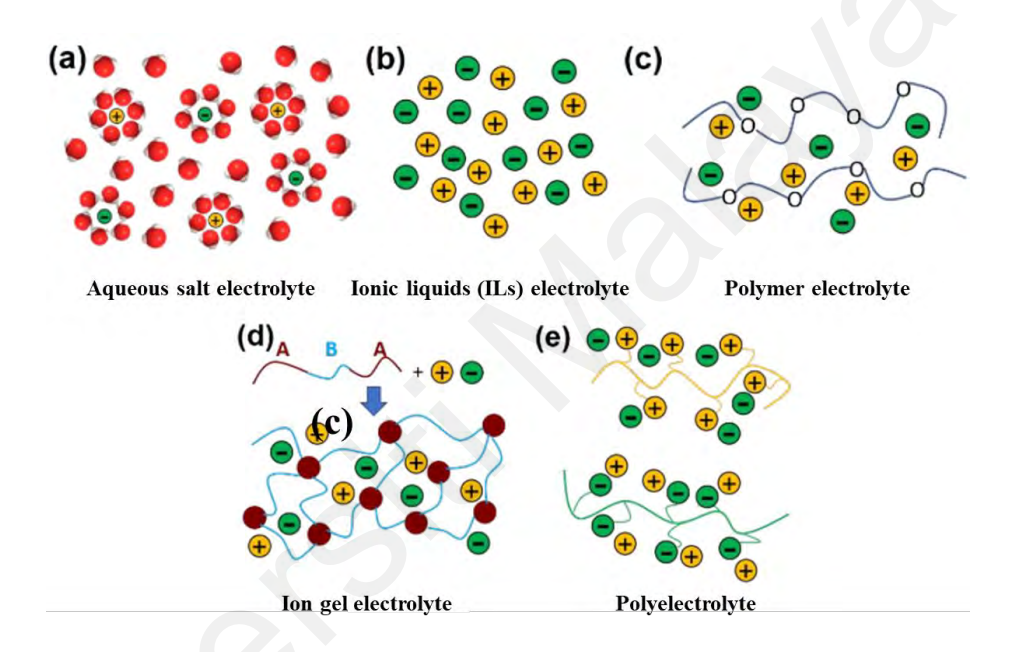


Figure 2.11: Illustrations of (a) Aqueous salt electrolyte, where the first solvation shells of both cations and anions are showed, (b) Ionic liquids (ILs) electrolyte, which contain pure cations and anions, (c) Polymer electrolytes, where the polyethylene oxide-like polymer chains align with the salt cations and anions, (d)

Ion gel electrolytes based on an ABA triblock copolymer and IL, (e)
Polyelectrolytes, where the bottom one is based on the polymerization of anions (polyanion), while the higher one is based on the polymerization of cations (polycation) (Huang et al., 2021)

The simplest electrolyte material is the aqueous salt electrolyte, such as sodium chloride (NaCl), potassium chloride (KCl) aqueous solutions and phosphate-buffered saline (PBS) solutions. Although aqueous salt electrolyte has been mostly adopted in several applications, it leaks easily, especially under deformations, which is challenging to be controlled in many small size electronics. Meanwhile, the ionic liquid electrolyte

is a good alternative, where salt is in the liquid phase at room temperature. Compared to aqueous electrolyte especially when bio-compatibility is not required, ionic liquid electrolyte is typically preferred due to the larger electrochemical window, the merits of low melting point and high boiling point. For ionic liquid electrolytes, the most common cations include diethylmethyl(2-methoxyethyl)ammonium (DEME⁺), 1-ethyl-3- methylimidazolium (EMIM⁺), 1-butyl-3-methylimidazolium (BMIM⁺) and 1-hexyl-3-methylimidazolium $(HMIM^{+})$ While and others. the anions are bis(trifluoromethylsulfonyl)imide bis(fluorosulfonyl) (TFSI-), imide (FSI⁻), dicyanamide (DCA⁻), tetrafluoroborate (BF4⁻) and others.

As both aqueous salt electrolyte and ionic liquid electrolyte leak easily, gel-type electrolyte has been developed to mitigate such issues. It has great advantages in future generation of flexible, printable, or wearable OECTs. As typical one of gel-type electrolyte, polymer electrolytes are created by dissolving salts in an ion-coordinating polymers, with the most extensively researched polymers including poly (ethylene oxide) (PEO) and poly(vinyl alcohol) (PVA) (Singaraju et al., 2019). It is important to note that while most salts used in liquid electrolytes can also be utilized in polymer electrolytes, lithium perchlorate (LiClO₄) is the most commonly used. Furthermore, ionic gel electrolytes are typically composed of an ionic liquid dissolved into a polymer network, achieved by crosslinking the polymer with acetone, which transforms the blended solution into a colloidal substance. Several copolymers have been investigated for the usage in ionic gel electrolytes, including polystyrene-b-poly(ethyl acrylate)-bpolystyrene (PS-PEA-PS) (Zare Bidoky et al., 2018), poly(styrene-b-methyl methacrylate-b-styrene) (PS-PMMA-PS) (Lee et al., 2018), and polyvinylidene fluoride (PVDF) (Lee et al., 2018). Due to the high dielectric constant of the polymer component and the formation of the EDL, these ionic gel electrolytes achieve high capacitance and efficient polarization. Finally, polymers containing repeating units that bear an ionic or ionizable group are classified as polyelectrolytes. Representative polyelectrolytes employed in OECTs include poly(styrene sulfonic acid) (PSSH), which utilizes H⁺ as a counterion (Sinno et al., 2013); poly(styrene sulfonic acid sodium salt) (PSSNa), featuring Na⁺ as a counterion (Du et al., 2018); and poly[(vinyl phosphonic acid)-co-(acrylic acid)] [P(VPA-AA)], also with H⁺ as a counterion (Zhao et al., 2017). Additionally, certain natural polymer derivatives are prevalent as polyelectrolytes in OECTs, including chitosan (Min & Cho, 2020), carboxymethyl cellulose (Dai et al., 2018) and dextran (Y. Yang, X. Zhao, C. Zhang, et al., 2020).

Owing to their tunable viscosity, gel-type electrolytes offer superior adaptability compared to the liquid state electrolytes, enhancing their suitability for flexible and biocompatible electronics. These properties facilitate the employment of various processing techniques, such as inkjet printing and spin-coating, making gel-type electrolytes particularly advantageous for advanced electronic applications.

2.4.4 Application of OECTs

In recent years, OECT-based devices have expanded beyond simulating biological synaptic behavior and have found wide applications in sensing, wearable electronics, and artificial nervous systems. This is attributed to their high transconductance, low driving voltage, low power consumption, and high flexibility. The latest advancements in OECTs within these application areas are introduced below.

Biological and Chemical Sensors: In these sensing applications, chemical or biological signals are converted into electrical outputs of the OECTs through chemical reactions or biological recognition (Marquez et al., 2020). To date, flexible OECT-based sensors have been applied in various fields, including health monitoring, environmental science, and medical applications.

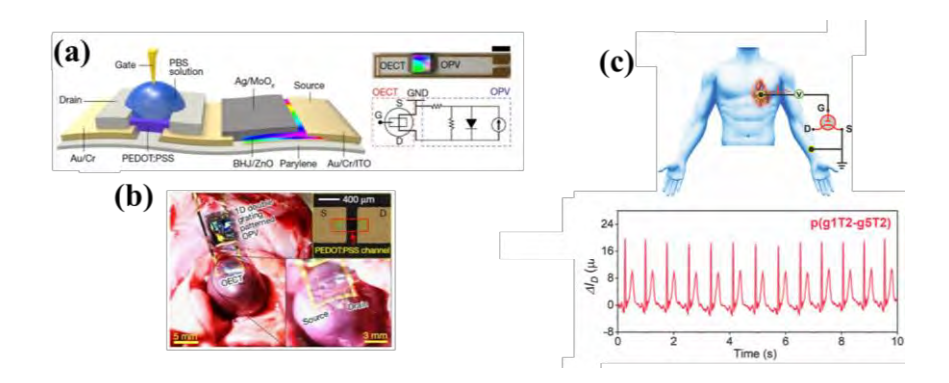


Figure 2.12: (a) Schematic of an OPV integrated with an OECT, with the associated circuit schematic and a picture of the combined device. (b) Photograph of the self-powered integrated device mounted to the rat heart (Park et al., 2018). (c) Schematic of the ECG monitoring and signals acquired by SSOECT based on p(g1T2-g5T2)

In the field of biological sensors, Park et al. (2018) have successfully developed a self-powered flexible electronic device that combined flexible organic photovoltaic cells (OPVs) with OECTs. This device can adhere to stretchable and wrinkled biological tissues to measure biometric signals (Figure 2.12 (a)). The device was installed on the open surface of a rat's heart, with PEDOT:PSS acting as the channel material and the bodily fluid on the surface acting as the electrolyte. The gate bias, or potential difference, between the OECT channel and the rat heart's bodily fluid affected the PEDOT:PSS channel's conductance (Figure 2.12 (b)). Consequently, when the rat heart's electrocardiogram (ECG) signals were recorded under LED lighting, they revealed robust ECG signals with an amplitude of 2.96 µA and a standard deviation of 25.2 nA, translating into a signal-to-noise ratio of 40.02 dB. Furthermore, Wu et al. (2023) have designed a solid-state OECT (SSOECT) for the detection of low-amplitude physiological signals. In this design, one electrode of the SSOECT was attached to the left forearm and connected to the source electrode, acting as a ground for measurement, while the other electrode was attached to the chest and connected to the gate electrode. The potential generated by cardiac activity was transmitted as a current signal through the SSOECT (Figure 2.12 (c)). The p(g1T2-g5T2) SSOECT produced high-quality

ECG results because the waveform morphology of the signals matched the usual electrical activity of the human heart.

Meanwhile, in the field of chemical sensing, OECT-based sensors are employed to detect chemical molecules, ions, and medicine. Ions such as H⁺, Na⁺, and Ca²⁺ in human body fluids are strongly correlated with health. Keene et al. (2019) have introduced a wearable patch-type OECT-based ion sensor designed to monitor physiological levels of NH⁴⁺ and Ca²⁺ ions in sweat. The device was attached to the forearm of each volunteer using a wearable patch, and changes in NH⁴⁺ and Ca²⁺ concentrations were measured during physical exercise (Figure 2.13 (a)). These findings show that wearable ion sensors are a useful tool for real-time analysis on human beings as well as ex-situ observations.

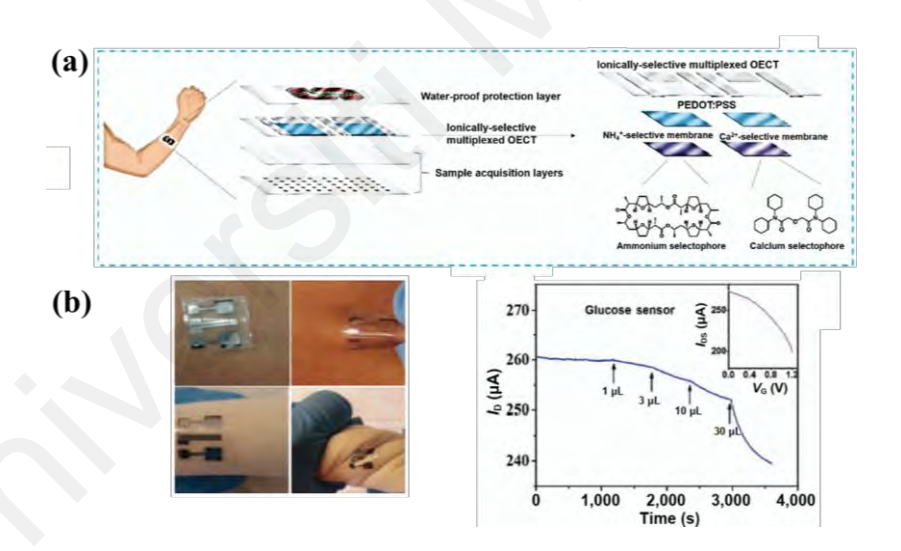


Figure 2.13: (a) Schematic components in the wearable OECT patch for multiplexed sensing of Al³⁺ and Ca²⁺ ions (Keene et al., 2019). (b) Photograph of flexible OECTs attached on different deformable surfaces and I_D response curve of the OECT to saliva under different volumes

Moreover, OECTs can also be utilized as medical sensors, providing an accurate, convenient, and non-invasive approach for rapid clinical diagnosis and therapy. For instance, monitoring serum glucose concentration is crucial for managing diabetes and reducing patient risk. (Liao et al., 2015) have designed a flexible OECT on a PET

substrate to detect glucose levels in saliva. The gate electrode of this OECT was further modified with glucose oxidase (GO_x) and graphene oxide (GO) to enhance enzyme immobilization. As a result, the OECT-based sensor exhibited a limit of detection (LOD) of 30 nM for glucose and demonstrated stable performance when attached to various surfaces (Figure 2.13 (b)). This design highlights the potential of the device for non-invasive detection of analytes in the human body.

Wearable Electronics: Recently, the wearable devices and electronic skin (e-skin) devices have garnered significant interest due to advancements in flexible materials. For instance, Trung et al. (2016) have integrated temperature sensing with flexible wearable devices to design a wearable temperature detection device. This design employed a transparent, stretchable gated sensor array that was highly responsive to the temperature of human skin (Figure 2.14 (a)). Based on this study, smart clothing that can automatically detect and control body surface temperature in real-time can be envisioned.

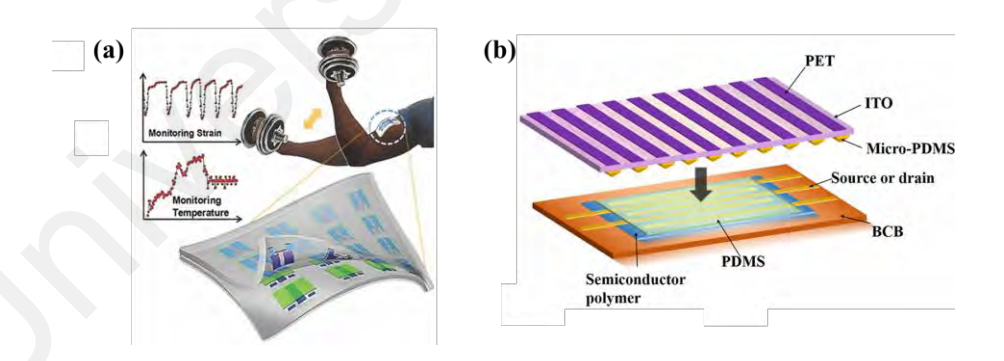


Figure 2.14: Schematics of (a) The transparent stretchable sensor array for temperature measurement on skin (Trung et al., 2016), (b) A flexible pressure sensor based on OECTs (Schwartz et al., 2013)

Furthermore, Schwartz et al. (2013) have developed a wearable pulse-detecting device based on a flexible pressure sensor with a sensing pressure of approximately 0.55 kPa and a short response time. The device was composed of several superimposed layers. The semiconductor polymer and source-drain electrode were in the first layer,

and the gate and a small electrolyte layer were located in the second layer (Figure 2.14 (b)). When pressure was applied to the device, it caused changes in the capacitance of the compressible electrolyte layer, thus altering the channel current. The author utilized this device to monitor pulse waves in human arteries, demonstrating its potential for real-time cardiovascular monitoring.

Human Nervous System: It is notable that the simulating functionalities of the human nervous system is another top research topic such as tactile senses, hearing and neuromorphic computing. In prosthetic design, an artificial tactile system achieves skinlike functioning, Kim et al. (2018) recently have demonstrated an artificial tactile system based on OECTs that actuated the legs of cockroaches, and a violent vibration observed. The system consisted of resistive pressure sensors, organic ring oscillators, and synaptic transistors. The pressure signal was converted into an electrical signal by the ring oscillators, which acted as nerve fiber to convert external tactile stimuli into voltage pulses. Next, postsynaptic potentials were then formed by activating the synaptic transistor (Figure 2. 15 (a)). Along this line, this tactile sensing system could be applied to actuation of the tibial extensor muscle in a detached cockroach leg (Figure 2.15 (b)). Inspired by this concept, such system can also be used to detect object shape and motion, as well as to distinguish braille characters.

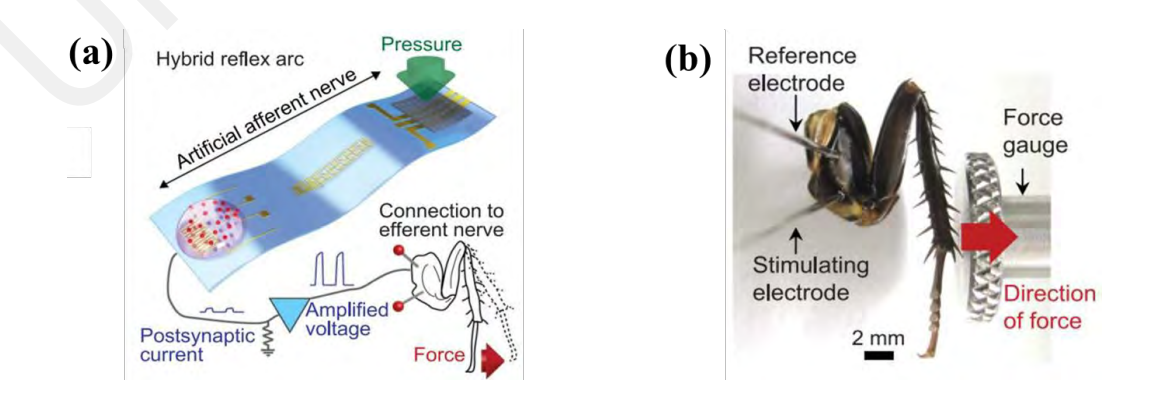


Figure 2.15: (a) Schematic of artificial tactile system made up by an artificial afferent nerve and a biological efferent nerve. (b) Photograph of action measurement of cockroach leg (Kim et al., 2018)

Besides, human auditory functions have also been successfully replicated. Wan et al. (2018) have designed a simplified artificial neural network to emulate the human brain's sound localization capability. The system comprised two gate electrodes and two sets of source/drain terminals, which were considered as pre-synapses (PREN1 and PREN2) and post-synapses (POSTN1 and POSTN2), respectively (Figure 2.16). The interaural time difference, which reflects the different distances between the ears and the sound source, was represented by the interval between the two stimuli. Consequently, the ratio of the amplitudes of the two post-synaptic currents can be directly correlated with the azimuth angle. This multi-terminal synaptic transistor design effectively simulated the brain's sound localization function.

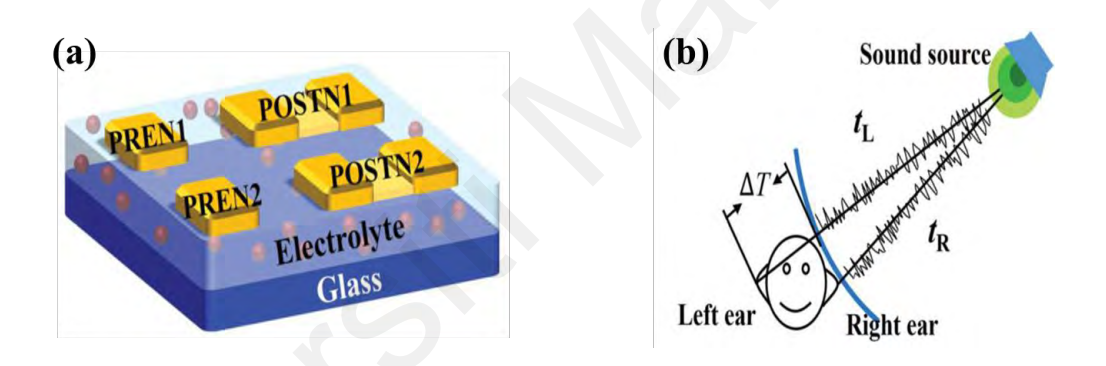


Figure 2.16: Schematics of (a) Sound location using a neuro-transistor-based artificial neural network, (b) Sound location by the human brain binaural effect (Wan et al., 2018)

2.5 Summary

In this chapter, the development of state-of-the-art transistor-based artificial synapse were systematically discussed. The synaptic functions of the biological synapse, and different artificial synaptic transistors were introduced. As the core components of synaptic transistor, the selection of materials are fundamental elements for the realization of synaptic functions. Moreover, the strengths and weaknesses of these four types of transistors are listed in Table 2.2.

Based on the statement mentioned above, OECTs based on solid-state biopolymer electrolytes will be selected and explored in this research due to the high transconductance, low-power operation, and bulk ionic doping, which enables superior synaptic plasticity. The solid-state biopolymer electrolyte enhances ionic mobility, stability, and biodegradability, addressing the limitations of liquid and synthetic electrolytes. PEDOT:PSS, with its mixed ionic-electronic conduction, ensures strong electrolyte coupling, flexibility, and efficient low-voltage operation. This combination is expected to offer a scalable, stable, and energy-efficient neuromorphic transistor, ideal for bioelectronics and AI-driven applications.

Table 2.2: Summary of material, synaptic function and application of new OECTs developed in recent years

Channel	Electrolyte	Synaptic function	Application	Refs
PEDOT:PSS and PSSNa	NaCl	PPD	Dynamic filtering	(Yamamoto & Malliaras, 2020)
PEDOT:PSS	Hydrogel	PPD, STP, LTP	Cold resistant devices	(Han et al., 2021)
PEDOT:PSS	Ion gel	IPSC, PPD	1	(Yan et al., 2020)
PEDOT:PSS	Chitosan	/	EEG physiologic signal acquisition	(Spyropoulos et al., 2019)
PEDOT:PSS/[EMIM][CI]	Ion gel	/	1	(Chen et al., 2020)
РЗНТ	[EMI][TFSA]and P(VDF-TrFE)	PPF	Neural network	(Kong et al., 2017)
РЗНТ	[EMI][TFSA]and P(VDF-HFP)	PPF, STDP	Multi-terminal flexible neural network	(Fu et al., 2018)
РЗНТ	[Li][TFSI]and polymer	PPD	Biosensors and digital logic	(Yan et al., 2020)
P(g1T2-g5T2)	PVDF-co-HFP/ EMIM BF ₄	1	Electrocardiography (ECG) signals detection	(Wu et al., 2023)
BBL	NaCl	1	Electrochemical complementary inverters	(H. Sun et al., 2018)
DNTT	Dextran	EPSC, STP, LTP	Biodegradable organic electronics	(Y. Yang, X. Zhao, C. Zhang, et al., 2020)
IGZO	Casein	EPSC, PPF, STDP	Handwritten pattern recognition	(Kim et al., 2022)

Inhibitory postsynaptic current: IPSC; Poly (4-styrenesulfonic acid-co-maleic acid) sodium salt: PSSNa; (Poly(benzimidazobenzophenanthroline)): BBL; Indium-gallium-zinc oxide: IGZO.

CHAPTER 3: RESEARCH METHODOLOGY

3.1 Introduction

This chapter outlines the design and fabrication processes employed to characterize two types of OECTs, based on different substrates, as well as methods for analyzing and optimizing device performance (Figure 3.1). The devices include rigid OECTs on silicon wafers and advanced flexible OECTs on PET substrates, both designed using SolidWorks, with various configurations explored. For fabrication, techniques such as screen printing, spin coating, and drop casting are employed, selected based on their suitability for specific material properties and the achievement of desired layer uniformity and thickness. The dielectric and chemical properties of the electrolyte are analyzed using the electrochemical impedance spectroscopy (EIS) and the Fourier transform infrared spectroscopy (FTIR), while electrical properties are assessed through current-voltage (I-V) and transconductance analyses. The mechanical properties of the devices are tested under bending and various temperature conditions, particularly for flexible OECTs, to ensure durability and operational reliability. Additionally, the biodegradability of the devices is examined. This research systematically explores the electrical, mechanical, and environmental performance of OECTs, supporting the optimization of device configurations and polymer choices, including adjustments in electrolyte composition and channel doping to enhance overall device functionality.

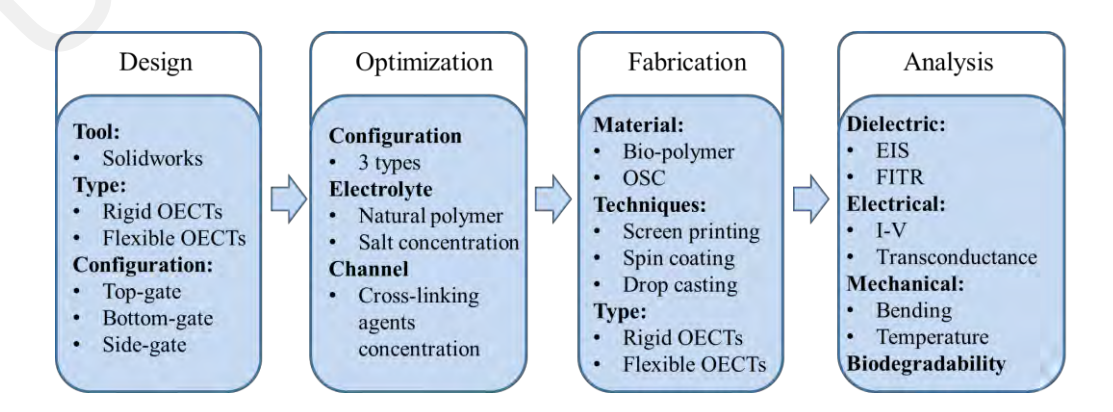


Figure 3.1: Research method for the development and analysis of flexible OECTs.

3.2 Flow Chart of Overall Project Methodology

The work structure for this research can be segmented into five key steps as shown in the flowchart in Figure 3.2. The first step is the identification of design specifications for the OECT which includes determining the appropriate design architecture, materials, fabrication techniques, and fabrication process. Secondly, it involves selecting the device structure and experimental conditions for fabrication. The specific configuration of the OECT has to be resolved, such as the choice of rigid substrate based on Silicon (Si) and flexible substrate based on polyethylene terephthalate (PET). Experimental conditions, including temperature and fabrication techniques, are carefully chosen based on the selected materials to optimize device performance. Thirdly, it revolves around the fabrication of OECTs using the chosen design specifications and experimental conditions. The fabrication process is carried out at low temperatures to ensure compatibility with organic materials. Depending on the selected materials, adjustments in temperature and manufacturing processes may be made to achieve the desired device characteristics. Additionally, depending on the chosen substrate, OECTs can be fabricated using either a rigid Si substrate or a flexible PET substrate. The fabrication process involves depositing the organic semiconductor and other necessary layers, as well as incorporating different organic polymer electrolytes to enhance device performance and functionality. Once the fabrication is complete, the fourth step involves the electrical and mechanical performance analysis of the fabricated OECTs. Electrical characterization involves measuring key parameters such as I-V characteristics, transconductance (g_m) , and threshold voltage (V_{Th}) stability. Mechanical analysis focuses on evaluating the bending robustness, and stability of the device under a broad range of temperatures, especially in the case of devices fabricated on flexible PET. Finally, the optimization of the OECTs involves enhancing the device's electrical performance by modifying the material composition in the electrolyte and organic

semiconductor, which serves as the foundation for further synapse function simulation.

Additionally, the degradation characteristic of OECTs is tested by exposing the devices to simulated natural environmental conditions.

In summary, the research workflow for OECTs involves identifying design specifications, selecting device structures and experimental conditions, fabricating the devices, analyzing their electrical and mechanical performance, and optimization. This systematic approach allows researchers to explore the potential of OECTs based on natural polymer for various applications in the field of flexible organic electronics and neuromorphic computing.

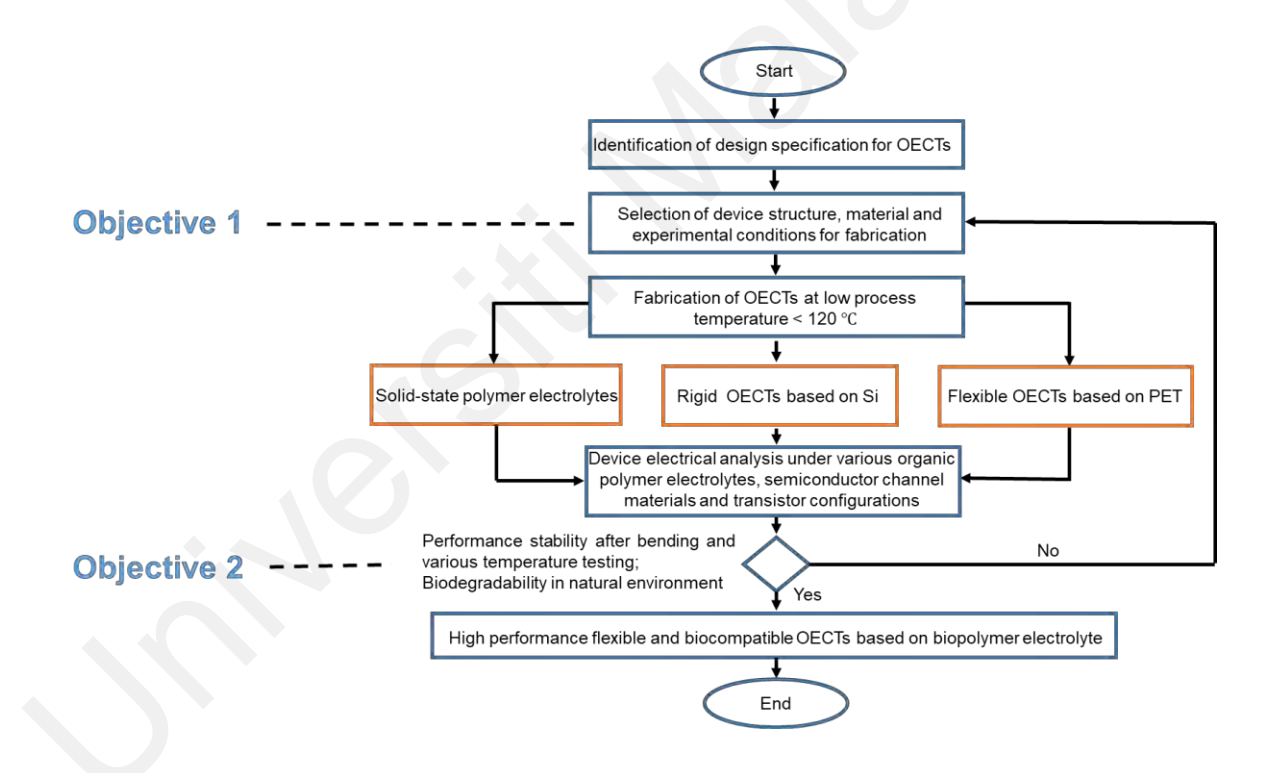


Figure 3.2: General overview of the research workflow

3.3 Experimental Section

In this section, the synthesis, fabrication, and characterization of OECTs based on different polymer electrolytes and PEDOT:PSS channel modifications are described. PEDOT:PSS is modified with different ethylene glycol (EG) concentrations to study conductivity effects. Various biopolymer electrolytes were formulated to optimize ion

transport. OECTs are fabricated on both rigid Si wafers (for controlled electrolyte comparison) and flexible PET substrates (for mechanical flexibility). Different device architectures are used to evaluate performance. Finally, material and electrical characterizations are conducted to assess film properties, conductivity, and device stability.

3.3.1 Organic Semiconductor Synthesis

PEDOT:PSS: The aqueous poly(3,4-ethylenedioxythiophene) polystyrene sulfonate (PEDOT:PSS, PH1000) was purchased from Ossila Ltd., Sheffield, UK. Based on previous studies (Ahmad et al., 2021) and experimental validation to enhance the conductivity of PEDOT:PSS while maintaining film stability, to test the effect of different conductivities of the PEDOT:PSS film, the PEDOT:PSS solution was added with different concentrations of ethylene glycol (EG) (2, 3, 4, 5, and 6 vol%), which is obtained from Sigma Aldrich. The PEDOT:PSS solution was stirred for 3 h and filtered by a 0.45 μm PTFE filter to eliminate impurity before being used to fabricate the channel layer of the OECTs, as depicted in Figure 3.3.

Table 3.1: Designation of the PEDOT:PSS with different amounts of EG

Material	Concentration of EG (vol%)				
PEDOT:PSS	20/	20/	40/	50/	<i>(</i> 0/
(PH1000)	2%	3%	4%	5%	6%

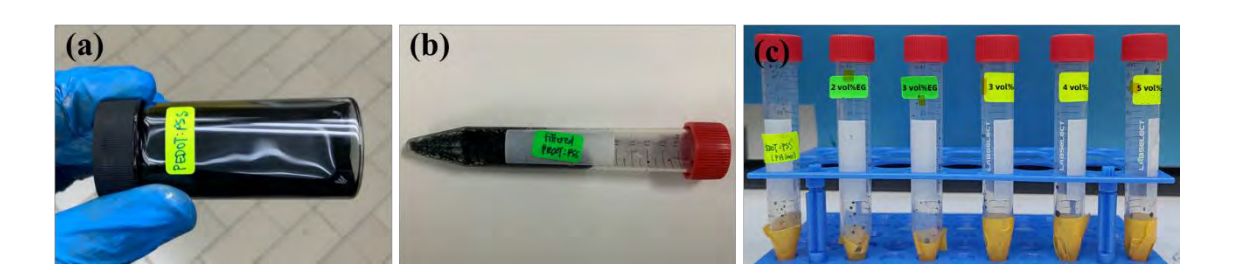


Figure 3.3: Illustration of (a) Pristine PEDOT:PSS solution, (b) Filtered by 0.45 µm filter and (c) Added with different amount of EG

3.3.2 Polymer Electrolyte Preparation

During the fabrication process of rigid OECTs, four distinct biopolymer electrolytes were employed to determine the most suitable polymer electrolyte for the final flexible device. Various biopolymers and salts (ion providers) were blended in different weight ratios to form the electrolytes, as listed in Table 3.2 and subsequently labeled.

Chitosan (CS): Dextran (Dex): Ammonium Bromide (NH₄Br) Polymer **Electrolyte** (CS:Dex:NH₄Br): Chitosan (CS),known for its abundance, biodegradability, non-toxic nature, and excellent film-forming capability, serves as an ideal solid-state polymeric matrix. CS-based polymer electrolytes have been described by Aziz et al (2021). The raw materials selected include Dex powder (average molecular weight of 35,000-45,000, Sigma-Aldrich) and high molecular weight CS (molecular weight of 310,000-375,000, Sigma-Aldrich). To prepare the CS:Dex based polymer electrolyte, 60 mL of 1% acetic acid was used to individually dissolve 40 wt% Dex and 60 wt% CS at ambient temperature for 1.5 h. Subsequently, a homogeneous blending solution was obtained by mixing and stirring for 180 min. For the preparation of CS:Dex:NH₄Br electrolytes, 30 wt% NH₄Br was incorporated into the blended solution of CS:Dex while being constantly stirred. The DC ionic conductivity was reported as 1.64×10^{-3} S cm⁻¹.

Methylcellulose (MC): Dextran (Dex): Ammonium Hexafluorophosphate (NH₄PF₆) Polymer Electrolyte (MC:Dex:NH₄PF₆): As a natural polymer, Methylcellulose (MC) contains numerous functional groups, such as oxygen, and possesses excellent film-forming properties and solubility, making it suitable for ionic conduction. MC-based polymer blend electrolytes have also been prepared by Aziz et al. (Aziz et al., 2022). In their preparation, 0.4 g of Dex and 0.6 g of MC were separately dissolved in 50 mL of 1 wt% acetic acid for 1.5 h at ambient temperature. Following

this, the Dex and MC solutions were homogenously mixed for 3 h. To enhance the ionic conductivity of the MC-Dex blend, 40 wt% NH₄PF₆ was added and stirred constantly until fully dissolved. Additionally, glycerol was added included as a plasticizer at 15 wt%. The resulting DC ionic conductivity was reported as 6.71×10^{-4} S cm⁻¹.

Fish gelatin (FS): Lithium Perchlorate (LiClO₄) Polymer Electrolyte (FS:LiClO₄): Furthermore, Kadir et al. (2021) have reported that fish gelatin-based polymer blend electrolytes. In this method, 2 g of gelatin derived from cold-water fish skin (FS) was stirred in 100 mL of distilled water at 60 °C for 30 min, with 25 wt% LiClO₄ added to create salted electrolytes (Kadir, 2021). The DC ionic conductivity of this blend was reported as $3.58 \pm 0.58 \times 10^{-6}$ S cm⁻¹.

Chitosan (CS): Dextran (Dex): Lithium Perchlorate (LiClO₄) Polymer Blend Electrolyte (CS:Dex: LiClO₄): Inspired by the successful blended electrolytes systems reported, a new polymer electrolyte based on CS was proposed and synthesized in this study. The new electrolyte consists of Chitosan (CS) (low molecular weight), dextran (Dex), and lithium perchlorate (LiClO₄) (purum p.a., ≥ 98%). To prepare the polymer electrolyte, CS and Dex were dissolved in a weight ratio of 6:4 in 30 mL of 1% acetic acid individually for 1.5 h to gain a homogeneous blending solution. For the preparation of CS:Dex:LiClO₄ electrolyte, the blended solution of CS:Dex was incorporated with 30 wt% of LiClO₄ while being constantly stirred for 12 h until the mixture turned into a homogeneous, clear, and viscous electrolyte. The polymer blend electrolyte was further filtered by a strainer to separate the suspended chitosan solids.

It is worth noting that all solution preparations were conducted at ambient temperature and relative humidity of ~64%, details shown in Figure 3.4. Moreover, the flexible conductive silver paste (Ag) (coverage: 250–270 cm²/g) was purchased from Sigma-Aldrich, St. Louis, USA, and used as electrodes of the OECTs.

Table 3.2: Designation of the electrolytes with different type of polymers

Wt%	Ionic conductivity	Designation
40:60:30	$1.64 \times 10^{-3} \text{ S cm}^{-1}$	CS:Dex:NH ₄ Br
40:60:40	$6.71 \times 10^{-4} \mathrm{S \ cm^{-1}}$	MC:Dex:NH ₄ PF ₆
40:10	$3.58 \pm 0.58 \times 10^{-6} \text{S cm}^{-1}$	FS:LiClO ₄
40:60:40	/	CS:Dex:LiClO ₄



Figure 3.4: General preparation process of biopolymer electrolytes

3.3.3 Fabrication of OECTs Based on Rigid Si Wafer Substrate

For the fabrication of OECTs on rigid Si wafers, the control variable method was employed to determine the optimal polymer electrolyte. In this procedure, only the electrolyte type was varied while all other components of the device were kept constant, maintaining the same materials and conditions throughout the procedure. Since the silicon wafer acts as gate electrode in this rigid device, as well as substrate, which provides strong electrolyte gating, the top-contact bottom-gate structure was utilized,

and a detailed diagram of the fabrication process is shown in Figure 3.5. First, heavily doped p-type Si wafers of size 1×1 cm² were cleaned sequentially in acetone, alcohol, and deionized water for 5 min each, which is enough size to fabricate one individual OECTs. The clean Si substrate was then treated with ultraviolet (UV) curing to render the surface more hydrophilic, facilitating active layer formation. Next, the chitosan-based electrolyte was spin-coated onto the surface of Si at 2000 rpm for 45 s, with the residual solvent removed by drying in a cabinet for 12 h at room temperature. Subsequently, a PEDOT:PSS solution was spin-coated onto the dielectric layer at 2500 rpm for 60 s and annealed at 80°C for 1 h to form a 0.55 µm active layer. Finally, 9.25 µm metal electrodes were deposited through a patterned mask using a screen printer with flexible silver (Ag) paste, followed by annealing at 80°C for 15 min. The source and drain electrodes were thus formed, with the channel width (W) and length (L) being 3.5 mm and 0.7 mm, respectively. Specific experimental conditions and parameters required for OECTs are listed in Table 3.3.

Table 3.3: Experimental conditions and facilities used for OECTs on Si wafer

Components	Material	Experimental conditions	Facilities
Substrate	P ⁺ Si wafer	1×1 cm ² UV curing, 10 min	UV curing machine
Electrolyte	4 polymer electrolytes	Spin-coating, 2000 rpm for 45 s Drying at room temperature, 1 day	Spin coater (MTI)
Channel	PEDOT:PSS	Spin-coating, 2500 rpm for 60 s Annealing at 80 ℃ for 1 h	Oven (Memmert)
Source & Drain	Ag	Screen-printing, $W \& L$: 3.5 × 0.7 mm Annealing at 80°C for 1 h	Desk screen printer
Structure	Top-contact box	ttom-gate	

⁴ polymer electrolytes: CS:Dex:NH₄Br, MC:Dex:NH₄PF₆, FS:LiClO₄, CS:Dex:LiClO₄.

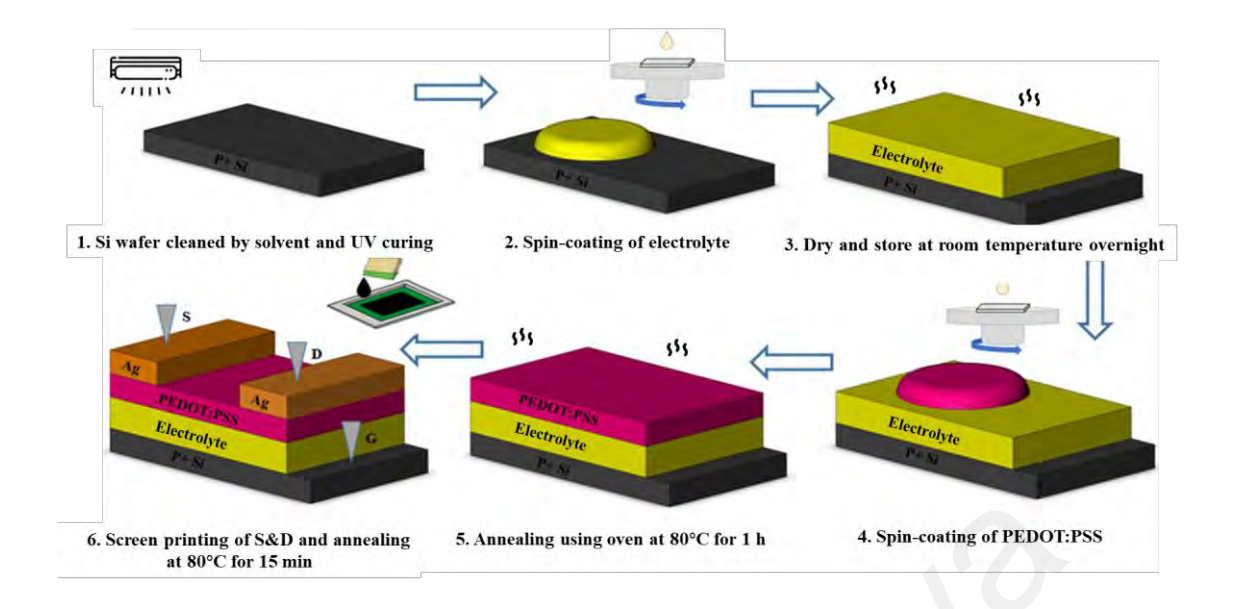


Figure 3.5: The overall step-by-step fabrication scheme of the OECT on silicon substrates

3.3.4 Fabrication of OECTs Based on Flexible PET Substrate

For the fabrication of a flexible chitosan-based OECT, the top-gate bottom-contact structure was employed at first due to the application of flexible PET substrate, which is particularly advantageous for neuromorphic computing and bioelectronic applications as strong ion-channel interaction. Then the electrode pattern was designed using a layout CAD tool with specific geometric parameters (channel length: 500 µm, width: 1500 µm) to prevent electrode overlapping or short circuits during screen printing. The devices were fabricated on a 150 µm-thick commercial low-cost poly (ethylene terephthalate) (PET) film. The fabrication process, detailed in Figure 3.6, began with cutting the PET into 9 × 3 cm² substrate to fit the screen printer platform followed by cleaning with isopropyl alcohol (IPA) and deionized water. Then, the PET surface's hydrophilicity was enhanced through UV exposure to ensure better adherence of channel and electrolyte layers. Prior to deposition of the source and drain electrodes, the PET was secured on a desktop screen printer. Precise calibration of the hinge clamp height ensured the minimal printing errors, as shown in Figure 3.6 g. A pair of 8.5 µm silver electrodes was then screen-printed onto the PET substrate using viscous silver paste, a

quicker and simpler process than conventional methods, taking only 3 s. Post-printing, the device was annealed at 100 °C for 30 min and cured under UV light at 405 nm for 15 min to smoothen the surface. Next, the device was attached to a PCB board using Kapton tape. A 1.2 µL PEDOT:PSS solution was drop-casted onto the source and drain (S&D) electrodes and annealed at 75 °C for 30 min to form a 4 µm active layer. The solid chitosan polymer electrolyte was then prepared by drop-casting 20 µL of the solution onto the PEDOT:PSS layer followed by a second annealing at 75 °C for 30 min. The residual solvent was removed in a controlled humid chamber for 12 h at room temperature, resulting in a 2.5 µm electrolyte layer. Finally, a silver electrode was deposited onto the chitosan polymer electrolyte layer as the gate electrode using the screen printer and annealed at 75 °C for 30 min. The devices were stored in a controlled humid chamber until further use.

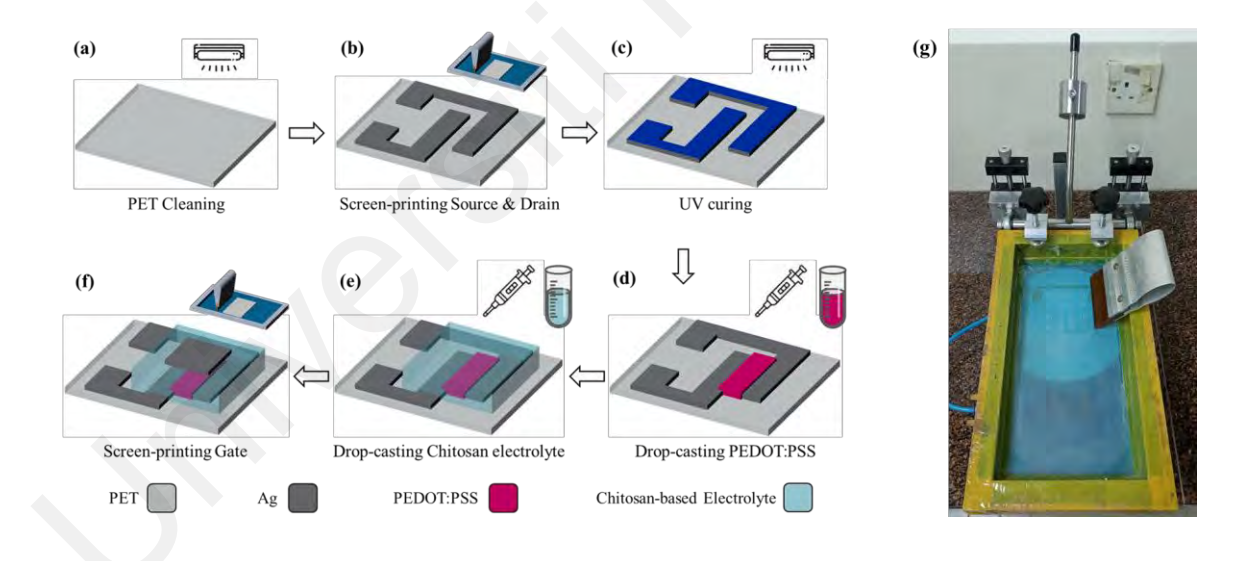


Figure 3.6: The procedure in fabricating OECT on flexible PET substrate

For comparison of the performance of the OECT in devices with different configurations, the bottom-gated and side-gated OECTs were fabricated subsequently (Figure 3.7). For the bottom-gated OECTs, a single silver electrode was screen-printed first as the gate electrode on the PET substrate. The following chitosan electrolyte and PEDOT:PSS channel were fabricated with the same process of top-gated OECTs, as

shown in Figure 3.6. It was noted that a pair of silver electrodes is finally screen-printed onto the PEDOT:PSS layer as the source and drain electrodes in the bottom-gated structure. Besides, in fabricating the side-gated OECTs, three silver electrodes were simultaneously screen-printed onto the PET substrate to be the source, drain, and gate electrodes. Following that, a PEDOT:PSS channel was patterned using drop-casting between the source and drain electrodes, and the chitosan electrolyte was finally deposited to connect the gate electrode with the PEDOT:PSS channel according to the methods described above. Unless stated otherwise, all devices were fabricated with channel $W/L = 1500 \,\mu\text{m}/500 \,\mu\text{m}$ and $d = 4 \,\mu\text{m}$, tested under ambient conditions ($\approx 26 \,^{\circ}\text{C}$, $\approx 65\%$ RH), details of specification and experimental conditions are listed in Table 3.4.

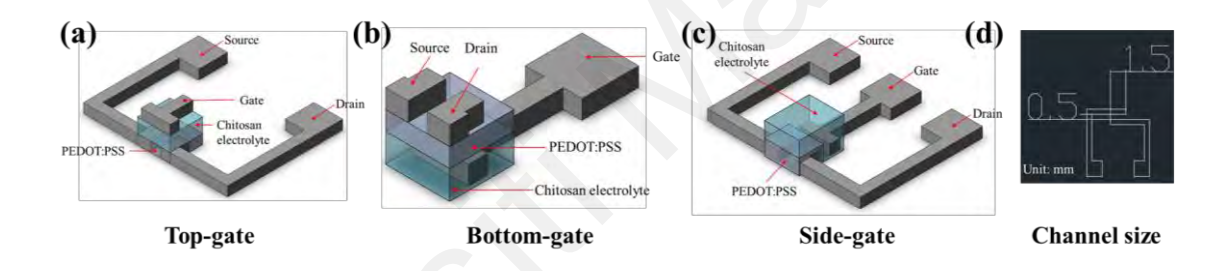


Figure 3.7: Schematic diagrams of OECT design of (a) Top-gated (b) bottom-gated (c) Side-gated, and (d) Channel size, $W\&L = 1.5 \times 0.5$ mm

Table 3.4: Experimental conditions and facilities used of flexible OECTs

Components	Material	Experimental conditions	Facilities
Substrate	PET	9 × 3 cm ² Cleaning in IPA and deionized water UV curing	UV curing machine
S&D	Ag	Screen-printing, $W \& L$: 1.5×0.5 mm Annealing at 100 °C for 30 min UV curing for 15 min	Desk screen printer Oven (Memmert)
Channel	PEDOT:PSS	Drop-casting, 1.2 μL Annealing at 75°C for 30 min	Pipette (Joanlab)
Electrolyte	CS:Dex:LiClO ₄	Drop-casting, 20 µL Annealing at 75°C for 30 min Storing in humid chamber overnight	Pipette (Joanlab)
Gate	Ag	Screen-printing Annealing at 75°C for 30 min	Desk screen printer Oven (Memmert)
Structure	Top-gate, bottom-gate, side-gate		

3.3.5 Characterization

Material Characterization: The surface morphologies of the films were recorded employing the field emission scanning electron microscopy (FESEM) (Quanta FEG 450) and digital microscope. For the analysis of the microstructure, the thickness of each layer of the OECTs was obtained with a stylus profilometer (Bruker Dektak XT).

Electrical Characterization: A digital multimeter (Fluke 15B+) was used to measure resistance of the PEDOT:PSS. The *I–V* characteristics of all the OECTs including output and transfer curves were conducted using a semiconductor characterization system (SCS) parameter analyzer (Keithley 4200A) in the atmosphere at room temperature. The temperature-dependent measurement of the OECTs was conducted by connecting a temperature control hotplate (IKA C-MAG HS 7) to the probe station of the Keithley 4200A. The fabricated OECTs were measured inside a constant temperature and humidity environment, which enables real-time and precise control of the operating temperature. The detailed specification of each facilities applied to characterize OECTs are listed in Table 3.5.

Table 3.5: Specification of each facility applied for OECTs measurement

Characterization	Facilities	Name	
Surface morphologies	FESEM	Quanta FEG 450	
Thickness	Stylus profilometer	Bruker Dektak XT	
	Digital multimeter	Fluke 15B+	
Electrical properties	SCS parameter analyzer	Keithley 4200A	
	Hotplate	IKA C-MAG HS 7	

3.4 Experimental Design of Electrical Characteristics

A comprehensive approach was proposed to evaluate the electrical characteristics of OECTs as introduced in Figure 3.8. Initially, the basic transfer curve (I_D - V_G), along with the hysteresis window and output curve (I_D - V_D), provided fundamental insights that how

the gate bias modulates its channel conductivity, highlighting the gate control over the device. The hysteresis window can prove the memory effect of the transistor, which is crucial for applications like neuromorphic computing. Key parameters such as transconductance (g_m) , on-off current ratio (I_{on}/I_{off}) , threshold voltage (V_{Th}) , and subthreshold swing (SS) are extracted to assess the transistor's efficiency and switching behaviour. Comparative analyses were performed to explore the differences in OECTs fabricated with various polymer electrolytes, which might affect the ion mobility and electronic properties. The investigation extended to understand how OECTs respond to different transistors configurations, including top-gated, bottom-gated and side-gated, emphasizing the comparable effect of structure layout on the device performance. Longterm stability tests were conducted to ensure the durability and reliability of the devices under prolonged operational conditions. Additionally, double sweeping techniques with varying scanning rates were employed to evaluate the hysteresis effects further, which were critical for understanding the memory and switching characteristics of the OECTs. This experimental design aims to encompass key aspects of electrical performance, ensuring a thorough understanding of OECT behaviour under different operational and environmental conditions.

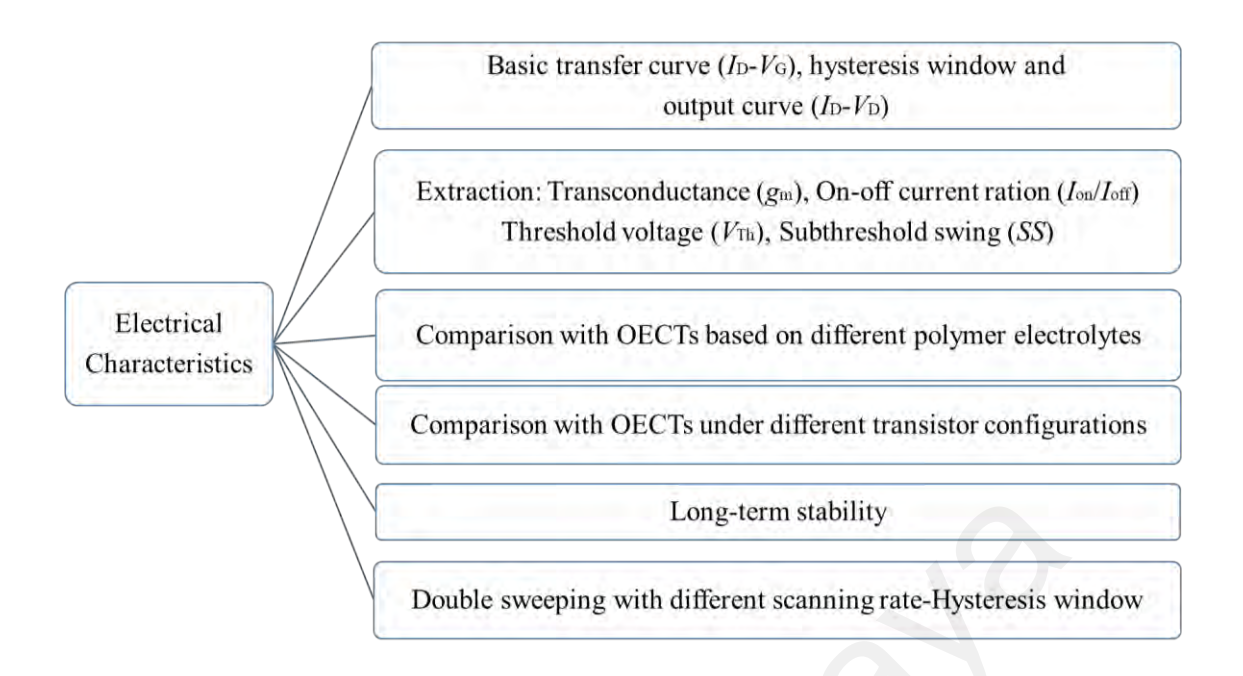


Figure 3.8: List of electrical characteristics investigated in this study

3.5 Experimental Design of Mechanical Properties

For assessing the mechanical properties of OECTs, the comprehensive flexibility and temperature testing were carried out to evaluate the stability of these devices under varying environmental conditions as shown in Table 3.6.

3.5.1 Mechanical Robustness Testing

To evaluate the flexibility of OECTs, a series of systematic bending tests were conducted. Initially, devices were bent over a semi-cylindrical mandrel to assess the performance changes due to bending stress. The pre- and post-bending characteristics of the OECTs were compared to identify any deviations in electrical behavior as shown in Figure 3.9. Further, the devices were subjected to repeated bending cycles ranging from 0 to 300 times and bending durations extending from 0 to 3 h. These tests were carried out using mandrels with different curvature radii, specifically varying from 40 mm to 100 mm. This establishes a correlation between the bending radius, the number of bending cycles, and the duration, providing a detailed insight into the mechanical endurance of the OECTs.

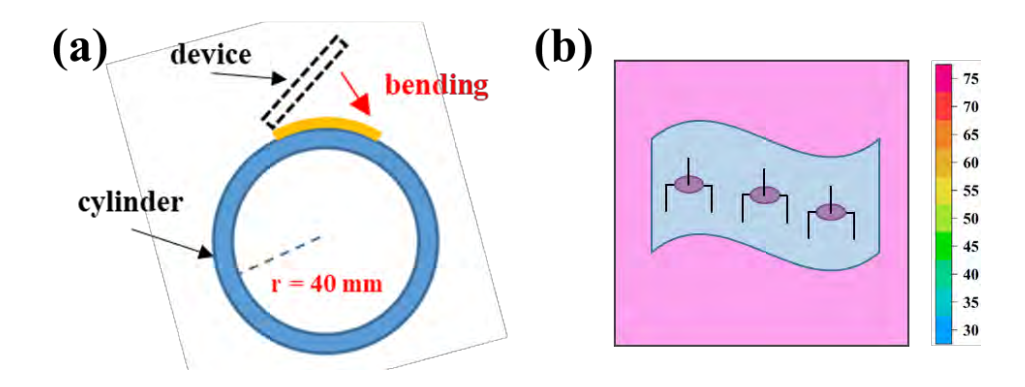


Figure 3.9: Schematics of (a) Bending testing and (b) Temperature testing

3.5.2 Temperature Testing

The temperature-dependent behavior of OECTs was examined by subjecting the devices to a controlled temperature range from 30 °C to 75 °C. At each temperature point, OECTs were equilibrated for a duration of 3 min to ensure thermal stabilization before any measurements are taken. This approach helps in understanding the thermal sensitivity of the OECTs and the impact of temperature fluctuations on their operational stability.

To assess the effect of both bending and temperature on the electrical performance of the OECTs, the transfer curves were measured, transconductance (g_m) and threshold voltage (V_{Th}) were extracted and analyzed respectively. The results were summarized in Table 3.6 to highlight how mechanical stress and temperature influence the fundamental electrical properties of the OECTs.

Table 3.6: Experimental design for mechanical properties of OECTs

]	Desig	gn	Condition		
	1	Pre & post-bending	On semi-cylindrical mandrel		
Mechanical robustness testing	2	Bending cycle	0 to 300 times,		
		Bending cycle	Bending radius 100 to 40 mm		
	2	Danding dynation	0 to 3 h,		
	3 Bending duration		Bending radius 100 to 40 mm		
Temperature testing	1	Temperature change	30 °C to 75 °C		

3.6 Optimization Solution

To optimize the performance of OECTs, the effects of device structure, material composition, and electrolyte modification were investigated (Figure 3.10). These optimization solutions are aimed at enhancing the electrical performance and stability of OECTs under operational conditions.

3.6.1 Effect of Structure in OECT

The impact of device architecture was explored by comparing top-gated, bottom-gated, and side-gated configurations of OECTs. Each structure influenced the charge carrier dynamics and electrochemical accessibility differently, potentially affecting the device's overall performance. By assessing the electrical characteristics and stability of each gating configuration, the optimal structural design could be determined, which offered the best performance in terms of I-V relationship, transconductance (g_m), and on-off ratio (I_{on}/I_{off}) respectively.

3.6.2 Effect of Ethylene Glycol (EG) Doping in PEDOT:PSS

Ethylene glycol (EG) was known to enhance the conductivity of PEDOT:PSS. To investigate this effect, an analysis was conducted where EG is added to PEDOT:PSS in varying concentrations from 2 to 6 vol%, in increments of 1 vol%. This study involved measuring the resulting sheet resistance of the PEDOT:PSS films and evaluating how these variations in EG concentration impact the electrical performance of OECTs. The objective is to establish a correlation between EG concentration and key electrical parameters such as on-state current (I_{on}) and transconductance (g_m), thereby identifying the optimal doping level for maximum conductivity and device efficiency.

3.6.3 Effect of Salt Addition to The Polymer Electrolyte

The addition of salt into the polymer electrolyte was another critical factor influencing the ionic conductivity and overall performance of OECTs. To investigate

this, different weight percentages of salt in the polymer electrolyte were examined, ranging from 20 to 40 wt% in increments of 10 wt%. This analysis included studying the changes in the surface morphology of the polymer electrolyte and the corresponding electrical performance of the devices. By understanding how salt concentration affected both morphology and ionic conductivity, the electrolyte composition could be optimized to enhance device operation and efficiency.

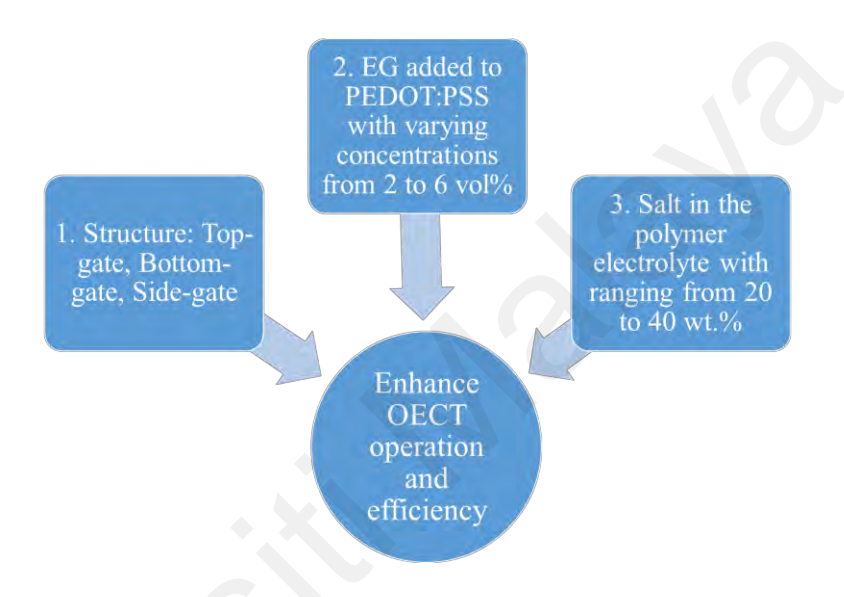


Figure 3.10: List of optimization methods for enhancing performance of OECTs

CHAPTER 4: RESULTS AND DISCUSSIONS

4.1 Introduction

This chapter discussed on the findings obtained in this work. The results are divided into two parts based on different type of substrate: rigid OECTs on Si wafer and flexible chitosan-based OECTs on PET. The analysis highlights on the meaningful findings and critical electrical performance by taking into accounts the material composition and mechanical considerations of each device types. Lastly, the degradability of flexible OECTs was carried out through water solubility tests.

4.2 Analysis on Performance of Rigid OECTs on Si Wafer

4.2.1 The Exhibition of Physical Rigid OECTs

Inspired by the fabrication of In₂O₃ thin film transistors proposed (Zhou et al., 2019), a heavily doped p-type Si wafer was utilized as the gate electrode in the OECTs reported in this study. Following the fabrication process for rigid OECTs described in Chapter 3, the p-type Si wafer served as the gate electrode, providing robust support for device operation and control. The pristine Si wafer was cleaned and precisely cut into multiple 1×1 cm² square substrates. Sequential deposition of the electrolyte and PEDOT:PSS was carried out on these substrates, forming channels with a length of 0.7 mm and a width of 3.5 mm. It was noted that the OECTs were fabricated using three distinct organic electrolytes: Chitosan, Methylcellulose, and Fish Gelatin. Figure 4.1 presents the physical images of the OECTs fabricated with these three types of polymer electrolytes, providing a visual representation of the devices' layout and highlighting the design differences based on the various polymer electrolytes employed.

Upon examining the physical images, several noteworthy observations could be made. Firstly, the methylcellulose-based OECT displayed a rough surface with numerous large particles visibly present on the OECT's surface, as shown in Figure 4.1

(c). These particles contributed to an uneven texture on the transistor channel. In contrast, the fish gelatin-based OECT exhibited significantly smaller particles compared to the methylcellulose-based OECT; however, the surface remained relatively rough, while a lesser extent (Figure 4.1 (d)). Notably, the chitosan-based OECT demonstrated a distinct characteristic: its surface appeared uniformly smooth, devoid of any noticeable particles (Figure 4.1 (b)). This indicated a high degree of surface uniformity and smoothness compared to the other two electrolyte-based OECTs. The absence of visible particles on the chitosan-based OECT's surface suggested superior surface quality and cleanliness. This visual analysis provided valuable insights into the physical characteristics and surface morphology of the OECTs fabricated using different polymer electrolytes.

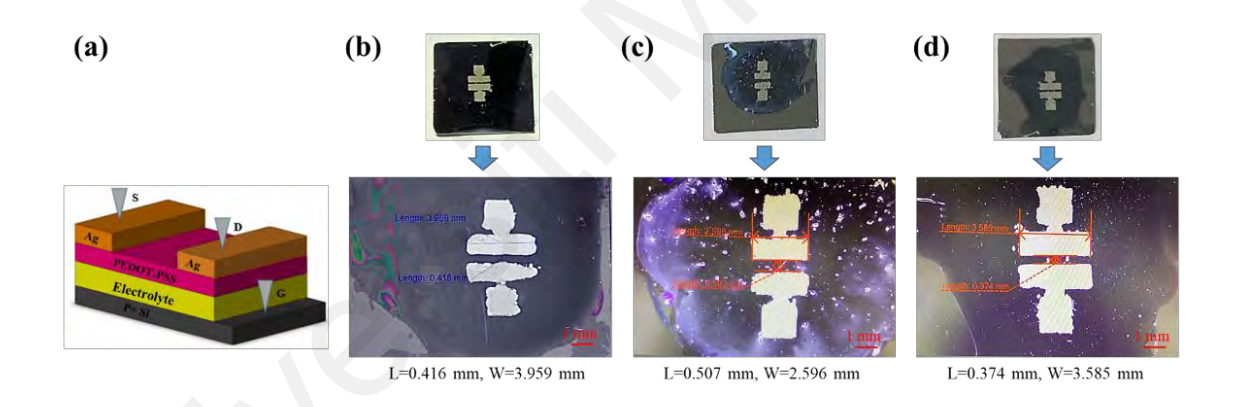


Figure 4.1: The photographs of rigid OECTs fabricated using three types polymer electrolytes on Si wafer. (a) Schematic diagram of structure of rigid OECT on Si wafer. Images of OECT based on (b) Chitosan, length and width are 0.416 mm and 3.959 mm, (c) Methylcellulose, length and width are 0.507 mm and 2.596 mm and (d) Fish gelatin, length and width are 0.374 mm and 3.585 mm

However, it was important to note that the actual channel sizes of the OECTs deviate from the original design. Most of the channel sizes were reduced, and a few were even larger, due to errors in manual screen printing, which cannot effectively control printing accuracy. High-precision and efficient screen-printing operations are urgently needed for future improvements.

4.2.2 Surface Morphology of Rigid OECTs

Thickness: The electrical performance of OECTs can be enhanced by increasing the thickness of the channel film, as described in the aforementioned Equation 2.1. The thickness of the semiconductor channel film is crucial for optimizing OECT performance. Accurate characterization and analysis require precise measurement of each layer's thickness. In this study, the thickness of each layer in three different OECTs was measured using a stylus profilometer, specifically the Bruker Dektak XT (Figure 4.2). This instrument provided precise and reliable measurements of the thicknesses in the OECTs.

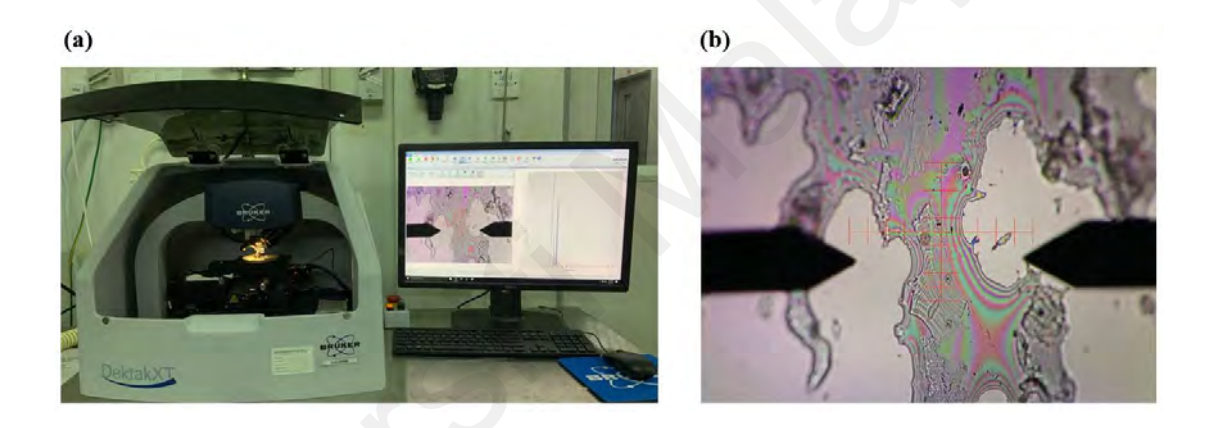


Figure 4.2: The photographs of (a) Bruker Dektak XT measuring the thickness and (b) The stylus of Bruker Dektak XT touching surface of Si substrate

The thicknesses of each layer for chitosan-based, methylcellulose-based, and fish gelatin-based OECTs are presented in Table 4.1. The results indicated that the average thickness of the spin-coated electrolyte layer was 0.6767 μm for chitosan, 0.3899 μm for methylcellulose, and 0.2455 μm for fish gelatin. Notably, the chitosan electrolyte layer was the thickest among the three types. Additionally, the average thickness of the PEDOT:PSS channel layer, also deposited by spin coating, ranged from 0.5498 μm to 2.3076 μm. This variation in thickness was likely due to errors of manual fabrication processes. Regarding the Ag electrode, which was screen-printed, its average thickness

ranged from 9.2505 μm to 12.1327 μm. Although the differences in thickness were not substantial, the Ag electrode exhibited the greatest overall thickness.

Table 4.1: Average thickness of each layer of three types OECTs

Matarial	Thickness (unit: μm)				
Material	Electrolyte	PEDOT:PSS	Ag		
Chitosan	0.6767	0.5498	9.2505		
Methylcellulose	0.3899	3.8644	11.0421		
Fish gelatin	0.2455	2.3076	12.1327		

Surface Morphology: Figure 4.3 presents a cross-sectional FESEM image of the solid-state chitosan electrolyte deposited on a Si substrate. The thickness of the solid chitosan electrolyte was measured to be approximately 0.6767 µm. An unconsolidated structure was observed within the chitosan electrolyte, as shown in Figure 4.3 (b), which could provide a larger specific surface area for the adsorption of water molecules (Colomer, 2011). Consequently, the hydroxyl groups in the chitosan electrolyte facilitated water absorption, leading to proton production through the ionization of water molecules and resulting in high proton conductivity. Additionally, a significant observation was the presence of a notable gap between the chitosan electrolyte film and the Si wafer. The chitosan electrolyte film did not exhibit close adhesion to the Si wafer, indicating a lack of proper connection. This inadequate adhesion compromised the effective establishment of an electric double layer (EDL) interface. The weakened connection between the chitosan and the gate electrode led to a diminished EDL effect. To optimize the performance of OECTs, it is crucial to address this issue of inadequate connectivity between the chitosan and the Si wafer, thereby ensuring a stronger and more effective EDL interface.

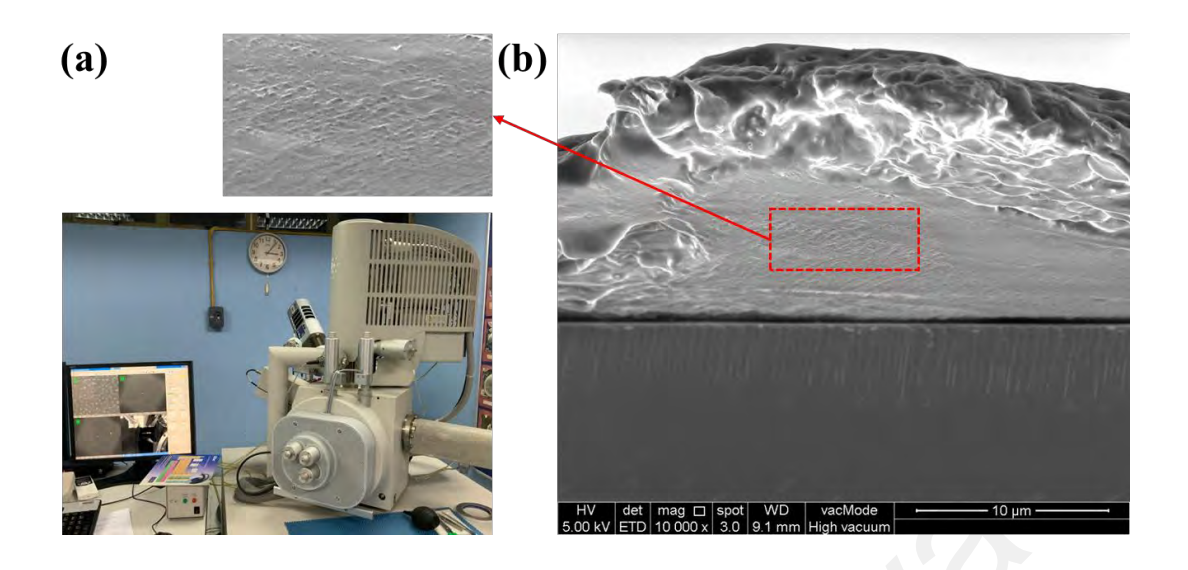


Figure 4.3: (a) The photograph of FESEM equipment, FEI QUANTA 450 FEG. (b) FESEM image of solid-state chitosan electrolyte on Si substrate

4.2.3 The Electrical Characteristics of Rigid OECTs

The transfer (I_D-V_G) and output (I_D-V_D) characteristics are critical in evaluating the electrical performance of OECTs, where I_D represents the drain current. These characteristics provide essential information into the operational behavior and performance of OECTs, which are crucial for their application in bioelectronics. Moreover, it is important to ensure that the maximum voltages $(|V_D|)$ applied to OECTs remain below 1 V to prevent electrolyte electrolysis (Giovannitti et al., 2020).

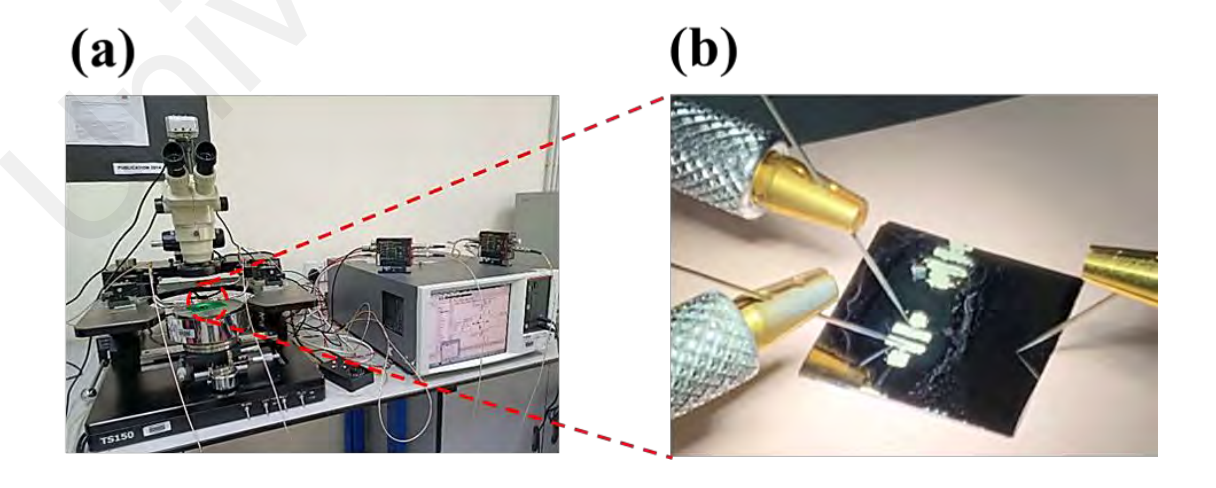


Figure 4.4: (a) The photograph of SCS parameter analyzer, Keithley 4200A and (b) Probes connected with electrodes of rigid OECTs to measure the electrical properties

To compare the effect of different polymer electrolytes on the electrical characteristics of rigid OECTs, the transfer and output curves of three types of OECTs were measured using an SCS parameter analyzer (Keithley 4200A) as shown in Figure 4.4. Typical p-type transfer curves were observed in these three devices, which were categorized based on the electrolyte material used: chitosan-based, methylcellulosebased, and fish gelatin-based (Figure 4.5). The double sweep transfer characteristics curves of OECTs were measured at a fixed V_D of - 0.5 V with V_G ranging from - 1.5 V to 1.5 V. The hysteresis window observed in each OECT is a necessary condition for simulating synaptic activity and indicates the presence of mobile ions in the polymer electrolytes (Chen et al., 2019). Among the tested devices, the methylcellulose-based OECT demonstrated a notable $I_{\rm on}/I_{\rm off}$ ratio of 4.1 \times 10⁶, accompanied by a relatively high threshold voltage ($V_{\rm Th}$) of - 0.75 V. The $V_{\rm Th}$ was determined by calculating the xaxis intercept of the square root of the I_D - V_G plot. Conversely, the fish gelatin-based OECT exhibited the lowest $V_{\rm Th}$ of - 0.65 V but had a significantly reduced $I_{\rm on}/I_{\rm off}$ ratio of 3.2 × 10⁶. In comparison, the chitosan-based OECT showed relatively superior performance characteristics, including an $I_{\rm on}/I_{\rm off}$ ratio of 3.5 \times 10⁶ and a low $V_{\rm Th}$ of - 0.7 V.

The corresponding I_D – V_D output characteristic curves are illustrated in Figure 4.5 (g-i), with V_G varying from 1 V to - 1.5 V in steps of 0.5 V. In the low V_D region, the output characteristics curves exhibited linear behavior, indicating good ohmic contact. In contrast, in the high V_D region, the drain current (I_D) of the OECTs gradually reached a saturation state. The EDL mechanism of the polymer electrolytes played a significant role in the drain current of the OECTs, as at higher V_D , the I_D progressively attains a saturated value.

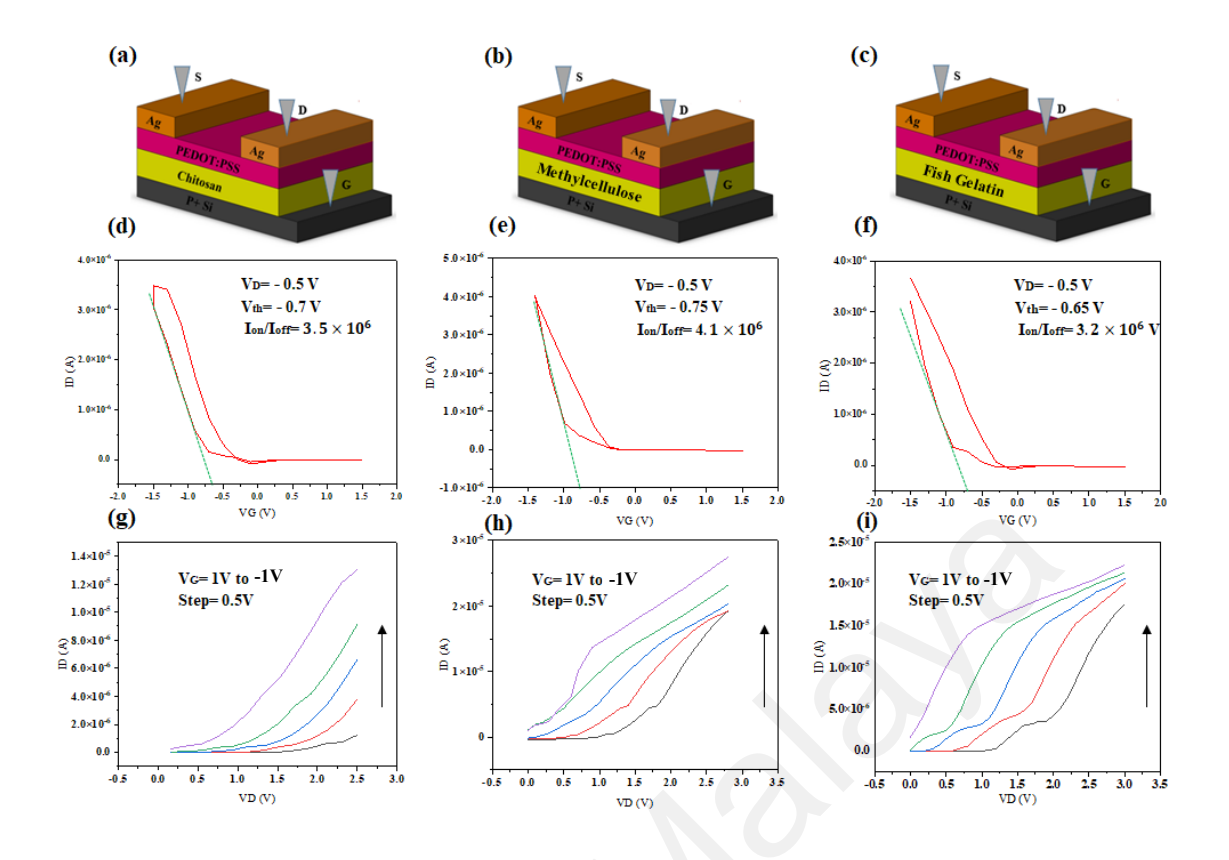


Figure 4.5: Schematics of rigid OECTs structures and corresponding electrical characteristics. Illustrations of OECT with (a) Chitosan-based electrolyte, (b) Methylcellulose-based electrolyte and (c) Fish gelatin-based electrolyte. (d-f) Transfer characteristics corresponding to (a-c). (g-i) Corresponding output curves of the transistors

4.2.4 Adjustment of Experimental Conditions

During the fabrication of rigid OECTs on Si wafers, several fabrication challenges were encountered, including the selection of spin-coating parameters (such as speed and duration) and annealing conditions (such as temperature and time). These factors required careful adjustment according to the specific materials used. Through continuous experimentation and optimization, the ideal rigid OECTs were successfully produced. The process involved meticulous adjustments to ensure the deposition of uniform and well-adhered layers, precise control of film thickness, and the achievement of desired electrical and mechanical properties.

Optimization of spin-coating parameters: Numerous studies have investigated spin-coating parameters in the fabrication of synaptic transistors. For example, Hwi-Su

Kim et al. (2022) employed a spin-coating method to deposit a casein-based electrolyte solution at 3000 rpm for 30 s (Kim et al., 2022), while J. Chen et al. (2019) spin-coated hydrogel at 1000 rpm for 60 s to form the film (Chen et al., 2019). Building on these established spin-coating parameters, a novel spin-coating parameter of 2000 rpm for 60 s was tailored and implemented for the deposition of the chitosan-based polymer electrolyte (Figure 4.6). This customized spin-coating parameter aimed to optimize the film formation and enhance the performance of the resulting OECTs.

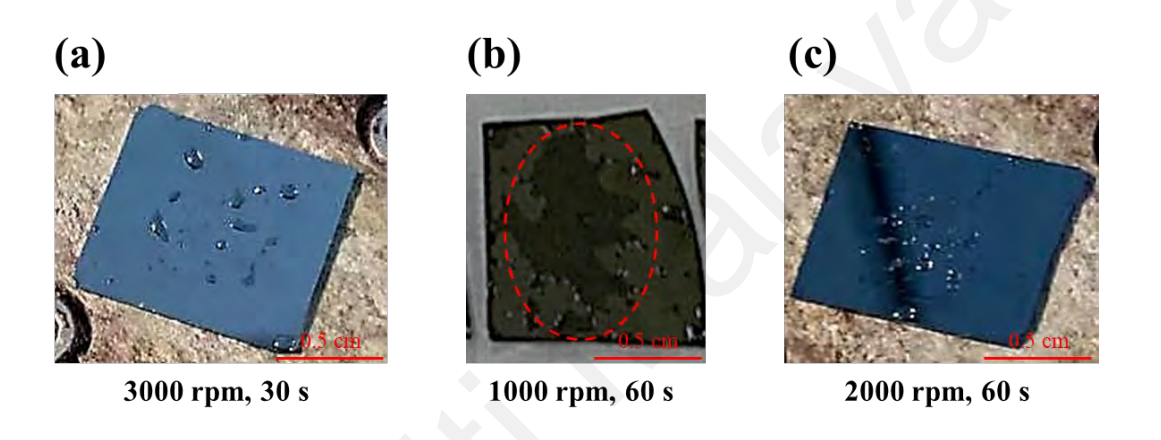


Figure 4.6: Photographs of deposition of chitosan-based electrolyte by spin-coating under (a) 3000 rpm for 30 s, (b) Under 1000 rpm for 60 s and (c) Under 2000 rpm for 60 s

The spin-coating results of the chitosan-based electrolyte revealed that a relatively uniform film was formed when spin-coated at 1000 rpm for 60 s, achieving consistent coverage of the Si wafer surface, but a small region exhibited non-uniform coverage. Poorer film quality was observed at other spin-coating parameters, likely due to the hydrophobic nature of the Si wafer surface. To address this issue, UV curing was applied to the Si wafer surface prior to the deposition of the chitosan film. This treatment facilitated the formation of chitosan films with improved uniform coating shapes under the same condition of 1000 rpm and 60 s of spin coating (Figure 4.7). The modified deposition process resulted in a more conducive surface to high-quality

Chitosan film formation, overcoming the challenges posed by the hydrophobic Si wafer surface.

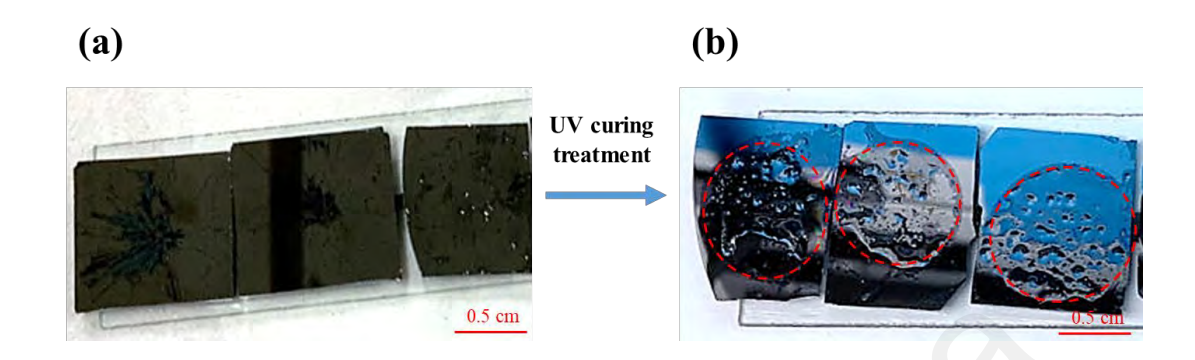


Figure 4.7: Photographs of chitosan-based electrolyte film formation under 1000 rpm for 60 s. (a) Before UV curing. (b) After UV curing

Optimization of Annealing Conditions: Thermal annealing of the deposited film is a crucial process as it expedites film formation and facilitates the removal of residual solvents, thereby enhancing the performance of OECTs. The temperature and duration of the annealing process are critical parameters. Excessive temperature or prolonged annealing can lead to film degradation and spontaneous detachment from the Si substrate (Figure 4.8 (b)). Experimental findings indicated that maintaining an annealing temperature of 80 °C and a duration between 10 to 15 min achieved optimal film formation without compromising its integrity (Figure 4.8 (a)). These controlled annealing conditions struck a balance between promoting film formation and preventing detrimental effects on the film structure.

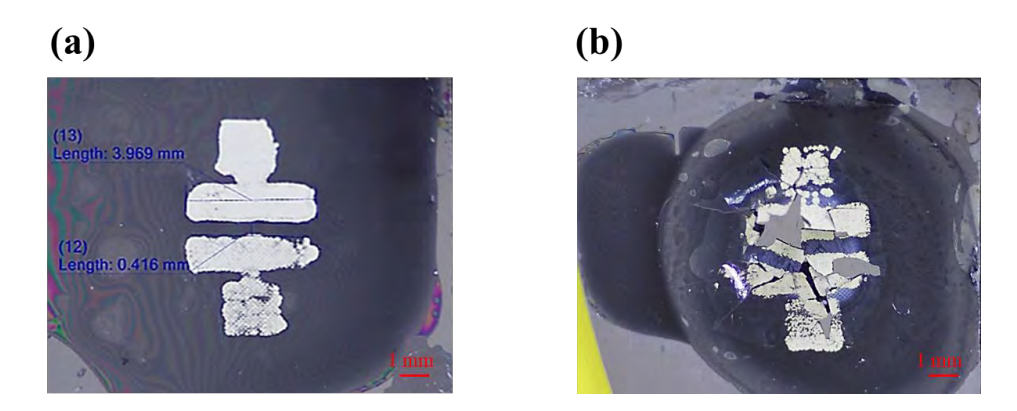


Figure 4.8: Annealing of chitosan-based electrolyte film under different temperature and duration. (a) Below 80 $\mathbb C$, less than 15 min. (b) Over 80 $\mathbb C$

4.3 Analysis on Performance of Flexible OECTs Based on Chitosan Electrolyte on PET Substrate

4.3.1 Dielectric Properties of The Solid-State Chitosan-Based Polymer Electrolyte

The chitosan-based electrolyte demonstrated effective proton conduction in rigid OECTs as stated before and, due to its intrinsic flexibility, was ideal candidature for the development of flexible and degradable OECTs. To further explore the potential of chitosan in flexible, degradable OECTs, a novel polymer electrolyte consisting of chitosan, dextran, and lithium salt (LiClO₄) was proposed in this study. Chitosan (CS), one of the most abundant biopolymers derived predominantly from shrimp waste is depicted in Figure 4.9 (a). Its chemical structure, rich in polar groups (NH₂ and OH), enables chitosan to function effectively as a sorbent with a high affinity for transition metal ions. Additionally, its biodegradability, nontoxicity, and excellent film-forming characteristics make chitosan an ideal host for the polymer electrolyte (Mohamed et al., 2020). Dextran (Dex), another widely available renewable polysaccharide as illustrated in Figure 4.9 (a), Dex chains are lined with numerous oxygen functional groups, endowing Dex with an excellent water solubility. This property is crucial for dissolving salt and facilitating the creation of uniform and ultrathin polymer electrolyte films through a straightforward drop-coating process. These characteristics make it possible

to combine chitosan and dextran to form a composite polymer electrolyte, as depicted in Figure 4.9 (b). Dannoun et al. highlighted a lithium ion-conducting green polymer blend electrolyte based on a CS:Dex mixture (Dannoun et al., 2021). Through electrical impedance spectroscopy (EIS) and Fourier transform infrared spectroscopy (FTIR) analyses, it can be confirmed that charge conduction in this electrolyte is primarily ionic. The chitosan-based electrolyte demonstrated a maximum ionic conductivity of $4.16 \times 10^{-4} \text{ S cm}^{-1}$, coupled with a low breakdown voltage of 2.2 V. These properties indicated the electrolyte's potential for effective performance in OECTs, which typically operated below 1.0 V.

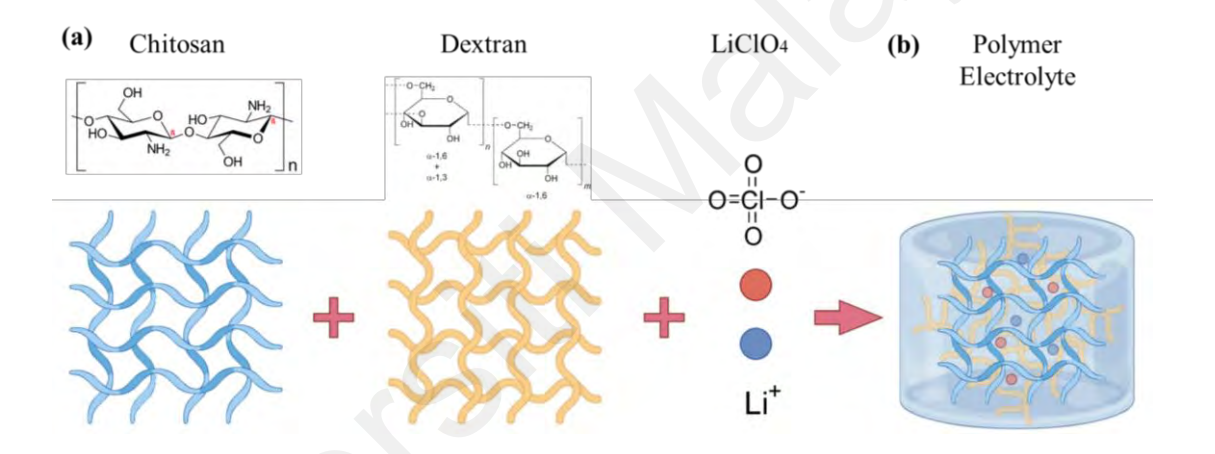


Figure 4.9: Design of the chitosan-based polymer electrolyte for the OECTs. (a) Microstructures and chemical structures of chitosan, dextran, and LiClO4. (b) Schematic diagram of the organic polymer electrolyte

4.3.2 Investigated Structures of Flexible Chitosan-based OECTs.

The device architecture of the top-gated OECTs and their photograph on a flexible substrate while being bent are shown in Figure 4.10 (a-b). To minimize the electrochemical impedance between the silver (Ag) electrodes and the chitosan ion membrane, a layer of PEDOT:PSS was strategically deposited onto the Ag contacts. This approach also directly determined the channel length (L), defined by the distance between the source and drain electrode contacts, as illustrated in Figure 4.10 (c). The advantage of this design was the ease with which the channel length can be adjusted by

modifying the metal contact patterns. The primary distinction between top-gated and bottom-gated OECTs lied in the placement of the gate electrode and the contact interface between the PEDOT:PSS and the metal contacts.

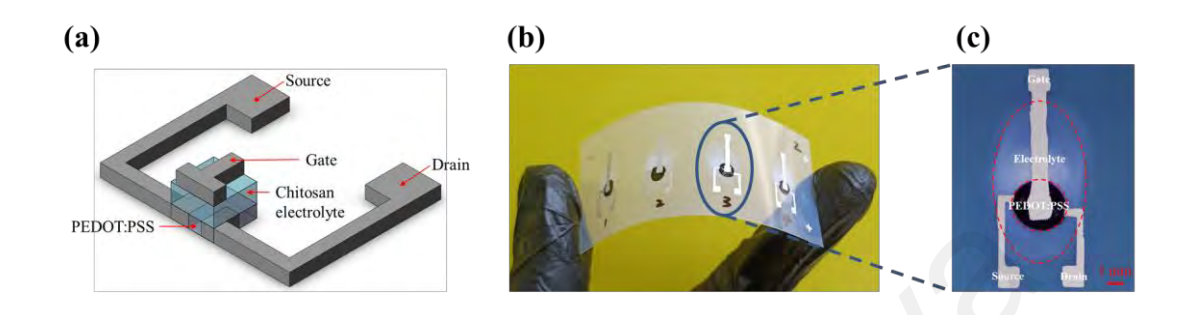


Figure 4.10: Flexible OECTs architecture. (a) Schematic illustration of the top-gated OECT. The channel length (L) and width (W) are 500 μm and 1500 μm, respectively. (b) Photographs of an array of top-gated OECTs on a flexible substrate while being bent and (c) One top-gated OECT, clearly showing the PEDOT:PSS layer and electrolyte layer. The green arrow indicates the direction of the transport of charge carriers

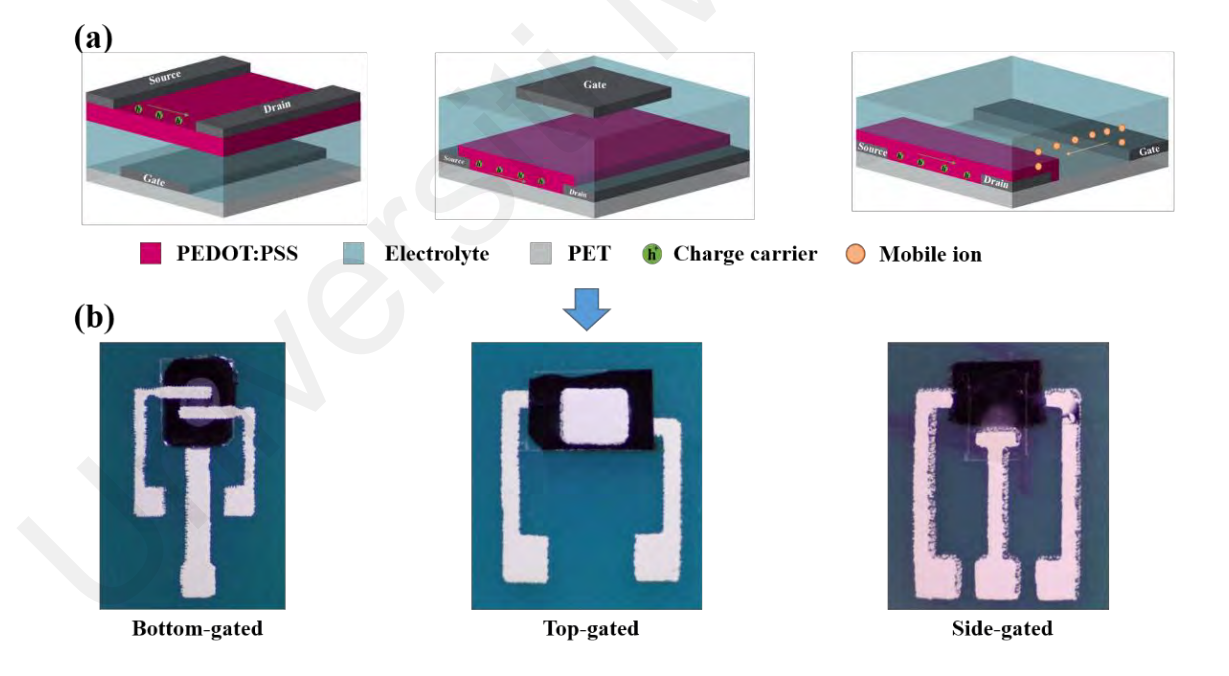


Figure 4.11: (a) Schematic illustration of bottom-gated OECTs, top-gated OECTs and side-gated OECTs. The green arrow indicates the direction of the transport of charge carriers. (b) Top views of OECTs with corresponding structures under digital microscope

As illustrated in Figure 4.11, the bottom-gated OECT was designed with a bottom gate and top contact configuration. In this structure, the source and drain electrode

contacts were placed directly on the active layer. However, this design limited the space available for the drain current to flow as only one side of the metal contact interfaces with the PEDOT:PSS layer. In contrast, the top-gated OECT featured a top gate and bottom contact arrangement. Here, the PEDOT:PSS channel layer has fully encompassed the source and drain contacts. This design allowed for a larger contact area between the channel layer and the metal contacts, facilitating broader transport of charge carriers, indicated by the green solid arrow in as shown in Figure 4.11. The sidegated OECT represented another common structure. In this design, both the source and drain electrode contacts and the gate electrode were positioned on the same plane, simplifying the fabrication process. However, this architecture faced limitations in field-effect strength and charge carrier injection efficiency (Huang et al., 2021) due to the relatively thick electrolyte layer.

4.3.3 The Electrical Characteristics of Flexible Chitosan-based OECTs.

Figure 4.12 displays the transfer and transconductance characteristics (red lines) of the top-gated OECTs. These devices demonstrated a low-voltage operation and characteristic depletion-type behavior, typical of electrolyte-gated transistors, which were distinct from the other two configurations. When a negative gate bias (V_G) is applied, anions from the electrolyte penetrate the PEDOT:PSS channel, leading to an accumulation of holes and a consequent increase in the drain current (I_D). A high average on-state current reaching 0.19 ± 0.03 mA was obtained at a V_G of -0.8 V when statistically analyzing 20 devices. This behavior was further evidenced by the typical pinch-off observed in the output characteristics, as illustrated in Figure 4.12 (c). The performance of these OECTs was further quantified by the corresponding maximum transconductance (g_m), which was derived from the slope of the transfer curve (g_m = $\partial I_D/\partial V_G$). As shown in Figure 4.12 (b), a large average g_m was recorded at 0.416 \pm 0.05 mS. Notably, the optimal g_m occurred at V_G of approximately -0.6 V, rather than at the

maximum applied V_G of -0.8 V. This finding indicated that the printed top-gated OECT operates most effectively at $V_G = -0.6$ V, particularly for applications requiring high transconductance (e.g., amplifiers).

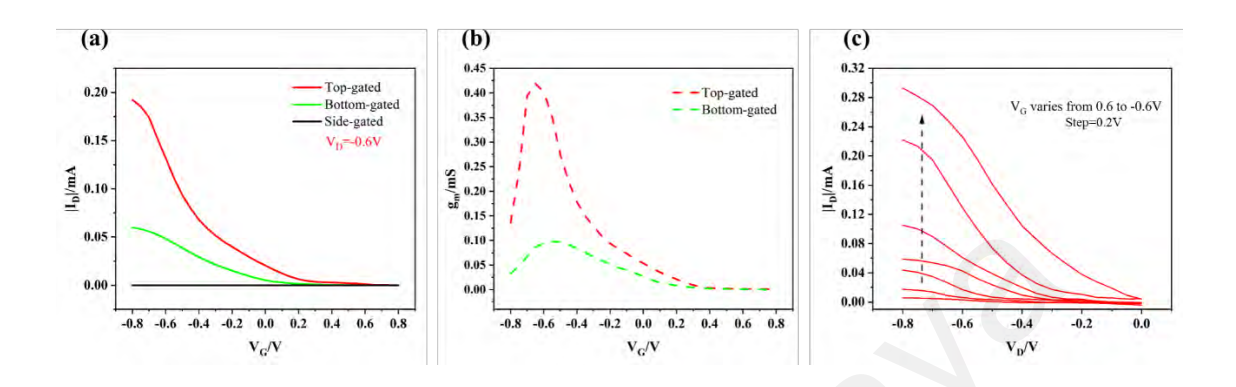


Figure 4.12: (a) Transfer characteristics of top-gated OECTs (red, solid line), bottom-gated OECTs (green, solid line), and side-gated OECTs (orange, solid line) measured at $V_D = -0.6$ V and (b) Their associated transconductances. (c) Output curve of top-gated OECTs. The inset arrows refer to the sweep direction. All measurements were performed in a chitosan-based polymer electrolyte with the PEDOT:PSS channel

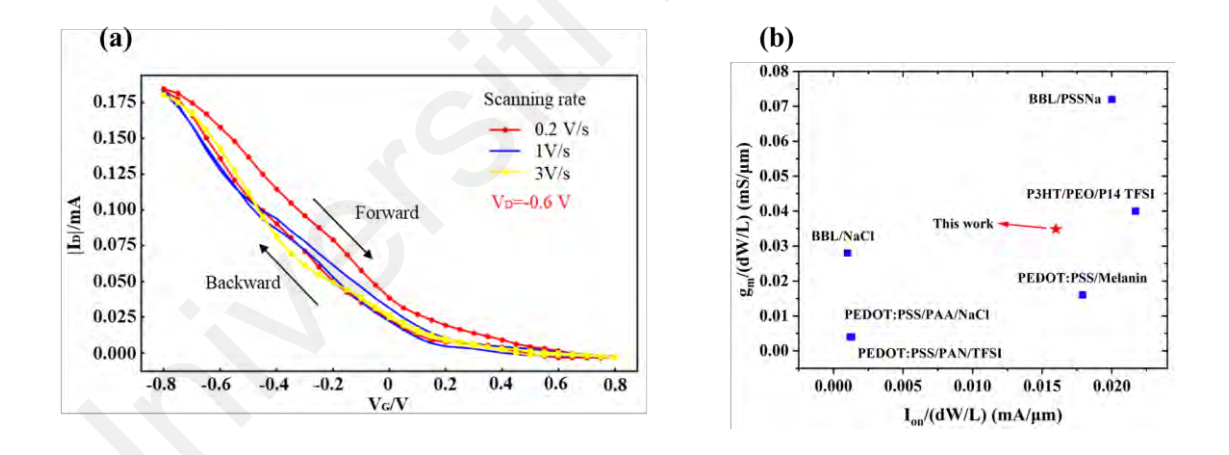


Figure 4.13: (a) Double sweeping transfer curves of top-gated OECTs with different scanning rates, showing slight hysteresis. (b) Comparison of normalized on-state current and maximum transconductance for previously reported OECTs and the chitosan-based OECT developed herein. To obtain a fair comparison among the reported works on the topic of OECTs, the peak on-current and maximum transconductance were normalized by the channel dimension (dW/L)

Moreover, the channel dimension is a critical role in the device's performance. When normalizing g_m by its channel dimension dW/L (where d, W, and L represent the channel thickness, width, and length, respectively), the normalized g_m was calculated as $0.035 \pm$

0.004 mS μ m⁻¹. Additionally, the high on–off current ratio (I_{on}/I_{off}) in printed top-gated OECTs can reach up to 0.3×10^3 . The low threshold voltage (V_{Th}) extracted from the transfer curve in the saturation region was found to be 0.4 ± 0.04 V. Additionally, slight hysteresis of the transfer characteristics of the top-gated OECTs was observed in Figure 4.13 (a), which indicated efficient doping/de-doping in the PEDOT:PSS channel. Its high electrical performance was mainly attributed to the hydrophilic PEDOT-rich domains in PEDOT:PSS, which enabled sufficient penetration and transport of ions in the bulk channel for electrochemical doping (Zeglio & Inganäs, 2018).

To highlight the superior performance of top-gated OECTs, the bottom-gated OECTs were fabricated with a channel length of 500 µm and a width of 1500 µm, as illustrated in Figure 4.11 (a). The transfer and transconductance characteristics of the bottom-gated OECTs, represented by green lines, were directly compared with those of the top-gated OECTs in Figure 4.12 (a-b). This comparison revealed that the on-state current and $g_{\rm m}$ of the top-gated OECTs were significantly higher, by more than an order of magnitude, than those of the bottom-gated OECTs. Furthermore, the subthreshold swing in the topgated OECTs was improved to 41.95 ± 1.21 mV/dec compared to 50 ± 1.4 mV/dec in the bottom-gated OECTs, indicating a more efficient ionic transport within their broader channel. In contrast to both top-gated and bottom-gated OECTs, the transfer characteristics of side-gated OECTs (depicted by the black solid line) exhibited a linear I_D - V_G relationship. This behavior was largely attributed to the high thickness of the electrolyte layer. The linear transfer characteristic can be explained by two primary factors: (1) A thicker electrolyte layer reduced the gate capacitance, diminishing the gate's ability to modulate the channel's charge carriers (Rivnay et al., 2018). This reduced modulation made the current less responsive to changes in voltage; (2) The considerable thickness of the electrolyte necessitated a longer path for ion travel and limited ion penetration into the semiconductor channel. This can cause a delayed electrochemical response, hindering the accumulation or depletion of charge carriers needed for effective current modulation. Consequently, the reduced gate capacitance and the extended ion path in the side-gated OECTs led to a minimal impact of gate voltage changes on the drain current, demonstrating the drawbacks in this architecture.

Moreover, to further evaluate the top-gated OECTs based on a solid-state chitosan polymer electrolyte, the electrical performances of other advanced OECTs are summarized and compared in Figure 4.13 (b) as a function of the normalized g_m and onstate current (I_{on}). The chitosan-based OECTs, while displaying a moderate I_{on} when compared to similar devices, offered a compensatory advantage with their high normalized g_m . Additionally, when incorporating PEDOT:PSS as the channel material, the devices not only achieved a high on-state current but also exhibited a superior normalized g_m . This dual advantage ensured that it remained competitive and surpasses the performance of numerous state-of-the-art OECTs based on a PEDOT:PSS channel, especially when considering its low-cost material such as chitosan and accessible screen-printing method. For a more comprehensive analysis, a detailed comparison of the electrical performances of various reported OECTs is provided in Table 4.2.

Table 4.2: Comparison of the electrical performances for recently reported OECTs

Active material	Electrolyte	W/L_{ch} $(\mu m/\mu m)$	d (μm)	(V)	Ion (mA)	g _m (mS)	$I_{on}/(dW/L_{ch})$ (mA/ μ m)	$g_m/(dW/L_{ch})$ (mS/ μ m)	Ref.
PEDOT:PSS	PAA/NaCl	4000/10	0.4	0.2	0.21	0.6	0.0013	0.004	(Rashid et al., 2021)
PEDOT:PSS	Hexamethyldisilozane/melanin	11200/100	0.1	-	0.2	0.175	0.0179	0.016	(Moser et al., 2020)
PEDOT:PSS	PAN/Li ⁺ TFSI ⁻	50/0.15	50	0.6	20.53	63.45	0.0012	0.004	(Yan et al., 2020)
BBL	PSSNa	2000/200	0.25	0.7	0.05	0.18	0.02	0.072	(Melianas et al., 2020)
BBL	NaCl	39000/20	0.18	0.6	3.5	9.8	0.001	0.028	(H. Sun et al., 2018)
РЗНТ	PEO/P14 TFSI	100/0.05	0.015	1	0.65	1.2	0.0217	0.04	(Wu et al., 2022)
PEDOT:PSS	Chitosan	1500/500	4	0.6	0.19	0.416	0.0158	0.035	This work

The electrolyte PSSNa is short for poly(sodium 4-styrenesulfonate); the polymer PEO/P14 TFSI was synthesized using polyethylene oxide (PEO) and 1-butyl-1-methylpiperidinium bis(trifluoromethylsulfonyl)imide (P14 TFSI); the active material P3HT is short for poly(3-hexylthiophene2,5-diyl); poly(benzimidazobenzophenanthroline) (BBL) is an n-type ladder-type conducting

polymer. Note that to obtain a fair comparison among the reported works on OECTs, the average $I_{\rm on}$ and the average $g_{\rm m}$ were normalized by the channel dimension (dW/L).

Furthermore, the chitosan-based OECTs with top-gated configuration were evaluated to have a good long-term stability without deteriorating performances after 21 days of aging at room temperature under ambient conditions as shown in Figure 4.14 via measuring the transfer characteristics over time. It was observed that the devices could be reliably operated for 21 days with a minor decrease in g_m of about 12.89%.

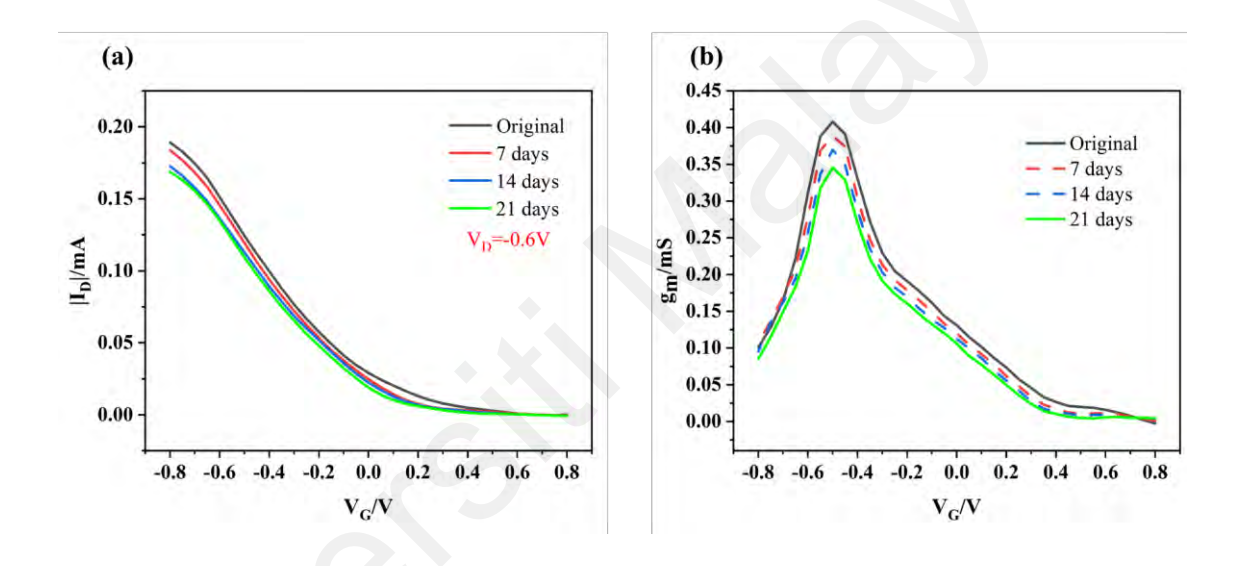


Figure 4.14: The long-term stability of chitosan-based OECTs. (a) Transfer and (b) The associated transconductance curves of chitosan-based OECTs measured over time

4.3.4 The Mechanical Properties of Flexible Chitosan-based OECTs.

Mechanical Robustness of Chitosan-based OECTs: Considering their potential application in wearable electronics, the mechanical robustness of the chitosan-based top-gated flexible OECTs was examined on flexible PET substrates. Figure 4.15 (a) presents the photograph of these OECTs bending on 3D printed semicylinders (Sun et al., 2021) with a 40 mm radius, demonstrating their flexibility. For a clearer comparison, Figure. 4.15 (b) shows the OECTs laid flat on a standard PCB board. When bent to a 40 mm radius, the flexible OECTs maintained an electrical performance similar to that of

their flat counterparts, as evidenced by their transfer and transconductance characteristics shown in Figure 4.15 (c). This consistency highlighted their suitability for flexible and wearable electronic applications.

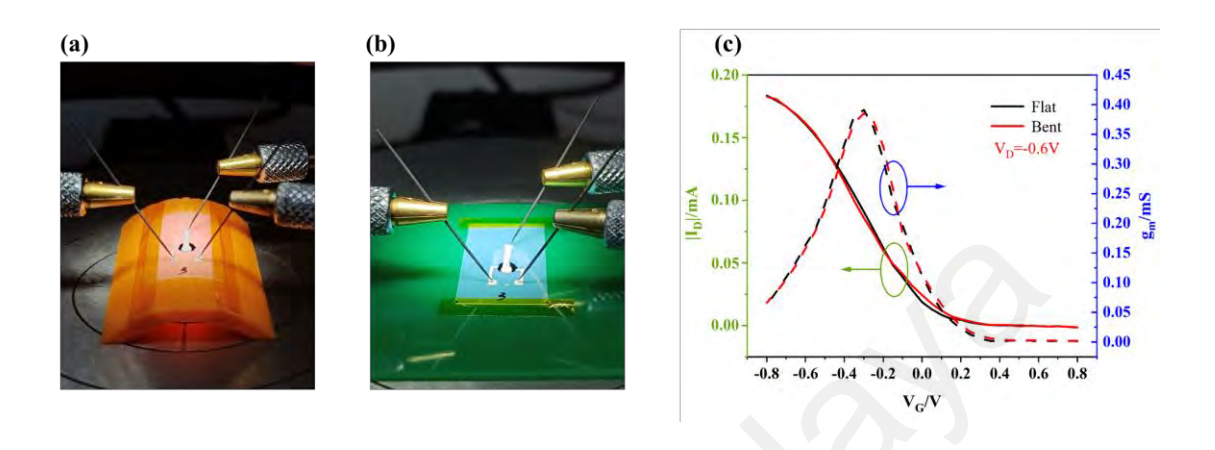


Figure 4.15: Device performance of flexible chitosan-based top-gated OECTs at two bending states. (a) Photographic images of the chitosan-based OECTs bended on a 3D printed rigid semicylinder and (b) Attached on a flat PCB board. (c) Corresponding transfer and gm characteristics for the flexible chitosan-based OECTs during bending at a bending radius of 40 mm and flat state

To gain more insights, the endurance of the flexible chitosan-based OECTs was assessed by examining their performance over a range of bending cycles (from 0 to 300) and at different bending radii (Figure 4.16). Figure 4.16 (b-c) show that both the peak I_{on} and g_{m} experienced a slight decline when the bending radius was reduced from 100 to 40 mm. Impressively, after even 300 bending cycles at a 40 mm radius, the peak I_{on} and g_{m} values were largely retained, registering at 0.132 mA and 0.359 mS, respectively. This represented only a 21% reduction in peak on-state current and a modest 5.3% decrease in g_{m} from their initial performance, indicating the excellent flexibility and reliability of the OECTs under repeated bending.

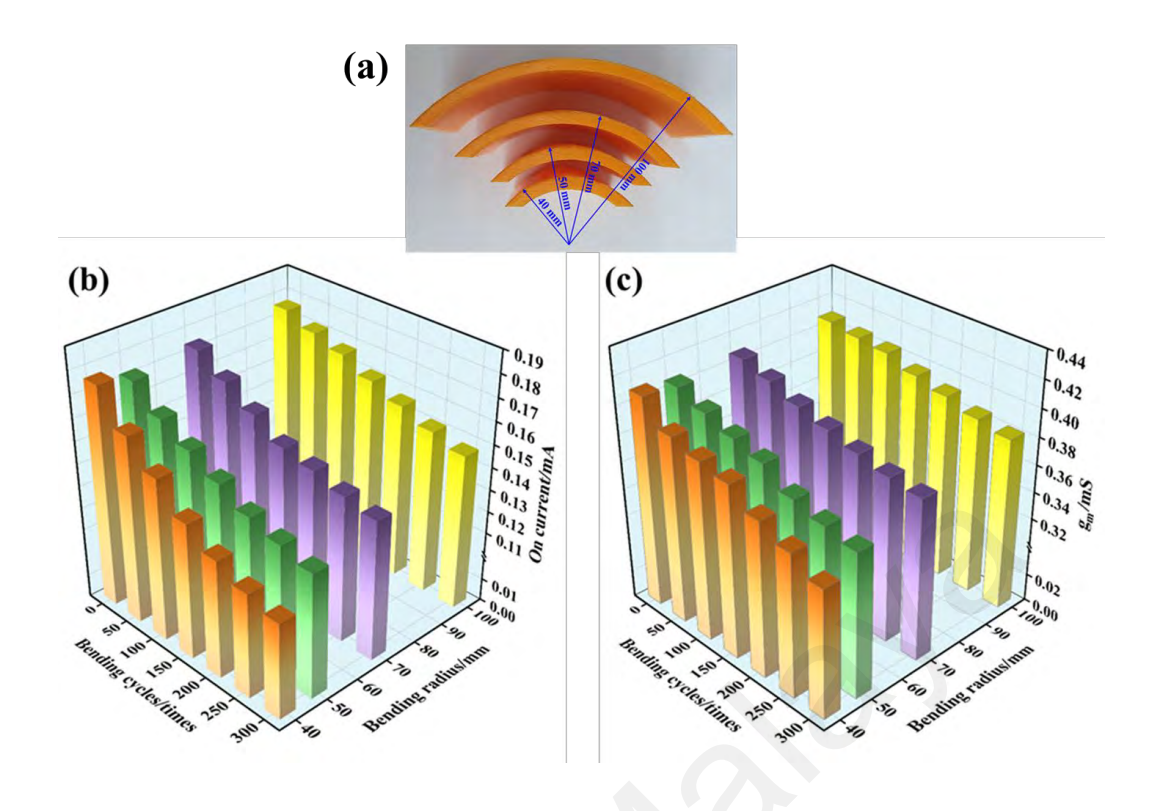


Figure 4.16: Device performance of flexible chitosan-based top-gated OECTs at different bending radii. (a) Photographic images of four 3D printed rigid semicylinders with different bending radii (R = 40, 50, 70, and 100 mm). Cycle stabilities of (b) Peak I_{on} and (c) g_m of flexible devices in terms of bending times at various bending radii (R = 40, 50, 70, and 100 mm)

In addition to bending cycles, the bending duration was a crucial factor in assessing the durability of flexible electronics (Huang et al., 2020), particularly for chitosan-based top-gated OECTs expected to remain bent for extended periods in practical applications. The durability of these devices was evaluated over bending durations ranging from 0.5 to 3 h, across four different radii of semicylinders. Both peak I_{on} and g_{m} of the flexible OECTs exhibited a gradual decrease with longer bending durations as shown in Figure 4.17. Remarkably, after even being bent for 3 h at the smallest radius of 40 mm, the devices maintained peak I_{on} and g_{m} values of 0.125 mA and 0.294 mS, respectively. These figures represented a reduction of 25% in peak I_{on} and 28% in g_{m} from their initial state, indicating the flexible OECTs' impressive mechanical durability and long-term reliability.

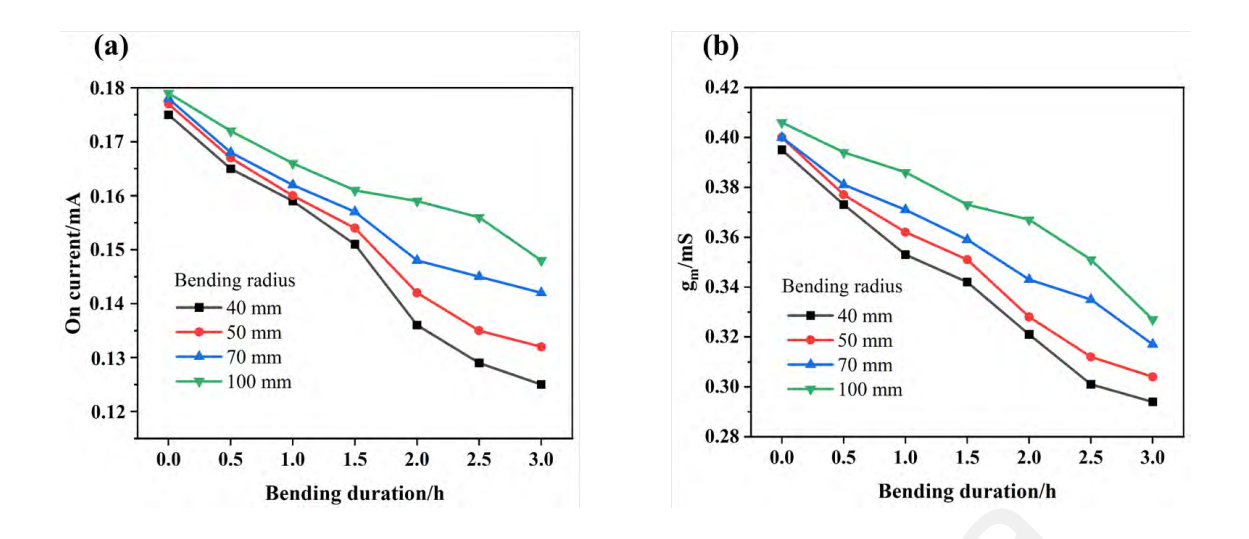


Figure 4.17: Long-term stability of the (a) peak $I_{\rm on}$ of flexible devices and (b) $g_{\rm m}$ as a function of bending duration at various bending radii (R = 40, 50, 70, and 100 mm). All measurements were performed in the chitosan-based top-gated OECTs

The remarkable mechanical robustness of the chitosan-based top-gated OECTs suggested that horizontal charge transport within the channel remained largely unaffected by in-plane cracks, which might result from strain during mechanical bending. However, the duration of bending posed a more significant challenge to the integrity of these bending OECTs.

Thermal Effect on Chitosan-based OECTs Performance: Next, the temperature effect on the ionic-electronic conduction properties of chitosan-based top-gated OECTs was investigated by analyzing their transfer characteristics at various temperatures. Figure 4.18 (a) illustrates the changes in transfer curves and the corresponding g_m values at elevated temperatures, ranging from 30 to 75 °C. With increasing operating temperatures (T), both the peak I_{on} and g_m showed a slight rise, with minimal changes in the threshold voltage (V_{Th}), as demonstrated in Figure 4.18 (b). This modest improvement in peak I_{on} and g_m was likely due to enhanced ion mobility and increased ionic conductivity of the polymer electrolyte at higher temperatures, aiding the doping and de-doping processes in the PEDOT:PSS semiconductor. Notably, at 75 °C, there was a sudden drop in both the peak I_{on} and g_m values. These results aligned with the

previously noted excellent performance of the organic channel and electrolyte materials at high temperatures (Aidit et al., 2023; Huang et al., 2020), confirming the suitability of chitosan-based OECTs for operation in environments up to human body temperature.

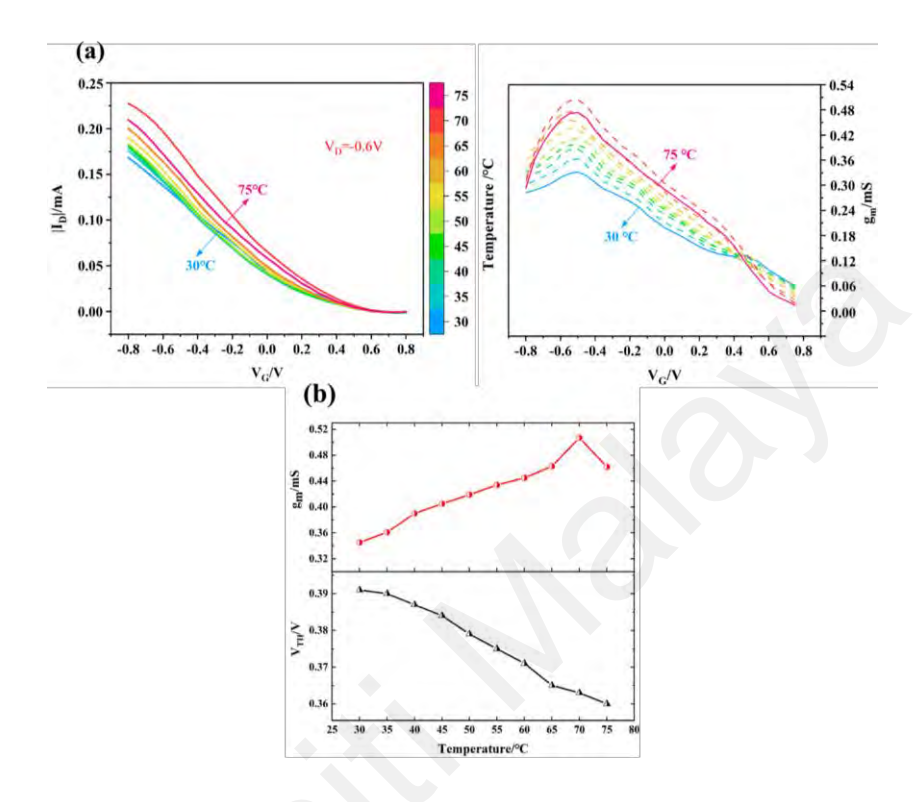


Figure 4.18: (a) Transfer characteristics and the associated transconductance of chitosan-based top-gated OECTs at different temperatures ranging from 30 to 75 °C. (b) Corresponding maximum g_m value and V_{Th} as a function of the operating temperature

4.3.5 Degradable Characterization

Current OECTs often rely on nondegradable and potentially toxic materials, posing significant environmental and ecological concerns (Lei et al., 2017; Y. Yang, X. Zhao, C. Zhang, et al., 2020). However, in chitosan-based top-gated OECTs, the polymer electrolyte used is made from low-cost, biodegradable chitosan combined with highly water-soluble dextran. Additionally, environmentally friendly PEDOT:PSS served as an active layer. As a result, our devices could physically disintegrate in water environments after fulfilling their intended functions, significantly reducing potential environmental impacts. The degradation characteristics of our chitosan-based top-gated OECTs are demonstrated in Figure 4.19. To demonstrate real-world applicability, a chitosan-based

top-gated OECT array (measuring 5 × 2 cm²) was partially buried in soil, simulating the scenario of device disposal in natural environments. In situations requiring rapid degradation and component recycling, the disintegration process can be expedited by simply dripping water on the devices (Y. Yang, X. Zhao, S. Wang, et al., 2020). Figure. 4.19 (b) shows the progressive disintegration of our OECTs after water application, illustrating how the device gradually shrinks and breaks down into smaller fragments. Remarkably, the entire chitosan-based top-gated OECT array nearly vanished within a brief 45 s period. This rapid decomposition process resulted in chitosan, dextran, and PEDOT:PSS being broken down by microorganisms and reintegrated into the ecosystem. Such efficient biodegradation not only mitigated recycling costs but also offered an ecofriendly solution to pressing environmental issues (Y. Yang, X. Zhao, C. Zhang, et al., 2020). This outcome strongly represented the potential of our chitosan and PEDOT:PSS-based OECTs for sustainable, "green" applications, particularly in neural technologies, due to their excellent biocompatibility and nontoxicity.

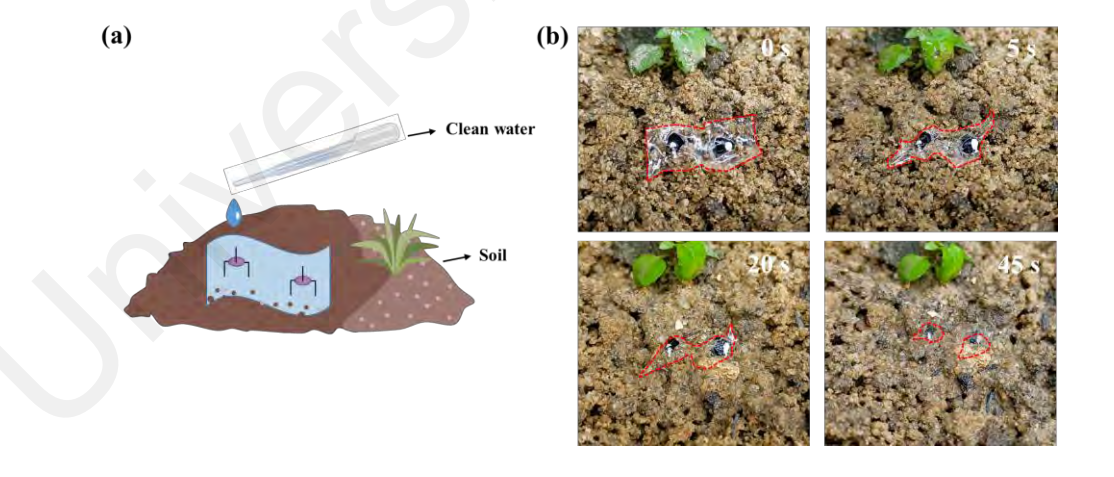


Figure 4.19: (a) Schematic illustration of the degradation experiment. (b) Degradable behavior of the self-supporting OECTs in watered damp soil in 45 s (humidity: 67%, temperature: 30 °C)

4.3.6 Optimization of Flexible Chitosan-based OECTs

Effect of Ethylene Glycol (EG) Doping in PEDOT:PSS on Chitosan-based OECTs: The conductivity of the active material PEDOT:PSS is crucial in determining

key performance metrics of the chitosan-based OECTs, such as the $I_{\rm on}/I_{\rm off}$ ratio, transconductance, operating voltage, and stability. A common method to enhance PEDOT:PSS conductivity was the addition of ethylene glycol (EG). EG works by disrupting the hydrogen bonds within the PSS matrix, leading to increased swelling in PEDOT-rich domains and consequently improved charge carrier transport (Kim et al., 2011). Additionally, EG doping benefits the film's morphology, creating a smoother surface (Wei et al., 2013), which is crucial for the consistent performance of the OECTs. To explore the impact of PEDOT:PSS conductivity on the device performance, the concentration of EG doping was varied. Figure 4.20 (a) illustrates how the sheet resistance ($R_{\rm sq}$) of the PEDOT:PSS film changed with EG doping. $R_{\rm sq}$ was a common measure of resistance of the thin PEDOT:PSS films: a lower $R_{\rm sq}$ indicated a higher electrical conductivity of the PEDOT:PSS layer, which facilitated efficient charge transport within the OECTs.

Strikingly, there was a reduction in normalized $R_{sq}/R_{sq}(0)$ by up to 72% when the EG concentration increased from 2 to 5%. This decrease implied that with the increase in EG doping concentration, the R_{sq} of PEDOT:PSS films decreased significantly, which was due to the fact that EG as a plasticizer within the PEDOT:PSS matrix facilitated an efficient connectivity among PEDOT-rich grains and optimized phase separation in the PEDOT:PSS film (Cui et al., 2019), thereby decreasing the sheet resistance and promoting the conductivity of PEDOT:PSS.

Increasing the concentration of EG in the PEDOT:PSS film led to a rise of peak on-state current in chitosan-based top-gated OECTs, from 0.07 to 0.18 mA, as illustrated in Figure 4.20 (b). This increase was attributed to the enhanced conductivity of the PEDOT:PSS film due to EG doping. However, when the EG concentration reached 6%, the device's transfer characteristic unexpectedly exhibited linear behavior, resembling a

resistor with apparent ohmic characteristics, rather than the typical behavior expected of OECTs. This linear I_D – V_G relationship was believed to be a consequence of the excessive EG doping, which resulted in an overly conductive PEDOT:PSS channel. The heightened conductivity reduced the gating effect, leading to inadequate modulation of the channel by the gate voltage. Besides, at an EG concentration of 5%, the g_m of the device experienced a slight decline, as shown in Figure 4.20 (c). This reduction was due to disruption of the PEDOT:PSS microstructure caused by the high EG concentration, resulting in an overly swollen polymer matrix and potential phase separation. Through this investigation, it was determined that a 4% concentration of EG represented the optimal balance for these chitosan-based top-gated OECTs, effectively enhancing the conductivity of PEDOT:PSS while improving the overall device performance.

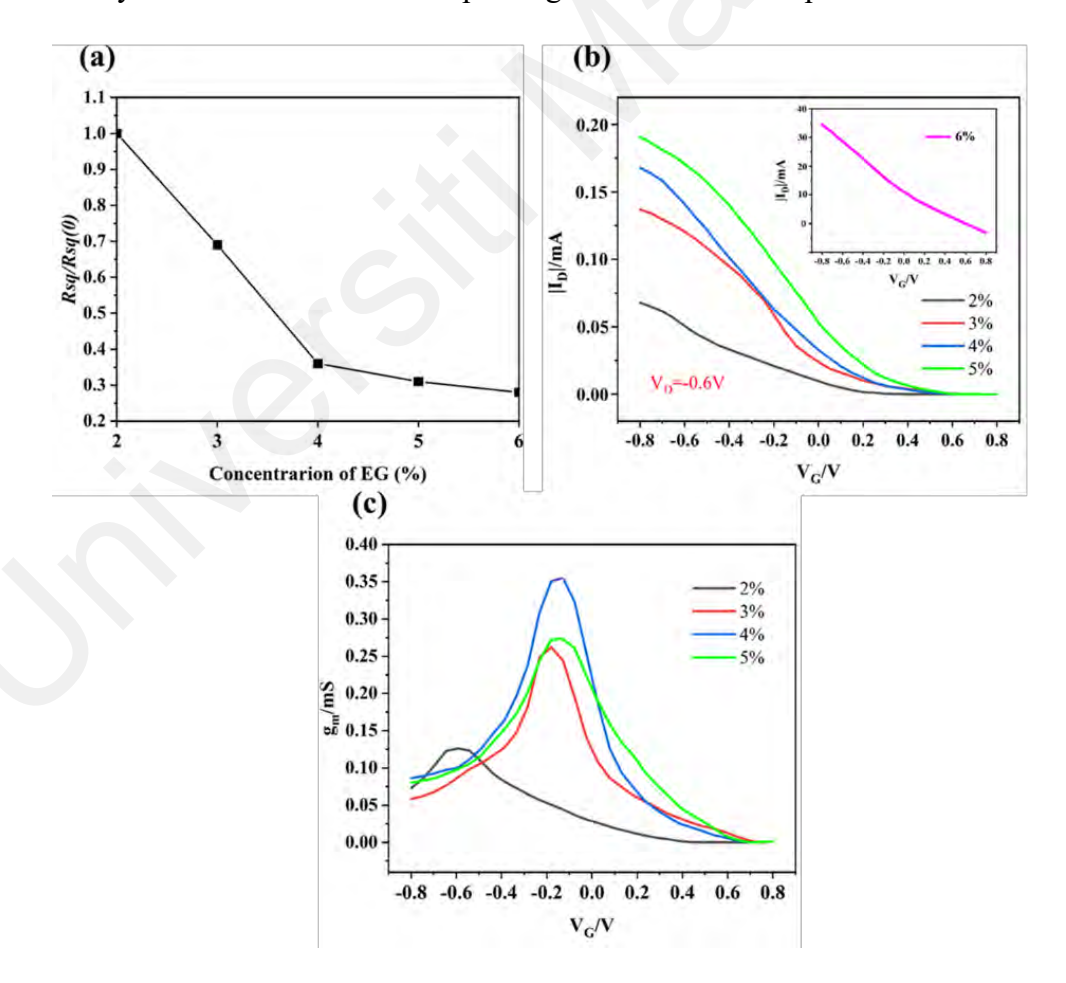


Figure 4.20: Effect of EG doping on the device performance. (a) Normalized $R_{sq}/R_{sq}(0)$ of the PEDOT:PSS film as a function of EG concentrations. (b) Transfer characteristics and (c) Associated transconductance of chitosan-based OECTs under different EG concentrations as a function of gate voltage

Effect of Salt (LiClO₄) Addition to The Chitosan Polymer Electrolyte on Chitosan-based OECTs: Following that, the incorporation of salts in the electrolyte was critical in chitosan-based top-gated OECTs for modulating the current through ion injection or removal. Consequently, the weight percentage of the salt played a crucial role, affecting the device's operational ions, efficiency, stability, and reliability (Timachova et al., 2015). It explored the impact of lithium perchlorate (LiClO₄) salt's morphology and ionic conductivity on the device performance by varying its weight percentage in the electrolyte. Figure 4.21 (a-c) displays the FESEM images, illustrating the effects of incorporating varying weight percentages of LiClO₄ salt into the chitosanbased electrolyte films. As the weight percentage of LiClO₄ increased, the electrolyte surface became rougher, characterized by protruding salt particles visible as small white specks. This altered surface morphology reflected changes in the blend of electrolyte films. Correspondingly, the measured DC ionic conductivity of the electrolyte film showed a significant increase, from 1.27×10^{-5} to 5.16×10^{-3} S cm⁻¹, with the rise of LiClO₄ weight percentage (Aziz et al., 2019). This could be explained by the fact that a higher salt concentration in the electrolyte provided more ions and cations, thereby increasing the availability of charge carriers. This enhancement, in turn, facilitated faster ion migration, ultimately dominating the ionic conductivity of the chitosan-based electrolyte.

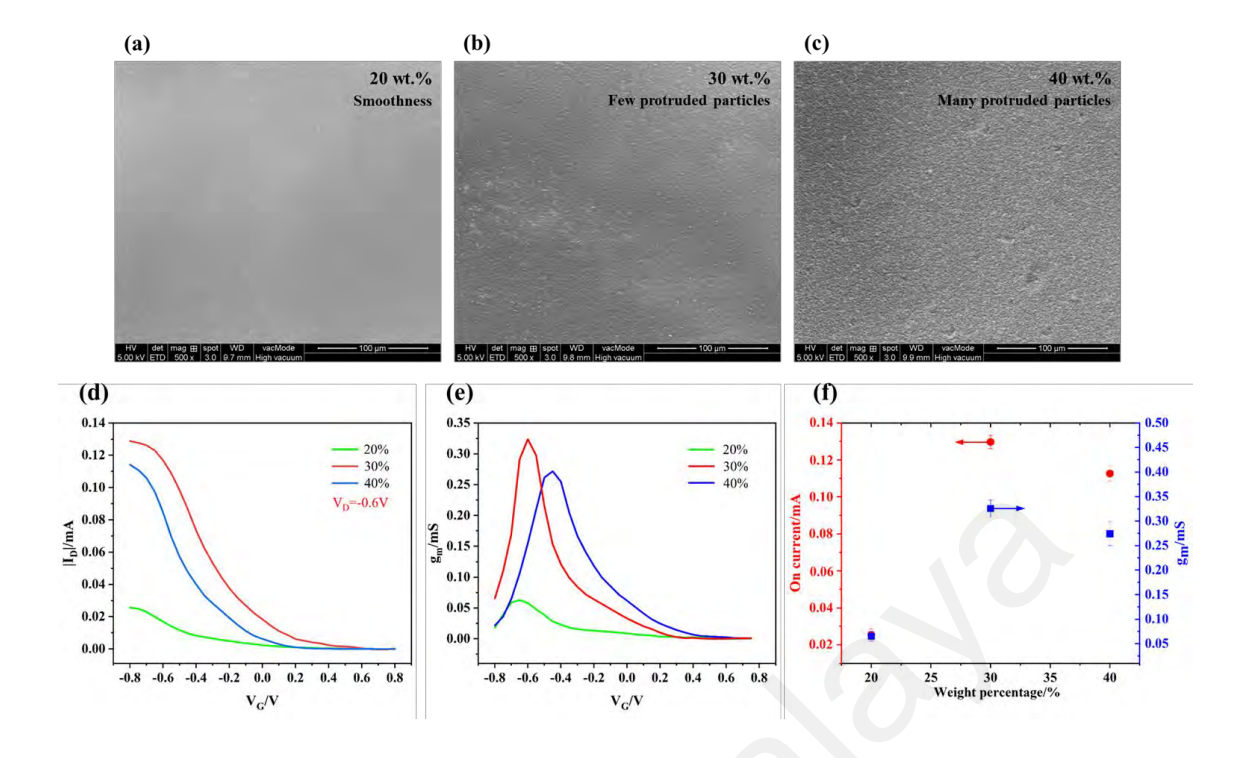


Figure 4.21: Effect of different weight percentages of LiClO₄ on device performance. FESEM images of LiClO₄ with weight percentages of (a) 20 wt%, (b) 30 wt%, and (c) 40 wt%. (d) Transfer characteristics and (e) Corresponding transconductance of chitosan-based OECTs with different LiClO₄ weight percentages as a function of gate voltage. (f) *I*_{0n} and *g*_m of the devices with different LiClO₄ weight percentages

Increasing the weight percentage of LiClO₄ in the electrolyte film led to an increase in peak I_{on} of devices, which varied from 0.026 to 0.131 mA seen in Figure 4.21 (d). This enhancement was attributed to the electrolyte's heightened ionic conductivity. Notably, the highest g_m was reached at a LiClO₄ concentration of 30 wt% shown in Figure 4.21 (e). This peak performance was due to the increased availability of charge carriers, which accelerated ion migration and enhanced the gate capacitance. The moderate amount of LiClO₄ created an optimal network within the amorphous regions of the electrolyte films, facilitating efficient ion movement. However, when the LiClO₄ concentration was further increased to 40 wt%, there was a decline in both the I_{on}/I_{off} ratio and transconductance, as depicted in Figure 4.21 (f). This decrease in device performance was linked to a reduction in ionic conductivity. At higher concentrations, the occurrence of salt recrystallization (Shukur & Kadir, 2015) became more prevalent,

reducing the number of free ions available for conduction. The recrystallization process had a limited capacity to integrate additional salts, leading to a diminished device efficiency. For more comprehensive insights, Table 4.3 presents the detailed electrical parameters of devices across various LiClO₄ weight percentages.

Table 4.3: Electrical properties of OECTs with different LiClO₄ weight percentage

Weight percentage (wt%)	Ionic conductivity (S cm ⁻¹)	Ion (mA)	g_m (mS)
20	1.27×10^{-5}	0.026	0.065
30	5.62 × 10 ⁻⁴	0.131	0.325
40	5.16×10^{-3}	0.113	0.275

4.4 Summary

The device performance of OECTs were analyzed in this section, which consist of the analysis on rigid OECTs on Si wafer substrate and flexible OECTs on PET substrate with chitosan electrolyte. The study enabled researchers to understand in details the potential performance of OECTs based on natural polymer and its optimization considerations by examining the impact of experimental conditions and material composition on critical electrical performance including, $I_{\rm on}$, $I_{\rm on}$ / $I_{\rm off}$ ratio, $g_{\rm m}$, $V_{\rm Th}$, etc.

In this work, it has been demonstrated that Si wafer can be effectively utilized with both organic and inorganic materials to fabricate OECTs. Among the rigid OECTs studied, the chitosan-based OECT exhibited a uniformly smooth surface. However, the errors of manual screen-printing and inadequate adhesion between the Si wafer and the chitosan electrolyte film might weaken the electric double layer (EDL) effect. Despite these issues, p-type transfer curves were observed in all three types of OECTs, and the chitosan-based OECT showed relatively superior performance characteristics, including an I_{on}/I_{off} ratio of 3.5×10^6 and a low threshold voltage (V_{Th}) of - 0.7 V. To optimize the OECTs, the ideal spin-coating parameter was identified as 1000 rpm for 60 s, forming uniform films on Si wafers pre-treated with UV curing. Additionally, maintaining an

annealing temperature of 80 °C for 10 to 15 min achieved optimal film formation for the polymer electrolyte without compromising its integrity. These adjustments collectively enhanced the performance and reliability of the polymer electrolyte-based OECTs.

Building on the excellent performance of chitosan-based electrolytes, a new flexible OECT utilizing a solid-state chitosan electrolyte was investigated, marking a significant first in the field. These flexible chitosan-based OECTs operated at a low driving voltage of 0.6 V, achieving an on-state current of 0.19 \pm 0.03 mA, a high on/off ratio of 0.3 \times 10^3 , and an impressive transconductance of up to 0.419 ± 0.05 mS. Besides, the study highlighted the critical role of ethylene glycol (EG) doping concentration in PEDOT:PSS and the salt weight percentage in the electrolyte on the electrical performance of the OECTs. The flexible chitosan-based OECTs demonstrated exceptional mechanical robustness, enduring various bending radii and durations without performance degradation. Furthermore, the devices maintained their electrical integrity across a broad temperature range, from 30 to 75 °C, underscoring their versatility. Importantly, the chitosan-based OECTs were capable of natural degradation without releasing harmful byproducts, significantly reducing environmental pollution and recycling costs. This research not only offered a viable approach to crafting flexible and eco-friendly OECTs but also opened new possibilities for their application in highperformance biosensors, digital logic circuits, and neuromorphic devices.

CHAPTER 5: CONCLUSION AND FUTURE WORKS

Organic electrochemical transistors (OECTs) are capable of emulating artificial synapses due to the similarity between the ion movement involved in the formation of an electrical double layer (EDL) and the process of information transmission in biological synapses. In OECTs, the gate is considered analogous to the pre-synapse, while the source-drain electrodes and the PEDOT:PSS channel represent the post-synapse. The chitosan-based electrolyte corresponds to the synaptic cleft, and neurotransmitters are similar to the ions that convey information. Consequently, an equivalent chitosan-gated flexible OECTs based on PEDOT:PSS has been proposed and developed as a new synaptic transistor. Hence, when a spike potential (V_G) is applied to the presynaptic gate in chitosan-based OECTs, the postsynaptic response can be detected through the reading of the voltage (V_D), resulting in an operational current (I_D), which can be seen as an excitatory postsynaptic current (EPSC) created in the biological synapse.

In this study, a biodegradable, flexible OECT based on a solid-state biopolymer electrolyte was introduced. The device featured a top-gate and bottom-contact architecture, comprising, from top to bottom, an Ag gate, a solid-state chitosan electrolyte, a PEDOT:PSS organic channel, and Ag source and drain electrodes. To optimize the device performance, various experimental conditions were compared, including the use of different biopolymers for the electrolyte, variations in spin-coating speed and duration, as well as different annealing temperatures and times. Through these comparisons, the most suitable polymer electrolyte was selected, leading to enhanced device performance. Furthermore, the impact of different structural configurations on the electrical performance of flexible OECTs was examined. Bending and temperature tests were conducted to assess the mechanical properties of the device.

The degradability of the organic device was confirmed through water solubility tests. By adjusting the material composition of each component in the OECT, such as incorporating EG into PEDOT:PSS and adding salt to the electrolyte, the device performance was further optimized.

In conclusion, polymer electrolytes based on natural material have been effectively demonstrated to work well with inorganic silicon wafer to be OECTs. This result was evidenced by the characteristic p-type transfer curves displayed by three types of devices, indicating efficient charge carrier mobility and effective interface interaction between the biopolymer electrolyte and the silicon substrate. Among various types of polymer electrolytes used, the chitosan-based electrolyte OECTs exhibited outstanding electrical properties, characterized by a high $I_{\rm on}/I_{\rm off}$ ratio of 3.5 \times 10⁶ and a low threshold voltage (V_{Th}) of - 0.7 V. These superior characteristics are attributed to the electrolyte's smooth and uniform surface and unsolid microstructure, which facilitates efficient ion transport and minimizes interface resistance. Furthermore, the top-gated flexible OECTs utilizing a chitosan-based compound as the gate electrolyte exhibited superior performance, as evidenced by their transfer and transconductance characteristics. These characteristics include an on-state current of 0.19 ± 0.03 mA, a high on/off current ratio of 0.3×10^3 , and a significant transconductance of 0.416 ± 0.05 mS. Such parameters highlighted the effective modulation of the channel conductivity and responsive electrical behavior of the devices. The flexible OECTs demonstrated remarkable endurance and mechanical robustness, maintaining operational stability after 300 bending cycles and long bending duration, and exposure to temperatures ranging from 30 to 75 °C. This durability demonstrated their suitability for applications in harsh environments characterized by physical stress and temperature fluctuations. Significantly, the flexible chitosan-based OECTs disintegrated through water solubility tests without releasing toxic byproducts. This degradability positioned these devices as a

sustainable alternative for bioelectronics and wearable technologies that demand ecological compatibility alongside technological functionality.

It is suggested that the optimization of channel dimensions is fundamental to enhancing the performance of OECTs. Future work should focus on systematically investigating the effects of changes of channel length, width, and thickness on device functionality. Building on this, another expand work is the synaptic behaviors simulation, such as excitatory postsynaptic current (EPSC), paired-pulse facilitation (PPF), depression (PPD), and short-term plasticity (STP). These studies will enhance the ability of OECTs to mimic neural responses, supporting their integration into neuromorphic systems and bio-inspired computing architectures. Additionally, exploring the applications of biocompatible OECTs in biomedical devices, particularly in biosensing like glucose monitoring, will develop real-time monitoring of physiological parameters. This could lead to significant advancements in personalized healthcare and effective disease management.

REFERENCES

- Ahmad, Z., Azman, A. W., Buys, Y. F., & Sarifuddin, N. (2021). Mechanisms for doped PEDOT: PSS electrical conductivity improvement. *Materials Advances*, 2(22), 7118-7138.
- Aidit, S., Rezali, F., Nor, N., Yusoff, N., Ma, L.-Y., Hatta, S., & Soin, N. (2023). Hydrothermal synthesis of zinc oxide/PEDOT: PSS composite for flexible temperature sensor application. *Flexible and Printed Electronics*, 8(2), 025008.
- Aziz, S. B., Dannoun, E. M., Murad, A. R., Mahmoud, K. H., Brza, M., Nofal, M. M., Elsayed, K. A., Abdullah, S. N., Hadi, J. M., & Kadir, M. (2022). Influence of scan rate on CV Pattern: Electrical and electrochemical properties of plasticized Methylcellulose: Dextran (MC: Dex) proton conducting polymer electrolytes. *Alexandria Engineering Journal*, 61(8), 5919-5937.
- Aziz, S. B., Hamsan, M. H., Kadir, M. F., Karim, W. O., & Abdullah, R. M. (2019). Development of polymer blend electrolyte membranes based on chitosan: Dextran with high ion transport properties for EDLC application. *International journal of molecular sciences*, 20(13), 3369.
- Backus, J. (1978). Can programming be liberated from the von Neumann style? A functional style and its algebra of programs. *Communications of the ACM*, 21(8), 613-641.
- Berggren, M., Nilsson, D., & Robinson, N. D. (2007). Organic materials for printed electronics. *Nature materials*, 6(1), 3-5.
- Bernards, D. A., & Malliaras, G. G. (2007). Steady state and transient behavior of organic electrochemical transistors. *Advanced Functional Materials*, 17(17), 3538-3544.
- Braendlein, M., Lonjaret, T., Leleux, P., Badier, J. M., & Malliaras, G. G. (2017). Voltage amplifier based on organic electrochemical transistor. *Advanced science*, 4(1), 1600247.
- Campana, A., Cramer, T., Simon, D., Berggren, M., & Biscarini, F. (2014). Electrocardiographic recording with conformable organic electrochemical transistor fabricated on resorbable bioscaffold. *Advanced Materials*, 26(23), 3874-3878.
- Cea, C., Spyropoulos, G. D., Jastrzebska-Perfect, P., Ferrero, J. J., Gelinas, J. N., & Khodagholy, D. (2020). Enhancement-mode ion-based transistor as a comprehensive interface and real-time processing unit for in vivo electrophysiology. *Nature materials*, 19(6), 679-686.
- Chae, S. S., Choi, W. J., Yang, C.-S., Lee, T. I., & Lee, J.-O. (2016). Simple interface engineering of graphene transistors with hydrophobizing stamps. *ACS Applied Materials & Interfaces*, 8(23), 14307-14312.

- Chen, J., Li, E., Yan, Y., Yang, Q., Cao, S., Zhong, J., Chen, H., & Guo, T. (2019). Flexible metal oxide synaptic transistors using biomass-based hydrogel as gate dielectric. *Journal of Physics D: Applied Physics*, 52(48), 484002.
- Chen, S., Surendran, A., Wu, X., & Leong, W. L. (2020). Contact modulated ionic transfer doping in all solid state organic electrochemical transistor for ultra high sensitive tactile perception at low operating voltage. *Advanced Functional Materials*, 30(51), 2006186.
- Cho, J. H., Lee, J., He, Y., Kim, B., Lodge, T. P., & Frisbie, C. D. (2008). High capacitance ion gel gate dielectrics with faster polarization response times for organic thin film transistors. *Advanced materials*, 20(4), 686-690.
- Cho, J. H., Lee, J., Xia, Y., Kim, B., He, Y., Renn, M. J., Lodge, T. P., & Daniel Frisbie, C. (2008). Printable ion-gel gate dielectrics for low-voltage polymer thin-film transistors on plastic. *Nature materials*, 7(11), 900-906.
- Colomer, M. (2011). Proton transport, water uptake and hydrogen permeability of nanoporous hematite ceramic membranes. *Journal of Power Sources*, 196(20), 8280-8285.
- Cramer, T., Kyndiah, A., Murgia, M., Leonardi, F., Casalini, S., & Biscarini, F. (2012). Double layer capacitance measured by organic field effect transistor operated in water. *Applied Physics Letters*, 100(14).
- Cui, H.-Q., Peng, R.-X., Song, W., Zhang, J.-F., Huang, J.-M., Zhu, L.-Q., & Ge, Z.-Y. (2019). Optimization of ethylene glycol doped PEDOT: PSS transparent electrodes for flexible organic solar cells by drop-coating method. *Chinese Journal of Polymer Science*, 37, 760-766.
- Dai, S., Chu, Y., Liu, D., Cao, F., Wu, X., Zhou, J., Zhou, B., Chen, Y., & Huang, J. (2018). Intrinsically ionic conductive cellulose nanopapers applied as all solid dielectrics for low voltage organic transistors. *Nature communications*, *9*(1), 2737.
- Dannoun, E. M., Aziz, S. B., Abdullah, S. N., Nofal, M. M., Mahmoud, K. H., Murad, A. R., Abdullah, R. M., & Kadir, M. F. (2021). Characteristics of plasticized lithium ion conducting green polymer blend electrolytes based on CS: dextran with high energy density and specific capacitance. *Polymers*, *13*(21), 3613.
- Dathbun, A., Kim, Y., Choi, Y., Sun, J., Kim, S., Kang, B., Kang, M. S., Hwang, D. K., Lee, S., & Lee, C. (2019). Selectively metallized 2D materials for simple logic devices. *ACS Applied Materials & Interfaces*, 11(20), 18571-18579.
- [Record #12 is using a reference type undefined in this output style.]
- Du, L., He, D., Liu, Y., Xu, M., Wang, Q., Xin, Q., & Song, A. (2018). Low-voltage, flexible IGZO transistors gated by PSSNa electrolyte. *IEEE Electron Device Letters*, 39(9), 1334-1337.
- Emelyanov, A., Lapkin, D., Demin, V., Erokhin, V., Battistoni, S., Baldi, G., Dimonte, A., Korovin, A., Iannotta, S., & Kashkarov, P. (2016). First steps towards the

- realization of a double layer perceptron based on organic memristive devices. *AIP advances*, 6(11).
- Fu, Y., Kong, L.-a., Chen, Y., Wang, J., Qian, C., Yuan, Y., Sun, J., Gao, Y., & Wan, Q. (2018). Flexible neuromorphic architectures based on self-supported multiterminal organic transistors. *ACS applied materials & interfaces*, 10(31), 26443-26450.
- Giovannitti, A., Rashid, R. B., Thiburce, Q., Paulsen, B. D., Cendra, C., Thorley, K., Moia, D., Mefford, J. T., Hanifi, D., & Weiyuan, D. (2020). Energetic control of redox active polymers toward safe organic bioelectronic materials. *Advanced Materials*, 32(16), 1908047.
- Gongadze, E., Van Rienen, U., & Iglič, A. (2011). Generalized stern models of the electric double layer considering the spatial variation of permittvity and finite size of ions in saturation regime. *Cellular & molecular biology letters*, 16, 576-594.
- Han, H., Yu, H., Wei, H., Gong, J., & Xu, W. (2019). Recent progress in three terminal artificial synapses: from device to system. *Small*, 15(32), 1900695.
- Han, S., Yu, S., Hu, S., Chen, H.-j., Wu, J., & Liu, C. (2021). A high endurance, temperature-resilient, and robust organic electrochemical transistor for neuromorphic circuits. *Journal of Materials Chemistry C*, 9(35), 11801-11808.
- Huang, H., Han, L., Li, J., Fu, X., Wang, Y., Yang, Z., Xu, X., Pan, L., & Xu, M. (2020). Super-stretchable, elastic and recoverable ionic conductive hydrogel for wireless wearable, stretchable sensor. *Journal of Materials Chemistry A*, 8(20), 10291-10300.
- Huang, W., Chen, J., Wang, G., Yao, Y., Zhuang, X., Pankow, R. M., Cheng, Y., Marks, T. J., & Facchetti, A. (2021). Dielectric materials for electrolyte gated transistor applications. *Journal of Materials Chemistry C*, *9*(30), 9348-9376.
- Jang, S., Jee, E., Choi, D., Kim, W., Kim, J. S., Amoli, V., Sung, T., Choi, D., Kim, D. H., & Kwon, J.-Y. (2018). Ultrasensitive, low-power oxide transistor-based mechanotransducer with microstructured, deformable ionic dielectrics. *ACS Applied Materials & Interfaces*, 10(37), 31472-31479.
- Jo, Y. J., Kim, H., Ok, J., Shin, Y. J., Shin, J. H., Kim, T. H., Jung, Y., & Kim, T. i. (2020). Biocompatible and biodegradable organic transistors using a solid state electrolyte incorporated with choline based ionic liquid and polysaccharide. *Advanced Functional Materials*, 30(29), 1909707.
- Kadir, M. F. Z. (2021). Non-faradaic-based supercapacitor fabricated with fish skin gelatin biopolymer electrolyte. *Ionics*, 27, 2219-2229.
- Kahng, D. (1960). Silicon-silicon dioxide field induced surface devices. IRE Solid State Device Res. Conf.,
- Keene, S. T., Fogarty, D., Cooke, R., Casadevall, C. D., Salleo, A., & Parlak, O. (2019). Wearable organic electrochemical transistor patch for multiplexed sensing of

- calcium and ammonium ions from human perspiration. Advanced healthcare materials, 8(24), 1901321.
- Kim, H.-S., Park, H., & Cho, W.-J. (2022). Biocompatible casein electrolyte-based electric-double-layer for artificial synaptic transistors. *Nanomaterials*, *12*(15), 2596.
- Kim, S., Choi, B., Lim, M., Yoon, J., Lee, J., Kim, H.-D., & Choi, S.-J. (2017). Pattern recognition using carbon nanotube synaptic transistors with an adjustable weight update protocol. *ACS nano*, 11(3), 2814-2822.
- Kim, Y., Chortos, A., Xu, W., Liu, Y., Oh, J. Y., Son, D., Kang, J., Foudeh, A. M., Zhu, C., & Lee, Y. (2018). A bioinspired flexible organic artificial afferent nerve. *Science*, 360(6392), 998-1003.
- Kim, Y. H., Sachse, C., Machala, M. L., May, C., Müller Meskamp, L., & Leo, K. (2011). Highly conductive PEDOT: PSS electrode with optimized solvent and thermal post treatment for ITO free organic solar cells. *Advanced Functional Materials*, 21(6), 1076-1081.
- Kong, L.-a., Sun, J., Qian, C., Fu, Y., Wang, J., Yang, J., & Gao, Y. (2017). Long-term synaptic plasticity simulated in ionic liquid/polymer hybrid electrolyte gated organic transistors. *Organic Electronics*, 47, 126-132.
- Koutsouras, D. A., Prodromakis, T., Malliaras, G. G., Blom, P. W., & Gkoupidenis, P. (2019). Functional connectivity of organic neuromorphic devices by global voltage oscillations. *Advanced Intelligent Systems*, *I*(1), 1900013.
- Lai, D., Li, E., Yan, Y., Liu, Y., Zhong, J., Lv, D., Ke, Y., Chen, H., & Guo, T. (2019). Gelatin-hydrogel based organic synaptic transistor. *Organic Electronics*, 75, 105409.
- Lee, K. H., Kang, M. S., Zhang, S., Gu, Y., Lodge, T. P., & Frisbie, C. D. (2012). "Cut and stick" rubbery ion gels as high capacitance gate dielectrics. *Advanced materials*, 24(32), 4457-4462.
- Lee, K. H., Zhang, S., Lodge, T. P., & Frisbie, C. D. (2011). Electrical impedance of spin-coatable ion gel films. *The Journal of Physical Chemistry B*, 115(13), 3315-3321.
- Lee, Y., Oh, J. Y., Xu, W., Kim, O., Kim, T. R., Kang, J., Kim, Y., Son, D., Tok, J. B.-H., & Park, M. J. (2018). Stretchable organic optoelectronic sensorimotor synapse. *Science advances*, 4(11), eaat7387.
- Lee, Y., Park, H.-L., Kim, Y., & Lee, T.-W. (2021). Organic electronic synapses with low energy consumption. *Joule*, 5(4), 794-810.
- Lee, Y. R., Trung, T. Q., Hwang, B.-U., & Lee, N.-E. (2020). A flexible artificial intrinsic-synaptic tactile sensory organ. *Nature communications*, 11(1), 2753.
- Lei, T., Guan, M., Liu, J., Lin, H.-C., Pfattner, R., Shaw, L., McGuire, A. F., Huang, T.-C., Shao, L., & Cheng, K.-T. (2017). Biocompatible and totally disintegrable

- semiconducting polymer for ultrathin and ultralightweight transient electronics. *Proceedings of the National Academy of Sciences*, 114(20), 5107-5112.
- Li, W., Liu, Q., Zhang, Y., Li, C. a., He, Z., Choy, W. C., Low, P. J., Sonar, P., & Kyaw, A. K. K. (2020). Biodegradable materials and green processing for green electronics. *Advanced materials*, 32(33), 2001591.
- Li, X., Liu, Y., Zhang, J., Wu, F., Hu, M., & Yang, H. (2022). Flexible artificial synapses based on field effect transistors: From materials, mechanics towards applications. *Advanced Intelligent Systems*, 4(9), 2200015.
- Liang, Y., Guo, T., Zhou, L., Offenhäusser, A., & Mayer, D. (2020). Label-free split aptamer sensor for femtomolar detection of dopamine by means of flexible organic electrochemical transistors. *Materials*, 13(11), 2577.
- Liao, C., Mak, C., Zhang, M., Chan, H. L., & Yan, F. (2015). Flexible organic electrochemical transistors for highly selective enzyme biosensors and used for saliva testing. *Adv. Mater*, 27(4), 676-681.
- Lu, P.-P., Shang, D.-S., Yang, C.-S., & Sun, Y. (2020). An organic synaptic transistor with Nafion electrolyte. *Journal of Physics D: Applied Physics*, 53(48), 485102.
- Luo, C., Zhang, Y., Shuai, W., He, K., Li, M., Tao, R., Chen, D., Fan, Z., Zhang, B., & Zhou, X. (2023). Ferroelectric Hf0. 5Zr0. 5O2-gated synaptic transistors with large conductance dynamic range and multilevel states. *Science China Materials*, 66(6), 2372-2382.
- Mao, J.-Y., Hu, L., Zhang, S.-R., Ren, Y., Yang, J.-Q., Zhou, L., Zeng, Y.-J., Zhou, Y., & Han, S.-T. (2019). Artificial synapses emulated through a light mediated organic inorganic hybrid transistor. *Journal of Materials Chemistry C*, 7(1), 48-59.
- Markram, H., Gerstner, W., & Sjöström, P. J. (2012). Spike-timing-dependent plasticity: a comprehensive overview. *Frontiers in synaptic neuroscience*, 4, 2.
- Marquez, A. V., McEvoy, N., & Pakdel, A. (2020). Organic electrochemical transistors (OECTs) toward flexible and wearable bioelectronics. *Molecules*, 25(22), 5288.
- Mead, C. (1990). Neuromorphic electronic systems. *Proceedings of the IEEE*, 78(10), 1629-1636.
- Melianas, A., Quill, T., LeCroy, G., Tuchman, Y., Loo, H. v., Keene, S., Giovannitti, A., Lee, H., Maria, I., & McCulloch, I. (2020). Temperature-resilient solid-state organic artificial synapses for neuromorphic computing. *Science advances*, 6(27), eabb2958.
- Menon, P., Hatta, S., & de Souza, M. (2023). After 75 Years of the Transistor: An Age of Neuromorphic Computing [Women in Electronic Devices]. *IEEE Electron Devices Magazine*, *I*(2), 57-58.

- Min, S.-Y., & Cho, W.-J. (2020). CMOS-compatible synaptic transistor gated by chitosan electrolyte-Ta2O5 hybrid electric double layer. *Scientific Reports*, 10(1), 15561.
- Mohamed, A., Shukur, M., Kadir, M., & Yusof, Y. (2020). Ion conduction in chitosanstarch blend based polymer electrolyte with ammonium thiocyanate as charge provider. *Journal of Polymer Research*, 27, 1-14.
- Moser, M., Hidalgo, T. C., Surgailis, J., Gladisch, J., Ghosh, S., Sheelamanthula, R., Thiburce, Q., Giovannitti, A., Salleo, A., & Gasparini, N. (2020). Side chain redistribution as a strategy to boost organic electrochemical transistor performance and stability. *Advanced materials*, 32(37), 2002748.
- Nagata, R., Yanagi, Y., Fujii, S., Kataura, H., & Nishioka, Y. (2015). Highly conductive DMSO-treated PEDOT: PSS electrodes applied to flexible organic solar cells. *IEICE Transactions on Electronics*, 98(5), 411-421.
- Nguyen, T. D., Trung, T. Q., Lee, Y., & Lee, N.-E. (2022). Stretchable and stable electrolyte gated organic electrochemical transistor synapse with a nafion membrane for enhanced synaptic properties. *Advanced Engineering Materials*, 24(4), 2100918.
- Palumbiny, C. M., Heller, C., Schaffer, C. J., K rstgens, V., Santoro, G., Roth, S. V., & M ller-Buschbaum, P. (2014). Molecular reorientation and structural changes in cosolvent-treated highly conductive PEDOT: PSS electrodes for flexible indium tin oxide-free organic electronics. *The Journal of Physical Chemistry C*, 118(25), 13598-13606.
- Park, S., Heo, S. W., Lee, W., Inoue, D., Jiang, Z., Yu, K., Jinno, H., Hashizume, D., Sekino, M., & Yokota, T. (2018). Self-powered ultra-flexible electronics via nano-grating-patterned organic photovoltaics. *Nature*, *561*(7724), 516-521.
- Paterson, A. F., Singh, S., Fallon, K. J., Hodsden, T., Han, Y., Schroeder, B. C., Bronstein, H., Heeney, M., McCulloch, I., & Anthopoulos, T. D. (2018). Recent progress in high mobility organic transistors: a reality check. *Advanced Materials*, 30(36), 1801079.
- Pecqueur, S., Mastropasqua Talamo, M., Guérin, D., Blanchard, P., Roncali, J., Vuillaume, D., & Alibart, F. (2018). Neuromorphic time dependent pattern classification with organic electrochemical transistor arrays. *Advanced Electronic Materials*, 4(9), 1800166.
- Rashid, R. B., Du, W., Griggs, S., Maria, I. P., McCulloch, I., & Rivnay, J. (2021). Ambipolar inverters based on cofacial vertical organic electrochemical transistor pairs for biosignal amplification. *Science advances*, 7(37), eabh1055.
- Rezali, F. A. M., Hatta, S. F. W. M., & Soin, N. (2022). Modelling of Thin-film Transistor for Glucose Sensing Application. 2022 IEEE International Conference on Semiconductor Electronics (ICSE),
- Rezali, F. M., Aidit, S., Nouxman, M., Hatta, S. W. M., & Soin, N. (2023). Development of Rapid Dispense-Printed Flexible Interdigitated Electrode

- Modified with rGO-TiO2 Nanohybrid for Glucose Detection. *Journal of The Electrochemical Society*, 170(7), 077516.
- Rivnay, J., Inal, S., Salleo, A., Owens, R. M., Berggren, M., & Malliaras, G. G. (2018). Organic electrochemical transistors. *Nature Reviews Materials*, 3(2), 1-14.
- Royer, S., & Paré, D. (2003). Conservation of total synaptic weight through balanced synaptic depression and potentiation. *Nature*, 422(6931), 518-522.
- Schwartz, G., Tee, B. C.-K., Mei, J., Appleton, A. L., Kim, D. H., Wang, H., & Bao, Z. (2013). Flexible polymer transistors with high pressure sensitivity for application in electronic skin and health monitoring. *Nature communications*, 4(1), 1859.
- Shao, L., Zhao, Y., & Liu, Y. (2021). Organic synaptic transistors: The evolutionary path from memory cells to the application of artificial neural networks. *Advanced Functional Materials*, 31(28), 2101951.
- Shim, H., Sim, K., Ershad, F., Yang, P., Thukral, A., Rao, Z., Kim, H.-J., Liu, Y., Wang, X., & Gu, G. (2019). Stretchable elastic synaptic transistors for neurologically integrated soft engineering systems. *Science advances*, *5*(10), eaax4961.
- Shukur, M., & Kadir, M. (2015). Hydrogen ion conducting starch-chitosan blend based electrolyte for application in electrochemical devices. *Electrochimica Acta*, 158, 152-165.
- Singaraju, S. A., Baby, T. T., Neuper, F., Kruk, R., Hagmann, J. A., Hahn, H., & Breitung, B. (2019). Development of fully printed electrolyte-gated oxide transistors using graphene passive structures. *ACS Applied Electronic Materials*, *1*(8), 1538-1544.
- Sinno, H., Fabiano, S., Crispin, X., Berggren, M., & Engquist, I. (2013). Bias stress effect in polyelectrolyte-gated organic field-effect transistors. *Applied Physics Letters*, 102(11).
- Smith, A. J., Owens, S., & Forsythe, I. D. (2000). Characterisation of inhibitory and excitatory postsynaptic currents of the rat medial superior olive. *The Journal of Physiology*, 529(3), 681-698.
- Spyropoulos, G. D., Gelinas, J. N., & Khodagholy, D. (2019). Internal ion-gated organic electrochemical transistor: A building block for integrated bioelectronics. *Science advances*, 5(2), eaau7378.
- Strakosas, X., Bongo, M., & Owens, R. M. (2015). The organic electrochemical transistor for biological applications. *Journal of Applied Polymer Science*, 132(15).
- Sun, B., Ma, Q., Wang, X., Liu, J., & Rejab, M. (2021). Additive manufacturing in medical applications: a brief review. IOP conference series: materials science and engineering,

- Sun, H., Vagin, M., Wang, S., Crispin, X., Forchheimer, R., Berggren, M., & Fabiano, S. (2018). Complementary logic circuits based on high performance n type organic electrochemical transistors. *Advanced Materials*, 30(9), 1704916.
- Sun, J., Fu, Y., & Wan, Q. (2018). Organic synaptic devices for neuromorphic systems. *Journal of Physics D: Applied Physics*, 51(31), 314004.
- Takagi, H. (2000). Roles of ion channels in EPSP integration at neuronal dendrites. *Neuroscience research*, *37*(3), 167-171.
- Tarabella, G., Vurro, D., Lai, S., D'Angelo, P., Ascari, L., & Iannotta, S. (2020). Aerosol jet printing of PEDOT: PSS for large area flexible electronics. *Flexible and Printed Electronics*, 5(1), 014005.
- Timachova, K., Watanabe, H., & Balsara, N. P. (2015). Effect of molecular weight and salt concentration on ion transport and the transference number in polymer electrolytes. *Macromolecules*, 48(21), 7882-7888.
- Torricelli, F., Adrahtas, D. Z., Bao, Z., Berggren, M., Biscarini, F., Bonfiglio, A., Bortolotti, C. A., Frisbie, C. D., Macchia, E., & Malliaras, G. G. (2021). Electrolyte-gated transistors for enhanced performance bioelectronics. *Nature Reviews Methods Primers*, 1(1), 66.
- Trung, T. Q., Ramasundaram, S., Hwang, B. U., & Lee, N. E. (2016). An all elastomeric transparent and stretchable temperature sensor for body attachable wearable electronics. *Advanced Materials*, 28(3), 502-509.
- Tuma, T., Pantazi, A., Le Gallo, M., Sebastian, A., & Eleftheriou, E. (2016). Stochastic phase-change neurons. *Nature nanotechnology*, 11(8), 693-699.
- Van De Burgt, Y., Lubberman, E., Fuller, E. J., Keene, S. T., Faria, G. C., Agarwal, S., Marinella, M. J., Alec Talin, A., & Salleo, A. (2017). A non-volatile organic electrochemical device as a low-voltage artificial synapse for neuromorphic computing. *Nature materials*, 16(4), 414-418.
- Wan, C., Chen, G., Fu, Y., Wang, M., Matsuhisa, N., Pan, S., Pan, L., Yang, H., Wan, Q., & Zhu, L. (2018). An artificial sensory neuron with tactile perceptual learning. *Advanced Materials*, 30(30), 1801291.
- Wang, H., Yang, M., Tang, Q., Zhao, X., Tong, Y., & Liu, Y. (2019). Flexible, conformal organic synaptic transistors on elastomer for biomedical applications. *Advanced Functional Materials*, 29(19), 1901107.
- Wang, S., He, C., Tang, J., Yang, R., Shi, D., & Zhang, G. (2019). Electronic synapses based on ultrathin quasi-two-dimensional gallium oxide memristor. *Chinese Physics B*, 28(1), 017304.
- Wang, T.-Y., He, Z.-Y., Chen, L., Zhu, H., Sun, Q.-Q., Ding, S.-J., Zhou, P., & Zhang, D. W. (2018). An organic flexible artificial bio-synapses with long-term plasticity for neuromorphic computing. *Micromachines*, 9(5), 239.

- Wei, Q., Mukaida, M., Naitoh, Y., & Ishida, T. (2013). Morphological change and mobility enhancement in PEDOT: PSS by adding co-solvents. *Advanced materials (Deerfield Beach, Fla.)*, 25(20), 2831-2836.
- White, H. S., Kittlesen, G. P., & Wrighton, M. S. (1984). Chemical derivatization of an array of three gold microelectrodes with polypyrrole: fabrication of a molecule-based transistor. *Journal of the American Chemical Society*, 106(18), 5375-5377.
- White, S. P., Frisbie, C. D., & Dorfman, K. D. (2018). Detection and sourcing of gluten in grain with multiple floating-gate transistor biosensors. *ACS sensors*, 3(2), 395-402.
- Williamson, A., Ferro, M., Leleux, P., Ismailova, E., Kaszas, A., Doublet, T., Quilichini, P., Rivnay, J., Rózsa, B., & Katona, G. (2015). Localized neuron stimulation with organic electrochemical transistors on delaminating depth probes. *Advanced Materials*, 27(30), 4405-4410.
- Wu, X., Chen, S., Moser, M., Moudgil, A., Griggs, S., Marks, A., Li, T., McCulloch, I., & Leong, W. L. (2023). High Performing Solid State Organic Electrochemical Transistors Enabled by Glycolated Polythiophene and Ion Gel Electrolyte with a Wide Operation Temperature Range from 50 to 110° C. Advanced Functional Materials, 33(3), 2209354.
- Wu, X., Tam, T. L. D., Chen, S., Salim, T., Zhao, X., Zhou, Z., Lin, M., Xu, J., Loo, Y.
 L., & Leong, W. L. (2022). All Polymer Bulk Heterojunction Organic Electrochemical Transistors with Balanced Ionic and Electronic Transport. Advanced materials, 34(42), 2206118.
- Yamamoto, S., & Malliaras, G. G. (2020). Controlling the neuromorphic behavior of organic electrochemical transistors by blending mixed and ion conductors. *ACS Applied Electronic Materials*, 2(7), 2224-2228.
- Yan, Y., Chen, Q., Wu, X., Wang, X., Li, E., Ke, Y., Liu, Y., Chen, H., & Guo, T. (2020). High-performance organic electrochemical transistors with nanoscale channel length and their application to artificial synapse. *ACS applied materials & interfaces*, 12(44), 49915-49925.
- Yang, C. S., Shang, D. S., Liu, N., Shi, G., Shen, X., Yu, R. C., Li, Y. Q., & Sun, Y. (2017). A synaptic transistor based on quasi 2D molybdenum oxide. *Advanced Materials*, 29(27), 1700906.
- Yang, F., Sun, L., Duan, Q., Dong, H., Jing, Z., Yang, Y., Li, R., Zhang, X., Hu, W., & Chua, L. (2021). Vertical organic nanocrystal arrays for crossbar memristors with tuning switching dynamics toward neuromorphic computing. *SmartMat*, 2(1), 99-108.
- Yang, X., Yu, J., Zhao, J., Chen, Y., Gao, G., Wang, Y., Sun, Q., & Wang, Z. L. (2020). Mechanoplastic tribotronic floating gate neuromorphic transistor. *Advanced Functional Materials*, 30(34), 2002506.

- Yang, Y., Zhao, X., Wang, S., Zhang, C., Sun, H., Xu, F., Tong, Y., Tang, Q., & Liu, Y. (2020). Exploration of the proton conduction behavior in natural neutral polysaccharides for biodegradable organic synaptic transistors. *Journal of Materials Chemistry C*, 8(46), 16542-16550.
- Yang, Y., Zhao, X., Zhang, C., Tong, Y., Hu, J., Zhang, H., Yang, M., Ye, X., Wang, S., & Sun, Z. (2020). Ultraflexible, degradable organic synaptic transistors based on natural polysaccharides for neuromorphic applications. *Advanced Functional Materials*, 30(51), 2006271.
- Yu, F., Zhu, L. Q., Gao, W. T., Fu, Y. M., Xiao, H., Tao, J., & Zhou, J. M. (2018). Chitosan-based polysaccharide-gated flexible indium tin oxide synaptic transistor with learning abilities. *ACS applied materials & interfaces*, 10(19), 16881-16886.
- Zare Bidoky, F., Hyun, W. J., Song, D., & Frisbie, C. D. (2018). Printed, 1 V electrolyte-gated transistors based on poly (3-hexylthiophene) operating at> 10 kHz on plastic. *Applied Physics Letters*, 113(5).
- Zeglio, E., & Inganäs, O. (2018). Active materials for organic electrochemical transistors. *Advanced Materials*, 30(44), 1800941.
- Zhang, H., Zhang, Y., Yu, Y., Song, X., Zhang, H., Cao, M., Che, Y., Dai, H., Yang, J., & Yao, J. (2017). Ambipolar quantum-dot-based low-voltage nonvolatile memory with double floating gates. *Acs Photonics*, 4(9), 2220-2227.
- Zhao, D., Fabiano, S., Berggren, M., & Crispin, X. (2017). Ionic thermoelectric gating organic transistors. *Nature communications*, 8(1), 14214.
- Zhou, Y., Li, J., Yang, Y., Chen, Q., & Zhang, J. (2019). Artificial synapse emulated through fully aqueous solution-processed low-voltage In2O3 thin-film transistor with Gd2O3 solid electrolyte. *ACS applied materials & interfaces*, *12*(1), 980-988.